Application of Polarimetric GPR to detection of subsurface objects

Application of Polarimetric GPR to detection of subsurface objects

by

TSEEDULAM Khuut

A Dissertation Presented in Partial Fulfillment of the
Requirements for the Degree of
Doctor Philosophy
in
Graduate School of Environmental Studies
of
TOHOKU UNIVERSITY

Supervised by
Prof. Dr. Motoyuki SATO

Committee in Charge
Prof. Dr. Motoyuki SATO
Prof. Dr. Noriyoshi TSUCHIYA
Prof. Dr. Hiroshi TAKAHASHI
Prof. Dr. Hiro WAKABAYASHI (NIHON University)

July, 2009

ACKNOWLEDGMENTS

I would like to offer my most sincere thanks to my supervisor, Professor Motoyuki Sato, for all his support and guidance, persistence, patience, and suggestions throughout the time of this project. I am grateful to the Satolab staff; Dr. M.Watanabe, Dr. T.Kido, Naoko Makino, and Yuko Iki for helping to solve my administrative problems.

I also thank my desertation committee members Prof. Hiro Wakabayashi, Prof. Noriyoshi Tsuchiya and Prof.Takahashi Hiroshi for their instructive suggestion and encouragement to complete the thesis.

I would like to thank for my colleagues of Satolab: T. Takayama, G.Mahmoud, M.G.Jose, G.Gilberto, M.Khamis, N.Ganchuluun, Kh.Badrakhgerel, Q.Lu, K.Kusano, N.Hayashi, Khamid, M.Matsumoto, Y.N.Tang, Y.J.Lee, D.H.Kim, N.Muratani and W.Zhao for your comments, ideas and presentations you made every week. Thanks to you all for sharing this PhD life with me and your wonderful friendship.

Grateful thanks to my friends, O.Aiymjan, B.Batkhishig, S.Myagmarsuren and Sh.Tsetsegjargal for inspiring and encouraging me.

I would also like to thank the Japanese Society for the Promotion of Science for supporting by JSPS Grant-in-Aid for Scientific Research (S) 18106008.

Finally, and most of all, I am extremely grateful to my dad Ch.Khuut, my mom D.Baasankhuu and my brothers; Kh.Batsukh, Kh.Bayanmunkh and sisters; Kh.Tserendulam and Kh.Tsetsegmaa.

Application of Polarimetric GPR for detection of subsurface objects

Abstract

The shallow subsurface information is of growing importance for environmental issues, engineering activities, and archaeological investigations. Because of this increased activity, it is important to obtain an image of the subsurface to disclose the presence and position of buried objects and the composition of the subsurface. The analysis of a detected signal to determine the electromagnetic characteristic of the target for target identification is an important radar application. Therefore the polarimetric GPR is adapted to get full polarimetric information in order to deal more successfully to describe the scattering behavior of the target.

In this research work, polarimetric GPR system, which was developed by the Sato Laboratory at the Tohoku University, Japan is proposed and evaluated for the detection and discrimination of the target at shallow depth.

In this research work presents description of polarimetric GPR system, calibration of system, some polarimetric signal processing algorithm and application of signal processing algorithm in experimental data. This work involves proposal of polarimetric decomposition algorithms to improve the target detection and identification at shallow depths. Using for known target we can understand and interpreted behavior of electromagnetic wave and scattering mechanism. In order to identify the target shape, polarimetric detection was examined to target a long metal wire, whose length is 3m. The concept of the target polarization basis changes has been tested using polarimetric data acquired over a buried metal wire and demonstrated the capability to accurate recover the target response signals, which would have the measured if the wire had been oriented with its preferential scattering axis aligned with antenna system. We represented the result of line of sight technique for experiment dataset, where target is oriented 0 and 45 degrees. As a result we could obtain more useful information related to the physics of scattering matrix. Target

decomposition techniques have been applied in various domains, providing a wealth of useful information about how target where is buried at shallow depth is seen by polarimetric radar. 3D reflectivity images obtained by polarimetric GPR experiments have been employed, together with decomposition techniques, for identifying the position, orientation and characteristics of the scattering mechanism in the buried target.

Polarization analysis applied two different applications obtained by RAMAC/GPR system. We applied the 3D GPR imaging method to detect and locate anomalous zones that could be associated with buried structures and buried pipe

In order to enhance our ability to interpretation the archaeological targets and buried pipe to recognize major reflections, we compared the GPR datasets acquired in two orthogonal survey directions. A good correlation is observed for the alignments of reflections acquired in the two directions. 3D GPR imaging has successfully mapped the 13th-century “Van Khan Tooril’s” castle and pipe detection.

CONTENTS

LIST OF FIGURES

LIST OF TABLES

CHAPTER 1. INTRODUCTION

1.1 Background of Ground Penetrating Radar……..1
1.2 Advanced concepts of polarimetry…….5
1.3 Research Objectives……7
1.4 Organization of the dissertation……..8

CHAPTER 2. THEORY OF RADAR POLARIMETRY

2.1 Wave Polarization……10
2.1.1. The Maxwell Equations……..10
2.1.2. Solution of the Wave Equation……...11
2.1.3. Polarization Description…….12
2.1.3.1. Polarization Ellipse……13
2.1.3.2. Typical Polarization States……14
2.1.3.3. Stokes Vector ……15
2.2. Polarization Scattering Matrix…….16
2.2.1. Scattering Matrix……16
2.2.2. Coherency and Covariance Matrices……..18
2.2.3. Mueller and Kennaugh Matrices…….21
2.3. Target Decomposition Theory…….22
2.3.1. Scattering by Random Media Partial Polarization……..22

2.3.2. Eigenvector Decomposition of the Coherency matrix……24
2.3.2.1. Symmetries……25
2.3.2.2. Parameterization of the Eigenvector Decomposition……27

CHAPTER 3. POLARIMETRIC GPR SYSTEM AND ITS EVALUATION

3.1. Principles of Polarimetric GPR Systems……29
3.2 Polarimetric Performance Evaluation……...32
3.2.1. Verification Measurement using a metal wire oriented
at different orientation angles……32
3.3 Polarimetric calibration……38
3.4 Summary……...44

CHAPTER 4. TEST EXPERIMENTS FOR BURIED OBJECT DETECTION AND DATA ANALYSIS

4.1 Introduction……...45
4.2 Polarimetric GPR measurement setup……..45
4.2.1 Experiment-1……..46
4.2.2. Experiment-2……63
4.3. Polarimetric Decomposition Technique……..66
4.2.1. The H/A/α Polarimetric Decomposition…….67
4.2.2. The Huynen-Kennaugh Matrix Decomposition……..70
4.4 Summary……...74

CHAPTER 5. POLARIZATION ANALYSIS FOR 3D GPR IMAGING

5.1. Introduction……..76
5.2. Methodology……76
5.3 Experiment 1. Archaeological Application……..77
5.3.1.Archaeological Background……77
5.3.2. GPR Data Acquisition and Processing……...78

5.3.3. Data Interpretation……..79
5.3.3.1. B-Scan image……79
5.3.2.2. C-Scan image……85
5.4. Experiment -2. Pipe Detection……89
5.4.1. GPR Data Acquisition……90
5.4.2. Signal Processing Result……92
5.4.2.1. Data Interpretation……96
5.5. Summary ……....99

CHAPTER 6. CONCLUSION ……..…...100

APPENDIX1 ……..….....A1

BIBLIOGRAPHY ……..….....i

ABSTRACT ……..….....

ACKNOWLEDGEMENTS ……..….....

PUBLICATION BY THE AUTHOR……..

LIST OF FIGURES

CHAPTER 1

Fig.1.1. GPR system ……...3

Fig.1.2. Stepped-frequency GPR system…….....4

Fig.1.3. Sketch map of radar system…….....8

CHAPTER 2

Fig.2.1. Spherical coordinate system for a plane wave…….……12

Fig.2.2. Polarization ellipse in the v-h plane and geometrical parameters.
The rotation corresponds to a right-handed polarization……..…13

Fig.2.3. Poincare sphere with Stokes parameters as Cartesian coordinates……..….16

CHAPTER 3

Fig.3.1.1. Sketch map of polarimetric GPR system…….…….....30

Fig.3.1.2. Polarimetric GPR system……...31

Fig.3.2.3. Return loss of Vivaldi antenna……...31

Fig.3.2.1. Experiment setup in anechoic-chamber…….33

Fig.3.2.2. Power spectrum of GPR data in different polarization state…….....34

Fig.3.2.3. GPR time domain data in different polarization states……..35

Fig.3.3.4. Scattering coefficient of co-polarization state……...36

Fig.3.3.5. Scattering coefficient of cross-polarization state……..37

Fig.3.3.1. Waveform of metal wire……....41

Fig.3.3.2. Calibration results of wire oriented by 30°, “M” –indicates
measured, “S” –calibrated, “T” –theoretical scattering coefficients……...42

Fig.3.3.3. relative amplitude and phase characteristics of 30° oriented metal wire;
a) Cross-polarization, b) co- polarization state……43

Fig.3.3.4. Cross talk……..…….....44

Fig.3.3.5. Gain balance……..44

CHAPTER 4

Fig.4.2.2. Sketch map of the experiment setup……..46

Fig.4.2.3. Spectrum of full polarization states; (a) Raw power spectrum,
(b) Spectrum of subtracted direct coupling signal……...48

Fig.4.2.4. Spectrogram of STFT; (a) Horizontal polarization
(b) Vertical polarization……...49

Fig.4.2.5. Spectrogram of STFT
(a) Power spectrum of STFT, (b) co polarized phase difference…….51

Fig.4.2.6. Raw C-scan images metal wire buried at a depth of 5cm in sand;
(a) target oriented at θ=0° (horizontal), (b) target is rotating
through the orientation angle θ=45°……..55

Fig.4.2.7. Raw B-scan images extracted from A-A' cross section
(a) target oriented at θ=0° (horizontal), (b) target is rotating through the orientation angle θ=45° ……56

Fig.4.2.8. Raw B-scan images extracted from B-B' cross section
(a) target oriented at θ=0° (horizontal), (b) target is rotating through the orientation angle θ=45°……..57

Fig.4.2.9. Time Domain wave form of metal wire buried at a depth of 5cm in sand, (a) target oriented at θ=0° (horizontal), (b) target is rotating through the orientation angle θ=45°……...58

Fig.4.2.10. B-scan images processed by Stokes matrix;
(a) Stokes images target is oriented at θ=0° (horizontal)
(b) Stokes images; target is rotating through the orientation angle θ=45°……..62

Fig.4.2.11. B-scan images of polarimetric analysis,
(a) Cross and co polarization images target is oriented at θ=0° (horizontal)
(b) Cross and co polarization images; target is rotating through the orientation angle θ=45°……....63

Fig.4.2.12. Photograph of the target used in the experiment……64

Fig.4.2.13. B-scan images of various targets in dry sand……..65

Fig.4.2.14. C-scan images of various targets in dry sand……..66

Fig.4.3.1. Polarimetric analysis of the metal wire oriented at 0 degrees
(a) absolute scattering coefficients, (b) the computed eigenvalues
(c) estimated anisotropy, (d) estimated orientation angle……...69

Fig.4.3.2. Polarimetric analysis of the metal wire oriented at 45 degrees,
(a) absolute scattering coefficients, (b) the computed eigenvalues
(c) estimated anisotropy, (d) estimated orientation angle……...70
Fig.4.2.3. C-scan images processed by Huynen parameter displayed at
depth at 3.8ns……74

CHAPTER 5

Fig.5.2.1. View of the archaeological site and the target……..77

Fig.5.2.2. Sketch map of the study area……78

Fig.5.2.3. GPR Profile, Profile-4 acquired along NS direction dashed circles
indicates reflections from tile and bricks ($v = 0.13m/ns$) ;
(a) Instantaneous amplitude, (b) Instantaneous phase……82

Fig.5.2.4. GPR Profile, Profile-10 acquired along NS direction dashed
circles indicates reflections from tile and bricks ($v = 0.13m/ns$);
(a) Instantaneous amplitude, (b) Instantaneous phase……83

Fig.5.2.5. GPR Profile, Profile-19 acquired along WE direction
dashed circles indicates reflections from tile and bricks ($v = 0.13m/ns$)
(a) Instantaneous amplitude, (b) Instantaneous phase……84

Fig.5.2.6. Instantaneous amplitude horizontal slice maps at 15cm
depth ($v = 0.13m/ns$), (a) horizontal slice obtained along NS survey direction,
(b) horizontal slice obtained along WE survey direction……87

Fig.5.2.7. Instantaneous amplitude horizontal slice maps from 15cm to 21cm
depths ($v = 0.13m/ns$);
(b) horizontal slice obtained along WE survey direction……88

Fig.5.3.1 Schematic diagram of the new 3D GPR system……89

Fig.5.3.2. Data acquisition by 3D GPR with PLPS; Two rotating laser transmitters (Tx1, Tx2) emit pulse sequences received by the laser detector mounted on the GPR antenna……..91
Fig.5.4.3. Sketch map of experiment……....91

Fig.5.4.4. C-scan images of 3D GPR in 2 different orthogonal directions at 35cm depth; dotted white lines indicates location of pipe;
(a) XX polarization; (b) YY polarization…….……94

Fig.5.4.5. Phase images obtained by Hilbert Transformation;
dotted white lines indicates location of pipe;
(a) XX polarization; (b) YY polarization……95

Fig.5.4.6. B-scan images extracted from 3D GPR imaging;
dotted black lines indicates hyperbola, where is representing location of the target; (a) XX polarization (b) YY polarization……..96

Fig.5.4.7. Polarimetric images processed by Stokes matrix;
(a) S_1 image processed by Stokes matrix;
(b) S_2 image processed by Stokes matrix;……..98

LIST OF TABLES

CHAPTER 4

Table.4.1.1.Experiment Parameters……...47

Table 4.1.2. Characteristics of targets……...65

Table 4.2.1. Geometrical significance of the Huynen parameters…….72

CHAPTER 1

INTRODUCTION

In recent years, there has been great interest in detecting and imaging subsurface targets in a wide variety of areas such as civil engineering [17], landmine detection [14], [15], [45], archeological investigations [8], [9], [28], [37], [43] and environmental applications [27], [47]. Various sensing tools have been used to get better performance in different situations. The main sensors used are electromagnetic induction (EMI), ground penetrating radar (GPR), seismic and infrared (IR) sensors. These sensors rely on different operating principles and provide different levels of information about the sensed medium based on their capabilities. An EMI sensor is sensitive to conductivity and basically is used to find objects with metallic content. IR is attractive for its high standoff distance sensing. Seismic sensors are sensitive to the mechanical properties of objects. GPR has been shown to be an efficient subsurface imaging tool due to its low cost nondestructive capability of detecting both metal and non-metal objects. In this thesis we will be mostly focusing on creating subsurface images and detecting features in those images using polarimetric GPR system.

1.1. BACKGROUND OF GROUND PENETRATING RADAR

Ground-penetrating radar (GPR) is a geophysical method that uses electromagnetic radiation in the microwave band of the radio spectrum, and detects the reflected signals from subsurface structures. GPR is the general term applied to techniques which employ radio waves, typically in the 1 to 5000 MHz frequency range, to map structure and features buries in the ground or in man-made structures.

Compared with other subsurface sensing technologies, GPR has a few advantages. First, it is sensitive to changes in all three electromagnetic characteristics of a medium, electric permittivity, electric conductivity, and magnetic permeability. Thus GPR is capable of detecting both metallic and nonmetallic objects. Second, unlike sensors that can only survey an area directly beneath them, GPR can survey an area in front of it [35]. Therefore, a GPR system can be used to detect dangerous objects before the system moves over and past them. This can be important for operations such as buried landmine detection and unexploded ordinance remediation. In practice, GPR data are either processed on-line or off-line. On-line processing can be fast and provides real-time detection and requires a more sophisticated hardware and powerful computer. Off-line processing requires a large amount of data storage and can use data of a full scan.

Basically, GPR can be divided into two categories, depending on their operating principles. They are as following;

- Time Domain Radar
- Frequency Domain Radar

The impulse radar and the chirp radar, which operates in time domain is called time domain radar. Most of the GPR are time domain radar, which sensitivity and the maximal detectable depth is usually limited by antenna. A typical GPR transmitter/receiver configuration is shown in Fig.1.1. The system consists of one transmitter and one receiver. The transmitter emits a short pulse of electromagnetic energy and the receiver collects the echo for a certain time period. The exact type of the transmitter and receiver, shape of the electromagnetic pulse, and system setup depend on the specific application of the GPR To improve performance and efficiency, a GPR array is usually employed to sweep a large area in a relatively short time. Fig. 1.1 shows a typical GPR array moving in the direction.

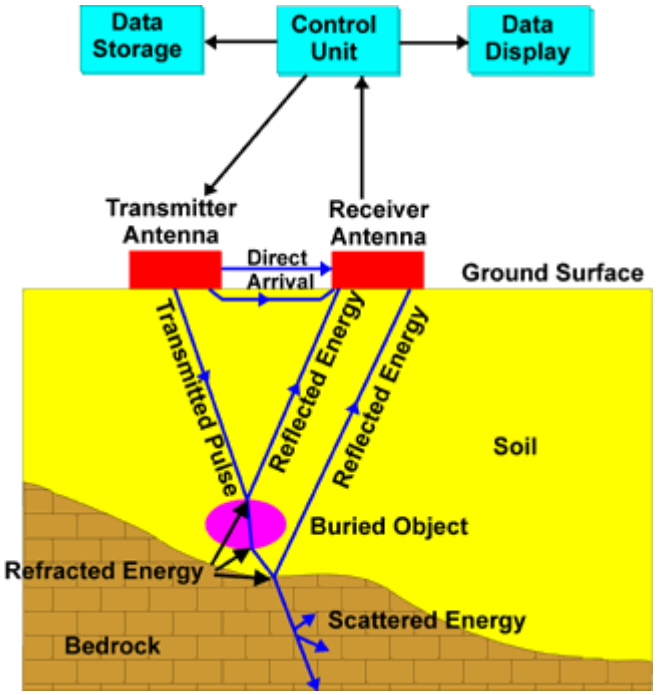

Fig.1.1. Time domain GPR system

At every stop of the array, the GPR array operates in the following sequence: 1) the first transmitter radiates a pulse into the ground and then turns off; 2) the first receiver turns on to collect reflected signal; and 3) the first receiver turns off after a short time, usually 10 to 20 ns. The above process repeats from every pair of transmitters and receivers and then the GPR array moves to next position. Based on the echoes, the processing objective is to determine if an object is present in the GPRs field of view. The inherent near-field nature of the GPR detection problem coupled with the fact that the objects of interest are embedded in an inhomogeneous half space with a typically rough interface present some significant challenges in the area of GPR signal processing.

Another type of GPR that is becoming increasingly popular is the stepped-frequency continuous wave (SFCW) GPR [24]. The SFCW radar, which operates in frequency domain, is called frequency domain radar. A stepped-frequency signal probes the environment with a discrete set of frequencies. The main advantage of a SFCW GPR is the greater measurement accuracy inherent in a frequency domain system and the flexibility to adjust the operating frequency range to suit the specific ground conditions. For both types of GPR the total subsurface response, formed from a combination of the responses from all reflectors within the medium, can be inverted

using various imaging algorithms; e.g., time-domain Standard Back-projection (SBP) [14], and Fourier domain Synthetic Aperture Radar (SAR) image formation techniques [37], [16].

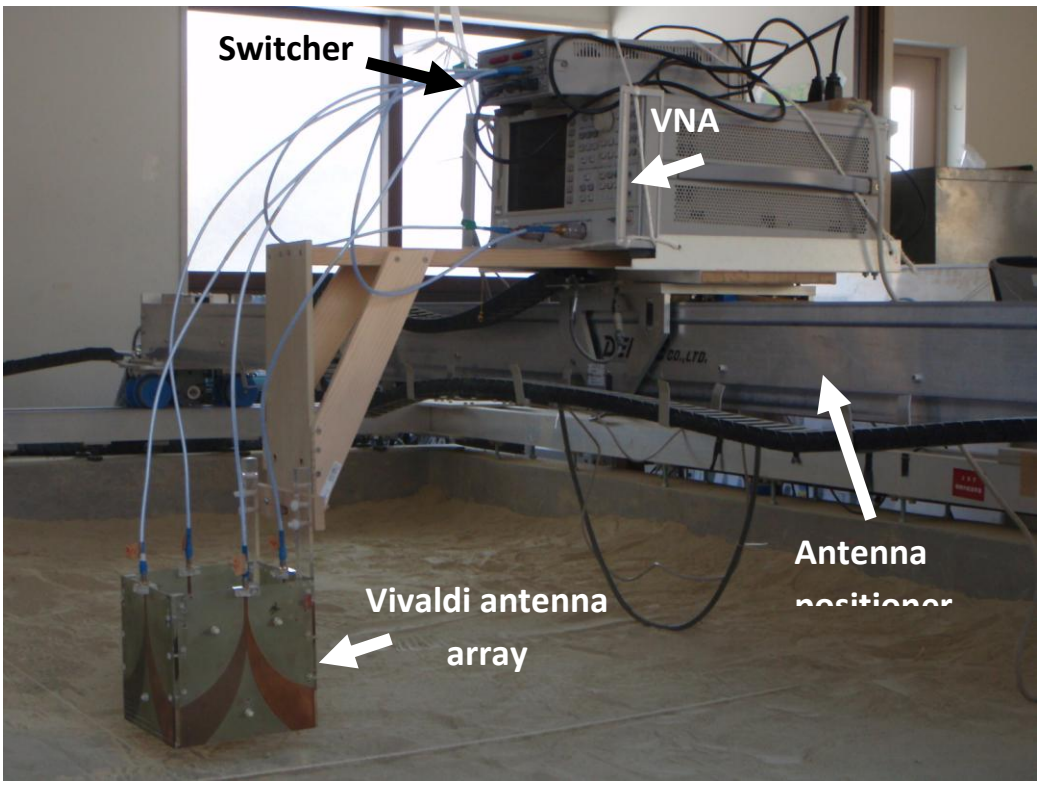

Fig.1.2. Stepped-frequency GPR system

All of these algorithms require fine spatial sampling and Nyquist-rate time sampling of the received signals, or a high number of frequency measurements. Then they perform matched filtering with the impulse response of the data acquisition process to form an image.

Limitations of GPR

- As with any other geophysical technique, GPR is extremely good in some circumstances and should not be used at some locations.
- GPR anomalies rely on a detectable contrast of subsurface electrical properties between two media or within a medium. In the absence of a detectable contrast, no anomaly will be evident. It is possible that ground conditions may contain

targets that are absent from the GPR data. Also, GPR data can contain weak anomalies, which are difficult to interpret.

- GPR signal cannot penetrate highly conductive material e.g., beneath metal sheets or very wet ground.
- Calibration should be carried out to obtain accurate depth estimates.
- GPR data processing and interpretation can be complicated - specialized analysis and interpretation is required.
- GPR is unsuited to absolute measurement, e.g., it can find wet areas, but at the moment cannot determine actual moisture content (currently under research).
- GPR is an interpretive method, based on the identification of reflectors, which may not uniquely identify an object.

1.2. ADVANCEMENT OF RADAR POLARIMETRY

Radar Polarimetry (Polar: polarization Metry: measure) is the science of acquiring, processing and analysing the polarization state of an electromagnetic field. The polarization information contained in the waves backscattered from a given medium is highly related to its geometrical structure and orientation as well as to its geophysical properties such as humidity, roughness and conductivity of soils.

Radar Polarimetry deals with the full vector nature of polarized electromagnetic waves, and when the wave passes through a medium of changing index of refraction, or when it strikes an object or a scattering surface and it is reflected; then, characteristic information about the reflectivity, shape and orientation of the reflecting body can be obtained by implementing polarization processing [3]. Whereas with radar polarimetry the textural fine-structure, target-orientation and shape, symmetries and material constituents of the Earth surface can be recovered with considerable improvements above that of standard “amplitude-only radar”; with radar interferometry the spatial structure can be explored. More recently, Radar Interferometry has matured as an important sensing technology for topographic mapping and land classification [11], [32]. By combining interferograms in different polarisation states it has been shown that important structural information relating to vegetation height and density can be obtained. Combining polarimetric and

interferometric SAR techniques (POL-IN-SAR) it is today possible to recover such co-registered textural plus spatial properties simultaneously. This has important consequences for the design of future space and airborne sensors for carbon sequestration and climate change studies.

An important development in our understanding of how to best extract physical information from the classical 2x2 coherent backscattering matrix [S] has been achieved through the construction of system vectors [11].

There is currently a great deal of interest in the use of polarimetry for radar remote sensing. In this context, an important objective is to extract physical information from the observed scattering of microwaves by surface and volume structures. The most important observable measured by such radar systems is the 3x3 coherency matrix [T]. This matrix accounts for local variations in the scattering matrix and is the lowest order operator suitable to extract polarimetric parameters for distributed scatterers in the presence of additive (system) and/or multiplicative (speckle) noise.

Many targets of interest in radar remote sensing require a multivariate statistical description due to the combination of coherent speckle noise and random vector scattering effects from surface and volume. For such targets, it is of interest to generate the concept of an average or dominant scattering mechanism for the purposes of classification or inversion of scattering data. This averaging process leads to the concept of the "distributed target" which has its own structure, in opposition to the stationary target or "pure single target".

Target Decomposition theorems are aimed at providing such an interpretation based on sensible physical constraints such as the average target being invariant to changes in wave polarization basis.

Target Decomposition theorems were first formalized by J.R. Huynen but have their roots in the work of Chandrasekhar on light scattering by small anisotropic particles. Since this original work, there has been much other proposed decomposition. We classify four main types of theorem:

- Those based on the dichotomy of the Kennaugh matrix (Huynen).
- Those using an eigenvector / eigenvalues analysis of the covariance or coherency matrix (Cloude, VanZyl, Cloude and Pottier).

A complete description of all these different Polarimetric Target Decomposition can be found in [9], and we focus here on the H/A/α decomposition theorem and Huynen Kennaugh decomposition.

1.3. RESEARCH OBJECTIVES

Radar techniques, developed originally for the detection of targets in the sky or on the surface of land or sea, are now being adapted as a means of investigating the composition and integrity of non-conducting materials and structures. The radar technique principally detect back-scattered energy from a target; anomalies within a material give rise to reflections and if the radar antenna is scanned over the material an image of the anomalies can be generated.

Radar polarimetry is fast growing and powerful remote sensing technique. It is anticipated the majority of new radars will have polarimetric or scattering matrix capability. The strength of the polarimetric approach is due to many important and key features of radar targets being vectorial in nature. Hence, making use of the inherent vector property of electromagnetic field interactions with the scatterer, results in a more comprehensive picture of the target.

Polarimetric radar detection is a powerful remote sensing technique for target recognition, identification and classification. The polarimetric approach is potent as it effectively explores radar target features (e.g., structure, change) by making use of the full vector properties of the electromagnetic (EM) field while interacting with the target scatterers.

Polarimetric GPR provides a target signature, which contains information about size, shape and material properties of the target being detected and it can be used for detecting target orientation. The analysis of a detected signal to determine the electromagnetic characteristic of the target for target identification is an important radar application. Therefore the polarimetric GPR is adapted to get full polarimetric information in order to deal more successfully to describe the scattering behavior of target.

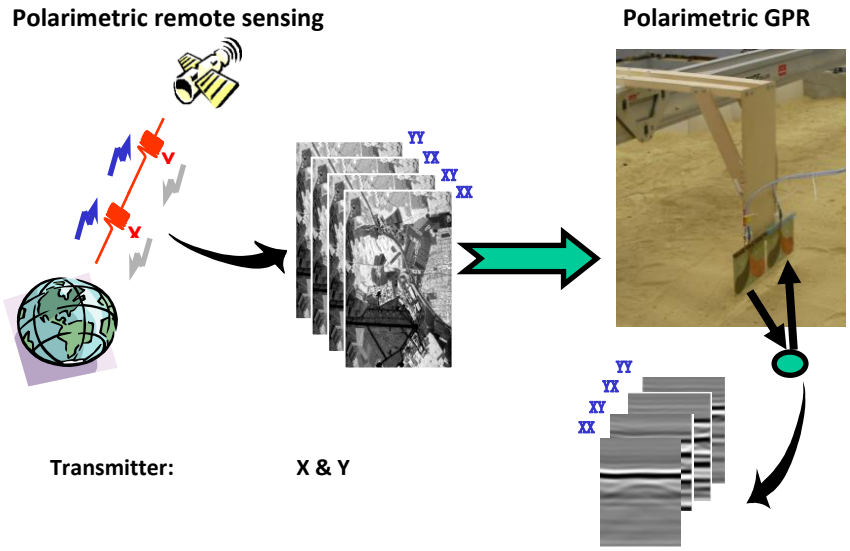

Fig.1.3. Sketch map of radar system

Therefore, we planed to develop a full polarimetric GPR system for detecting of different subsurface targets. For application of the full polarimetric GPR system, the following research objectives:

(a) Development of a full polarimetric GPR system
(b) System evaluation with polarimetric calibration
(c) Test experiments for known target
(d) Full polarimetric GPR data processing
(e) Extend the information of target
(f) Polarimetric analysis & interpretation of full polarimetric GPR data
(g) Potential application of subsurface target

1.4. ORGANIZATION OF THE DISSERTATION

The dissertation on the "Application of Polarimetric GPR for detection of subsurface objects" covers principles of Polarimetric GPR system, polarimetric calibration, polarimetric analysis and processing as well as interpretation for subsurface target.

This dissertation is composed of six chapters. Chapter 2 covers theory of radar polarimetry. All the polarimetric theory has been published already in the literature, but the issues directly related with the thesis are rewritten in this chapter for the sake of completeness. Chapter 3 defines design and features evaluation of a full Polarimetric GPR system. The last section of Chapter 3 discusses polarimetric performance evaluation outlines the basic experiment test and polarimetric calibration. Chapter 4 describes experimental test of shallow subsurface polarimetric measurement and results of polarimetric analysis. Chapter 5 contains GPR experiment of field experiment and signal processing and visualization. We tried to process polarimetric analysis to dataset obtained by RAMAC/GPR system. In chapter 6, summary of the preceding chapters and shortcomings are presented. Hilbert transformation formulas are described in Appendix-1.

CHAPTER 2

THEORY OF RADAR POLARIMETRY

The purpose of this chapter is the definition of the basic concepts that will be used throughout the thesis.

2.1. WAVE POLARIZATION

2.1.1. THE MAXWELL EQUATIONS

In 1864, J.C. Maxwell established and synthesized preceding results obtained by M. Faraday, and A. Ampere and K.F. Gauss [5], [6], [30], [31], about the interaction between the electric field, the magnetic field and currents, generalizing them to variable regimes in time. The Maxwell equations represent the starting point to solve electromagnetic problems as they govern the generation and propagation of electromagnetic waves, as well as the interaction of these waves with the matter. For electromagnetic sources in non-conducting lossless, isotropic media, the Maxwell equations can be written as

$$\begin{aligned} \nabla \times \mathbf{E} &= -\frac{\partial \mathbf{B}}{\partial t} \\ \nabla \times \mathbf{H} &= \mathbf{J} + \frac{\partial \mathbf{D}}{\partial t} \\ \nabla \cdot \mathbf{B} &= 0 \\ \nabla \cdot \mathbf{D} &= \rho_v \\ \mathbf{D} &= \varepsilon \cdot \mathbf{E} \\ \mathbf{B} &= \mu \cdot \mathbf{H} \end{aligned} \tag{2.1}$$

where

E -the electric field intensity vector in Volt/meter

B -the magnetic flux density vector in Tesla

H -the magnetic field intensity vector in Ampere/meter

D -the current displacement vector in Coulomb/meter^2

J -the electric current density vector in Ampere/meter^2

ρ -the electric charge density in Coulomb/meter^3

2.1.2. SOLUTION OF THE WAVE EQUATION

In a source-free, isotropic, lossless homogeneous medium, Maxwell's equations can be combined to obtain the form of the electric field in the medium;

$$\nabla^2\mathbf{E}(\mathbf{r},t)+k^2\mathbf{E}(\mathbf{r},t)=0\,. \tag{2.2}$$

Where

$$k=\omega\sqrt{\mu\varepsilon}'=\frac{\omega}{c} \tag{2.3}$$

is the wave number, and c is the velocity of the light.

A general solution that satisfies Eq .2.2 is the following;

$$\mathbf{E}(\mathbf{r})=\mathbf{E}\cdot e^{-j\mathbf{k}\cdot\mathbf{r}}=\mathbf{E}\cdot e^{-jk\hat{\mathbf{k}}\cdot\mathbf{r}} \tag{2.4}$$

which is a plane wave propagating in the direction of **k**. The magnitude of **k** is the wave number *k*, so the direction of propagation is completely defined by the unit vector $\hat{\mathbf{k}}=\mathbf{k}/k$.

If the direction of propagation does not change in the space, and the magnitude of the fields does not attenuate with propagation, then this solution of the wave equation is named a plane wave.

2.1.3. POLARIZATION DESCRIPTION

In order to describe the polarization of a wave, a coordinate system must be established. In the following, a generic spherical coordinate system is described in Fig.2.1.

A plane wave traveling in the direction of $\hat{\mathbf{k}}$ has an electric field vector **E** that can be characterized in terms of two orthogonal components; horizontal polarization $E_h\,\hat{\mathbf{h}}$ and vertical polarization $E_v\,\hat{\mathbf{v}}$.

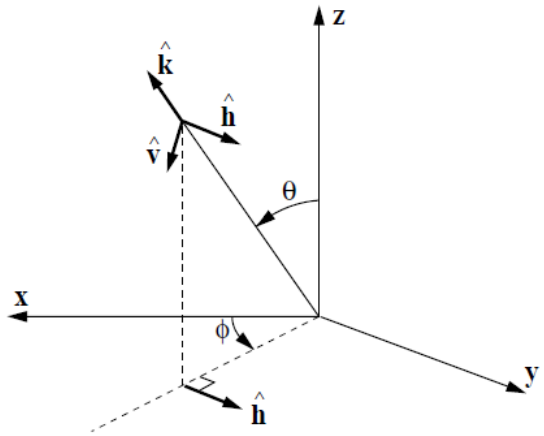

Fig.2.1. Spherical coordinate system for a plane wave

It can be conveniently done by defining the coordinate system $\left(\hat{\mathbf{k}},\hat{\mathbf{v}},\hat{\mathbf{h}}\right)$ in coincidence with the standard spherical coordinate system. $\left(\hat{\mathbf{r}},\hat{\boldsymbol{\theta}},\hat{\varphi}\right)$. This is depicted in Fig.2.1.

$$\mathbf{E}(\mathbf{r}) = \left(E_v\hat{\mathbf{v}} + E_h\hat{\mathbf{h}}\right)e^{-jk\hat{\mathbf{k}}\cdot\mathbf{r}} \tag{2.5}$$

where, according to Fig.2.1,

$$\hat{\mathbf{h}} = \frac{\hat{\mathbf{z}}\times\hat{\mathbf{k}}}{\left|\hat{\mathbf{z}}\times\hat{\mathbf{k}}\right|} \tag{2.6}$$

$$\hat{\mathbf{v}} = \hat{\mathbf{h}}\times\hat{\mathbf{k}} \tag{2.7}$$

These vectors can be also defined in terms of spherical angles

$$\hat{\mathbf{k}} = \sin\theta\cos\varphi\cdot\hat{\mathbf{x}} + \sin\theta\cos\varphi\cdot\hat{\mathbf{y}} + \cos\theta\cdot\hat{\mathbf{z}} \tag{2.8}$$

$$\hat{\mathbf{h}} = -\sin\varphi\cdot\hat{\mathbf{x}} + \cos\varphi\cdot\hat{\mathbf{y}} \tag{2.9}$$

$$\hat{\mathbf{v}} = \cos\theta\cos\varphi\cdot\hat{\mathbf{x}} + \cos\theta\sin\varphi\cdot\hat{\mathbf{y}} - \sin\theta\cdot\hat{\mathbf{z}} \tag{2.10}$$

2.1.3.1. **POLARIZATION ELLIPSE**

In general, the tip of the electric field vector moves on a monochromatic plane in time along an ellipse, which is known as the polarization ellipse (Fig2.2). The ellipse corresponds to the most general case of polarization, so every polarization state can be described by means of a set of a few geometrical values. The most important concepts are summarized here. If a_v, a_h and phase difference Δφ are given, referred to an arbitrary set of axes, and if α denotes an angle such that

$$\tan\alpha = \frac{a_h}{a_v}, \qquad 0 \le \alpha \le \pi/2 \tag{2.11}$$

then the principal semi-axes a and b of the ellipse, the orientation angle ψ which the major axis makes with $\hat{v}$, and the ellipticity angle χ which specifies the ratio of the ellipse axes, are specified by the following formulae;

$$a^2 + b^2 = a_v^2 + a_h^2 \tag{2.12}$$

$$\tan 2\psi = \tan 2\alpha \cos\Delta\varphi, \qquad 0 \le \varphi \le \pi \tag{2.13}$$

$$\sin 2\chi = \sin 2\alpha \sin\Delta\varphi \tag{2.14}$$

$$\tan\chi = \pm b/a \qquad -\pi/4 \prec \chi \le \pi/4 \tag{2.15}$$

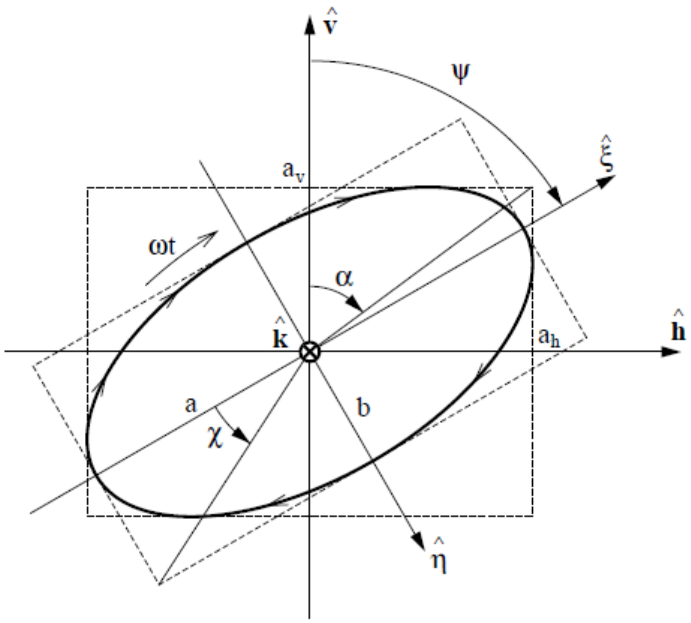

Fig.2.2. Polarization ellipse in the v-h plane and geometrical parameters; the rotation corresponds to a right-handed polarization

2.1.3.2. **TYPICAL POLARIZATION STATES**

Attending to define parameters of the polarization ellipse, some important particular cases of polarization states can be recognized. The first special type is the reduction of the ellipse to a straight line. It occurs when

$$\Delta\varphi = \varphi_h - \varphi_v = m\pi, \qquad m = 0,\pm1,\pm2,\ldots \tag{2.16}$$

leading to

$$\frac{\mathbf{E}_h}{\mathbf{E}_v} = (-1)^m \frac{a_h}{a_v} \tag{2.17}$$

In this case the field is said to present linear polarization. The ellipticity angle χ is zero, and the orientation angle ψ coincides with α whose tangent is given by Eq.2.17. In the $v-h$ basis, $\psi = 0$ corresponds to vertical polarization, and $\psi = \pi/2$ to horizontal polarization.

Another special case is that of a wave with circular polarization, the ellipse then degenerated to a circle. A necessary condition for this is that the circumscribed rectangle becomes a square;

$$a_v = a_v = a \tag{2.18}$$

In addition, one of the components must be zero when the other has an extreme value;

$$\Delta\varphi = \varphi_h - \varphi_v = m\pi/2, \qquad m = \pm1,\pm3,\pm5,\ldots \tag{2.19}$$

When the wave has a right-handed circular polarization, $\sin\Delta\varphi \prec 0$, so that

$$\Delta\varphi = -\frac{\pi}{2} + 2m\pi, \qquad m = 0,\pm1,\pm2,\ldots \tag{2.20}$$

$$\mathbf{E}_v = a\cos(\omega t - \mathbf{kr} + \varphi_v) \tag{2.21}$$

$$\mathbf{E}_h = a\cos\left(\omega\cdot t - \mathbf{kr} + \varphi_v - \pi/2\right) = a\sin\left(\omega\cdot t - \mathbf{kr} + \varphi_v\right) \tag{2.22}$$

2.1.3.3. STOKES VECTOR

A different representation of the polarization of plane waves that has been widely used in optics and radar is the Stokes vector **g**;

$$\mathbf{g} = \begin{bmatrix} \mathbf{I} \\ \mathbf{Q} \\ \mathbf{U} \\ \mathbf{V} \end{bmatrix} = \begin{bmatrix} |\mathbf{E}_v|^2 + |\mathbf{E}_h|^2 \\ |\mathbf{E}_v|^2 - |\mathbf{E}_h|^2 \\ 2\Re\left(\mathbf{E}_v\mathbf{E}_h^*\right) \\ 2\Im\left(\mathbf{E}_v\mathbf{E}_h^*\right) \end{bmatrix} \tag{2.23}$$

where the asterisk denotes the complex conjugate operation, $\Re$ and $\Im$ stand for the real and imaginary part, respectively.

A particular characteristic of those parameters are that all real and have the same physical dimensions. The parameter **I** is proportional to the total intensity to the wave, **Q** is the difference of the intensities in both polarizations, while **U** and **V** contain the phase information.

Although the Stokes vector has four components, only three of them are independent because they must satisfy

$$\mathbf{I}^2 = \mathbf{Q}^2 + \mathbf{U}^2 + \mathbf{V}^2 \tag{2.24}$$

The relationship between the Stokes parameters and the other sets of parameters is;

$$\mathbf{g} = \begin{bmatrix} \mathbf{I} \\ \mathbf{Q} \\ \mathbf{U} \\ \mathbf{V} \end{bmatrix} = \begin{bmatrix} a_v^2 + a_h^2 \\ a_v^2 - a_h^2 \\ 2a_v a_h \cos\Delta\varphi \\ 2a_v a_h \sin\Delta\varphi \end{bmatrix} = \mathbf{I}\begin{bmatrix} 1 \\ \cos 2\psi\cos 2\chi \\ \sin 2\psi\cos 2\chi \\ \sin 2\chi \end{bmatrix} \tag{2.25}$$

The relationship in Eq.2.25 indicates that the state of polarization of a plane wave can be geometrically represented by regarding $(\mathbf{Q}, \mathbf{U}, \mathbf{V})$ as the Cartesian coordinates of a point P.

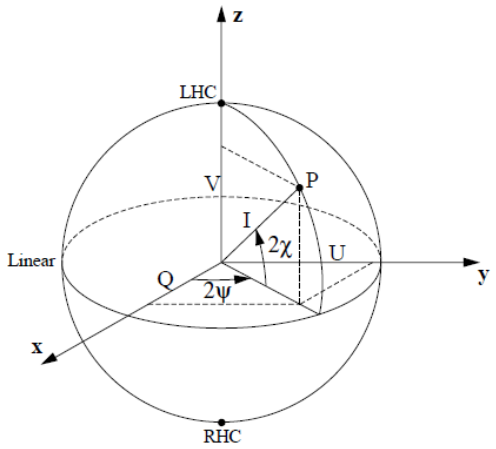

Fig.2.3. Poincare sphere with Stokes parameters as Cartesian coordinates

In fact, there is a unique mapping of every polarization state P on the surface of a sphere of radius I. The angles 2χ and 2ψ define the latitude and longitude of the point P, and the sphere is usually called a Poincare sphere (Fig.2.3).

2.2. **POLARIZATION SCATTERING MATRIX**

When dealing with the scattering produced by an object of interest, we will have to relate the polarization characteristics of two waves; a wave generated by the radar for illuminating the target, and a wave scattered by the target and the received by the radar receiving antenna.

2.2.1. SCATTERING MATRIX

When an object illuminated by an electromagnetic plane wave with incident and scattered electric field

$$\mathbf{E}^i = E_v^i \widehat{\mathbf{v}}_i + E_h^i \widehat{\mathbf{h}}_i \tag{2.26}$$

$$\mathbf{E}^s = E_v^s \widehat{\mathbf{v}}_s + E_h^s \widehat{\mathbf{h}}_s \tag{2.27}$$

where in the phase factor has been suppressed for convenience, $\hat{\mathbf{v}}_i$ and $\hat{\mathbf{h}}_i$ have been arbitrarily defined according to section 2.1.3, and the incident direction is denoted as $\hat{\mathbf{k}}_i$.

For the polarization description of the scatterer will be useful to adopt the following matrix notation for the electric field in Eq.2.26 and Eq.2.27.

$$\mathbf{E}^i = \begin{bmatrix} E_v^i \\ E_h^i \end{bmatrix} \qquad \mathbf{E}^s = \begin{bmatrix} E_v^s \\ E_h^s \end{bmatrix} \tag{2.28}$$

By using this matrix notation, the component of $\mathbf{E}^{\mathrm{i}}$ and $\mathbf{E}^{\mathrm{s}}$ are related by a complex 2×2 matrix in the following manner;

$$\begin{bmatrix} E_v^s \\ E_h^s \end{bmatrix} = \frac{e^{-jkr}}{r} \begin{bmatrix} S_{vv} & S_{vh} \\ S_{vh} & S_{hh} \end{bmatrix} \cdot \begin{bmatrix} E_v^i \\ E_h^i \end{bmatrix} = \frac{e^{-jkr}}{r} [S] \cdot [E^i] \tag{2.29}$$

where r is the distance between the scatterer and the antenna, and k is the wave number of the illuminated field. The phase factor represents the delay due to the travel of the wave from the scatterer to the antenna.

The $[S]$ matrix is called the scattering matrix. The elements of the scattering matrix are known as the complex amplitudes. S_{vv} –is the complex ratio of the electric field of the vertically polarized parts of the scattered wave and the incident wave; thus to measure S_{vv}, a vertically polarized wave is transmitted, and both amplitude and phase of the vertically polarized part of the scattered wave are measured. The other elements of the scattering matrix can be measured in a similar manner by choosing the appropriate combination of transmitted and received polarizations and measuring both amplitude and phase of the desired component of the scattered field.

The scattering matrix is formulated in forward scatter alignment (FSA) and back scatter alignment (BSA) conventions [51]. The FSA convention is generally used in problems with bistatic geometries or with multiple scattering. The reason is that the directions of the vertical and horizontal unit vectors are always defined with

respect to the direction of the wave propagation. Thus, this convention is also known as wave coordinates. The BSA convention is more commonly used in communications and radar because the unit vectors are defined with respect to the antenna polarization. The antenna is equally characterized in transmission and reception, so the unit vectors of the incident and scattered wave, when defined according to the BSA, are identical in the backscattering case. The BSA convention is also known as antenna coordinates.

2.2.2. COHERENCY AND COVARIANCE MATRICES

If the target vector is defined using the Pauli matrices basis [3], [10], [19], [42], [46], the result is called the coherency matrix $[T]$; whereas if ψ is used, the new matrix is known as the covariance matrix, $[G]$. Then following this definition, these matrices

$$[\mathbf{T}] = \mathbf{k}_P \cdot \mathbf{k}_P^{*T} = [T]^{*T} \tag{2.30}$$

$$[\mathbf{C}] = \mathbf{k}_L \cdot \mathbf{k}_L^{*T} = [C]^{*T} \tag{2.31}$$

Both matrices are related by the transformation

$$[C] = [A]^{*T}[T]\cdot[A] \tag{2.32}$$

where in

$$[A] = \frac{1}{2}\begin{bmatrix} 1 & 0 & 0 & 1 \\ 1 & 0 & 0 & -1 \\ 0 & 1 & 1 & 0 \\ 0 & j & -j & 0 \end{bmatrix} \tag{2.33}$$

These matrices share some interesting properties: both are hermitian positive semi-definite and have the same eigienvalues. The eigenvectors information $[T]$ and $[G]$ form orthonormal sets of vectors that can be used as a suitable basis for the vectorization operation detailed previously.

For future use, it is useful at this point to present a parameterization of the coherency matrix, that reads;

$$[T]=\begin{bmatrix} A_0+A & C-jD & H+jG & I-jJ \\ C+jD & B_0+B & E+jF & K-jL \\ H-jG & E-jF & B_0-B & M+jN \\ I+jJ & K+jL & M-jN & A_0-A \end{bmatrix} \tag{2.34}$$

The important case of backscattering from a reciprocal target is expressed in the following for the coherency matrix. Two cases are distinguished, depending on the polarization convention.

In case of FSA, the target vector results;

$$k_p=\frac{1}{2}\begin{bmatrix} a+d \\ a-d \\ 0 \\ 2jb \end{bmatrix} \tag{2.35}$$

and the coherency matrix is

$$[T]_{FSA}=\begin{bmatrix} A_0+A & C-jD & 0 & I-jJ \\ C+jD & B_0+B & 0 & K-jL \\ 0 & 0 & 0 & 0 \\ I+jJ & K+jL & M-jN & A_0-A \end{bmatrix} \tag{2.36}$$

Since there are only 9 nonzero elements, a reduced 3×3 coherency matrix can be defined as;

$$[T]_{FSA}=\begin{bmatrix} A_0+A & C-jD & I-jJ \\ C+jD & B_0+B & K-jL \\ I+jJ & K+jL & A_0-A \end{bmatrix} \tag{2.37}$$

In contrast, when the BSA convention is used, the target vector is;

$$k_p=\frac{1}{\sqrt{2}}\begin{bmatrix} a+e \\ a-e \\ 2b \\ 0 \end{bmatrix} \tag{2.38}$$

and the coherency matrix yields;

$$[T]_{BSA} = \begin{bmatrix} A_0 + A & C - jD & H + jG & 0 \\ C + jD & B_0 + B & E + jF & 0 \\ H - jG & E - jF & B_0 - B & 0 \\ 0 & 0 & 0 & 0 \end{bmatrix} \tag{2.39}$$

Again, a reduced 3×3 coherency matrix can be defined as;

$$[T_3]_{BSA} = \begin{bmatrix} A_0 + A & C - jD & H + jG \\ C + jD & B_0 + B & E + jF \\ H - jG & E - jF & B_0 - B \end{bmatrix} \tag{2.40}$$

As stated before, the parameterization in Eq.2.32 and successive equations will be useful in next section for stating a relationship between the coherency and covariance matrices and other important matrices. At this point, however, it is necessary to present an explicit expression of $[T]$ and $[C]$ for the backscattering case, with reciprocity, and by means of the BSA convention. This specific situation is in turn the most common in radar polarimetry and, hence, will always be used in this thesis when dealing with target decomposition applications. By substituting the reduced target vectors into the definitions of both coherency and covariance matrices Eqs.230-231, the new simplified matrices are;

$$[T_3]_{BSA} = \frac{1}{2}\begin{bmatrix} |S_{VV} + S_{HH}|^2 & (S_{VV} + S_{HH})(S_{VV} - S_{HH})^* & 2(S_{VV} + S_{HH})^* \\ (S_{VV} - S_{HH})(S_{VV} + S_{HH})^* & |S_{VV} - S_{HH}|^2 & 2(S_{VV} - S_{HH})^* \\ 2S_{VH}(S_{VV} + S_{HH})^* & 2S_{VH}(S_{VV} - S_{HH})^* & 4|S_{VH}|^2 \end{bmatrix} \tag{2.41}$$

$$[C_3]_{BSA} = \frac{1}{2}\begin{bmatrix} |S_{VV}|^2 & \sqrt{2}S_{VV} \cdot S_{VH}^* & S_{VV} \cdot S_{HH}^* \\ \sqrt{2}S_{VH} \cdot S_{VV}^* & 2|S_{VH}|^2 & \sqrt{2}S_{VH} \cdot S_{HH}^* \\ S_{HH} \cdot S_{VV}^* & \sqrt{2}S_{HH} \cdot S_{VH}^* & |S_{HH}|^2 \end{bmatrix} \tag{2.42}$$

and are related by the following matrix products

$$[C_3]_{BSA} = \frac{1}{2}[A_3]^T [T_3]_{BSA}[A_3] \qquad [T_3]_{BSA} = \frac{1}{2}[A_3]\cdot[C_3]_{BSA}[A_3]^T \qquad (2.43)$$

where

$$[A_3] = \begin{bmatrix} 1 & 0 & 1 \\ 1 & 0 & -1 \\ 0 & \sqrt{2} & 0 \end{bmatrix} \qquad \text{and} \qquad [A_3]^T = \begin{bmatrix} 1 & 1 & 0 \\ 0 & 0 & \sqrt{-12} \\ 1 & -1 & 0 \end{bmatrix} \qquad (2.44)$$

2.2.3. MUELLER AND KENNAUGH MATRICES

In the previous sections we have seen the scattering matrix characterizes a scatterer, from the polarization point of view, by providing a relationship between the incident and scattered field vectors. In an analogous way, a matrix could be defined for relating the Stokes vector of the incident and scattered fields. This new matrix is known as Mueller matrix, and is defined in the following.

The Mueller matrix is a 4×4 real matrix, that can be expressed in terms of the elements of the coherency matrix according to parameterization in Eq.2.34. For a general case, the Mueller matrix has the form

$$[M] = \begin{bmatrix} A_0 + B_0 & C + N & H + L & F + I \\ C - N & A + B & E + J & G + K \\ H - L & E - J & A - B & D + M \\ I - F & K - G & M - D & A_0 - B_0 \end{bmatrix} \qquad (2.45)$$

If the backscatter case with reciprocity is examined, the resulting Mueller matrices for both polarization conventions are

$$[M]_{FSA} = \begin{bmatrix} A_0 + B_0 & C & L & I \\ C & A + B_0 & J & K \\ -L & -J & A - B_0 & D \\ I & K & -D & A_0 - B_0 \end{bmatrix} \qquad (2.46)$$

and

$$[M]_{BSA} = \begin{bmatrix} A_0 + B_0 & C & H & F \\ C & A_0 + B & E & G \\ H & E & A_0 - B & D \\ -F & -G & -D & A_0 - B_0 \end{bmatrix} \qquad (2.47)$$

The new matrix is therefore usually known as the Kennaugh matrix $[K]$, and in the backscattering case with reciprocity yields;

$$[K]=\begin{bmatrix} A_0+B_0 & C & H & F \\ C & A_0+B & E & G \\ H & E & A_0-B & D \\ F & G & D & B_0-A_0 \end{bmatrix} \tag{2.48}$$

Thus the Kennaugh matrix is symmetric under the BSA convention, whereas the Mueller matrices are not symmetric. As already explained, the Mueller matrix and the Kennaugh matrix do not differ so much; only the elements of one row have opposite signs. The key point to avoid any confusion is the origin of their definition, since the two matrices corresponds to two distinct operations: Mueller matrix relates the scattered field to the incident fields by using the Stokes formalism, whereas the Kennaugh matrix provides the received power, given the receiving antenna polarization characteristics. It seemed important to clarify their definitions in order to ease a possible comparison between results obtained by the coherency matrix and those from the Mueller or Kennaugh matrices.

2.3. TARGET DECOMPOSITION THEORY

As explained in section 1.2, the main point of this thesis is the extraction of physical information about the target by means of an analysis of the polarization matrices that describe the target. This analysis is known as target decomposition.

2.3.1. SCATTERING BY RANDOM MEDIA. PARTIAL POLARIZATION

In section 2.2 the description of the polarization characteristics of a scatterer has been carried out by using several matrices, and the relation between all these matrices has also been shown. The common point of this polarization descriptors presented so far is that all of them have been defined by considering the polarization of the wave to behave in a deterministic manner, i.e. the wave is monochromatic, and ω, a_v, a_h and $\Delta\varphi$ are deterministic or constant. Such wave is said to be completely

polarized. However, the wave transmitted by radar can be considered completely polarized in most cases, the field scattered by any natural scatterer is seldom completely polarized when observed as a function of time or spatial position. This loss of polarization is due to randomness of the illuminated scene, unavoidable noise. The extreme case is that of a wave whose polarization state changes in a totally random way, so that is equally probable to find any possible polarization state from a single observation. Such a wave is known as unpolarized. The common situation is between the two extremes, and the wave is said to be partially polarized.

One of the most widely used polarization descriptor of a wave is based on the Stokes vector. For radar scattering from a natural scene, the electric field components are random variables, and averaging must be performed to express the polarimetric information of the wave. In the case of the Stokes vector, the averaging is incoherent, since the elements of such a vector are defined as intensities. The Stokes vector of a partially polarized wave is defined as;

$$\langle \mathbf{g} \rangle = \begin{bmatrix} \langle \mathbf{I} \rangle \\ \langle \mathbf{Q} \rangle \\ \langle \mathbf{U} \rangle \\ \langle \mathbf{V} \rangle \end{bmatrix} = \begin{bmatrix} \langle |\mathbf{E}_V|^2 \rangle + \langle |\mathbf{E}_H|^2 \rangle \\ \langle |\mathbf{E}_V|^2 \rangle - \langle |\mathbf{E}_H|^2 \rangle \\ \langle 2\Re |\mathbf{E}_V \mathbf{E}_H^*| \rangle \\ -\langle 2\Im |\mathbf{E}_V \mathbf{E}_H^*| \rangle \end{bmatrix} = \begin{bmatrix} \langle a_V^2 \rangle + \langle a_H^2 \rangle \\ \langle a_V^2 \rangle - \langle a_H^2 \rangle \\ \langle 2 a_V a_H \cos \Delta\varphi \rangle \\ \langle 2 a_V a_H \sin \Delta\varphi \rangle \end{bmatrix} \tag{2.49}$$

where $\langle \cdot \rangle$ denotes the ensemble averaging over the available samples. For example;

$$\langle \mathbf{I} \rangle = \frac{1}{N} \sum_{n=1}^{N} \mathbf{I}_n \tag{2.50}$$

where in $\mathbf{I}_n$ is the total intensity measured in the *n*-th individual measurements.

For an unpolarized wave, $\langle a_V^2 \rangle = \langle a_H^2 \rangle$ and $\mathbf{E}_V$ and $\mathbf{E}_H$ are uncorrelated, thus leading to an averaged Stokes vector with only one zero element, I since $\mathbf{Q} = \mathbf{U} = \mathbf{V} = 0$ for a partially polarized case, the equality in Eq.2.24 becomes

$$\mathbf{I}^2 \geq \mathbf{Q}^2 + \mathbf{U}^2 + \mathbf{V}^2 \tag{2.51}$$

and the degree of polarization of a wave is defined as

$$m = \frac{polarized \cdot power}{Total \cdot power} = \frac{\sqrt{\mathbf{Q}^2 + \mathbf{U}^2 + \mathbf{V}^2}}{\mathbf{I}}, \qquad 0 \le m \le 1 \tag{2.52}$$

In the same way as the polarization of the wave can be described with the average Stokes vector, the polarization characteristics of a scatterer can be presented by an average matrix. The averaging can be performed in two alternative ways; coherently and incoherently. Coherent averaging is suitable to be applied, by definition, to the scattering matrix, whereas the incoherent averaging is appropriate for the other matrix descriptors defined in Mueller, Kennaugh, coherency and covariance matrices. Following the final objective of target decomposition theories, to decompose or express such an average matrix into a sum of matrices representing independent elements with associated physical mechanisms, there have been different approaches in the literature. The Huynen type decompositions attempt the extraction of a single scattering matrix from an incoherent averaged matrix, and the remainder is assigned to a distributed target or a "noise" contribution, but separation into single scattering plus noise is not appropriate for many natural targets. Finally, in contrast, the goal of the eigenvector based target decomposition analysis is to present the averaged data as a summation of single scattering mechanisms, and this separation is well founded in the underlying mathematical properties of any eigenvalue approach.

2.3.2. EIGENVECTOR DECOMPOSITION OF THE COHERENCY MATRIX

Let us assume that we have a measured coherency matrix, obtained after an ensemble averaging, $\langle |T| \rangle$, and defined according to Eq.2.30 and Eq2.41, from a scene with reciprocity and in the backscatter direction;

$$\langle [T] \rangle = \left\langle \mathbf{k}_{3P} \cdot \mathbf{k}_{3P}^{*T} \right\rangle \tag{2.53}$$

Then, the eigenvector-based decomposition states that the coherency matrix can be written in the form;

$$\langle [T] \rangle = [U_3][\Sigma][U_3]^{-1} \tag{2.54}$$

where

$$[\Sigma] = \begin{bmatrix} \lambda_1 & 0 & 0 \\ 0 & \lambda_2 & 0 \\ 0 & 0 & \lambda_3 \end{bmatrix} \tag{2.55}$$

is a 3×3 diagonal matrix with positive real elements, $\lambda_1 \geq \lambda_2 \geq \lambda_3 \geq 0$, which are the eigenvalues of the coherency matrix; and

$$[U_3] = [e_1 e_2 e_3] = \begin{bmatrix} \cos\alpha_1 & \cos\alpha_2 & \cos\alpha_3 \\ \sin\alpha_1 \cos\beta_1 e^{j\delta_1} & \sin\alpha_2 \cos\beta_2 e^{j\delta_2} & \sin\alpha_3 \cos\beta_3 e^{j\delta_3} \\ \sin\alpha_1 \cos\beta_1 e^{j\gamma_1} & \sin\alpha_2 \cos\beta_2 e^{j\gamma_2} & \sin\alpha_3 \cos\beta_3 e^{j\gamma_3} \end{bmatrix} \tag{2.56}$$

U_3 is a 3×3 matrix whose columns are the eigenvectors of the coherency matrix; e_1, e_2 and e_3.

Equivalently, we can express the coherency matrix as a linear combination of the outer products of the eigenvectors. The weights of this linear combination are the eigenvalues;

$$\langle |T| \rangle = \sum_{i=1}^{3} \lambda_i e_i e_i^{*T} \tag{2.57}$$

The interpretation of Eq.2.57 is that the coherency matrix can be decomposed as a weighted sum of three scattering mechanisms.

2.3.2.1. SYMMETRIES

Symmetry assumptions about the distribution of the elementary scattering centers in such partial scatterers leads to a simplification of the scattering problem and allows quantitative conclusions about their scattering behavior [2], [48], [49]. If their scattering matrix of a particular position and a particular direction are known, then the scattering matrix of its mirrored or rotated image in certain symmetrical positions are also known. Van de Hulst was the first one formulating symmetry properties of the scatterer and implementing it on the Mueller matrix.

- Reflection Symmetry

The first case is a distributed target that have one plane of symmetry containing the line of sight (LOS). This implies that any scatterer P located at one side of the plane characterized by a scattering matrix/vector

$$[S_P]=\begin{bmatrix} S_{HH} & S_{XX} \\ S_{XX} & S_{VV} \end{bmatrix} \quad \text{and} \quad \bar{k}_P = \frac{1}{\sqrt{2}}[S_{HH}+S_{VV} \quad S_{HH}-S_{VV} \quad 2S_{XX}]^T \qquad (2.58)$$

there is a mirrored scatterer Q at the other side of the plane with scattering matrix/vector given by [21]

$$[S_Q]=\begin{bmatrix} S_{HH} & -S_{XX} \\ -S_{XX} & S_{VV} \end{bmatrix} \text{ and } \bar{\mathbf{k}}_Q = \frac{1}{\sqrt{2}}[S_{HH}+S_{VV} \quad S_{HH}-S_{VV} \quad 2S_{XX}]^T \qquad (2.59)$$

$[S_P]$ and $[S_Q]$ differ only in the sign of the off-diagonal elements. Accordingly, the coherency matrix $[T]$ of such a medium can be written as the superposition of the coherency matrices for both symmetrical components.

$$[T]=[T_P]+[T_Q] \qquad (2.60)$$

The coherency matrix can be completely described by 5 parameters corresponding to the three real elements on the diagonal and remaining a complex cross-correlation between the co-polarized channels.

- Rotation Symmetry

The second special case is that of a medium with rotation symmetry, the coherency matrix is invariant when the target (or alternatively the antenna) is rotated about the line of sight (LOS).

$$[T(\theta)]=[U_3^R(\theta)]\cdot[T]\cdot[U_3^R(\theta)]^{-1} \qquad (2.61)$$

where

$$[U_3(\theta)] = \begin{bmatrix} 1 & 0 & 0 \\ 0 & \cos 2\theta & \sin 2\theta \\ 0 & -\sin 2\theta & \cos 2\theta \end{bmatrix} \text{ and}$$

$$[U_3(\theta)]^{-1} = [U_3]^T = \begin{bmatrix} 1 & 0 & 0 \\ 0 & \cos 2\theta & -\sin 2\theta \\ 0 & \sin 2\theta & \cos 2\theta \end{bmatrix} \quad (2.62)$$

2.3.2.2. PARAMETERIZATION OF THE EIGENVECTOR DECOMPOSITION

Having formulated the eigenvector decomposition of the coherency matrix, the underlying physical meaning of the resulting parameters is studied in this section from the point of view of the extraction of information about the target.

The idea of the eigenvector approach is to use the diagonalisation of the coherency matrix $[T]$ of a distributed scatterer, in order to decompose it into a non-coherent sum of three independent coherency matrices $[T_i]$.

There are important physical features arising directly from the eigenvalues of the coherency matrix. The first is the polarimetric scattering entropy H defined by using the logarithmic sum of the eigenvalues of $[T]$.

$$H = -\sum_{i=1}^{3} P_i \log_3 P_i \quad (2.63)$$

where

$$P_i = \frac{\lambda_i}{\sum_{i=1}^{3} \lambda_i} \quad (2.64)$$

are the probabilities of each eigenvalue, and the entropy is defined in the range $0 \le H \le 1$. Also $\sum_{i=1}^{3} P_i = 1$;

- Roll-Invariant parameters

Some parameters related to the randomness of the process and scattering mechanisms that are present in the scene can be retrieved from the coherency matrix. An important question arises at this point; Are these retrieved parameters dependent

on the relative orientation of the antenna with respect to the target? If this was the situation, the scattering mechanism that we extract would depend on the orientation, thus not being reliable. For example, think about a target whose dominant scattering mechanism is dipole-like, but when it is rotated about the LOS it becomes a surface-like or a dihedral scattering mechanism.

In this following we will analyze which of the parameters obtained from the eigenvector decomposition are independent of the orientation of the target about the LOS. These parameters will be called roll-invariant. In this way, the coherency matrix of a target rotated by angle θ about the LOS is

$$[T(\theta)] = [U_3(\theta)] \cdot [T] \cdot [U_3(\theta)]^{-1} \tag{2.65}$$

If we substitute the eigenvalue decomposition of the original coherency matrix Eq.2.53 into Eq.2.65, it yields;

$$\langle [T(\theta)] \rangle = [U_3^R(\theta)] \langle [T] \rangle [U_3^R(\theta)]^{-1} = [U_3^R(\theta)] \cdot [U_3] \cdot [\Sigma] \cdot [U_3]^{-1} [U_3^R(\theta)]^{-1} \tag{2.66}$$

$$[U_3(\theta)] = \begin{bmatrix} \cos\alpha_1 & \cos\alpha_2 & \cos\alpha_3 \\ \sin\alpha_1 \cos\beta_1 e^{j\delta_1} & \sin\alpha_2 \cos\beta_2 e^{j\delta_2} & \sin\alpha_3 \cos\beta_3 e^{j\delta_3} \\ \sin\alpha_1 \cos\beta_1 e^{j\gamma_1} & \sin\alpha_2 \cos\beta_2 e^{j\gamma_2} & \sin\alpha_3 \cos\beta_3 e^{j\gamma_3} \end{bmatrix} \tag{2.67}$$

The eigenvalues are the same as before, so any parameter derived directly from them is roll-invariant. For example, the entropy and probabilities previously defined, and other two parameters widely used, namely; total power and anisotropy.

The total power TP is the trace or sum of the eigenvalues, and represents the total power scattered by the target and collected by an orthogonally polarized antenna pair.

$$TP = \lambda_1 + \lambda_2 + \lambda_3 \tag{2.68}$$

The anisotropy A, is defined from the ratio between eigenvalues and complements the target entropy.

$$A = \frac{P_2 - P_3}{P_2 + P_3} = \frac{\lambda_2 - \lambda_3}{\lambda_2 + \lambda_3} \tag{2.69}$$

Eq.2.67 says that the three scattering mechanisms α_i are the same as before the rotation. Hence, the dominant scattering mechanism $\overline{\alpha}$ is roll-invariant. This fact is important when we observe a scene with radar and want to retrieve the present scattering mechanisms, since we do not have to take care about the orientation of the targets about the LOS in order to know their behavior.

CHAPTER 3

POLARIMETRIC GPR SYSTEM AND ITS EVALUATION

The key point of polarimetric GPR data is that measurements are carried out at multiple frequencies and polarizations. The obtained multidimensional information allows the identification of different scatterers via discrimination of different scattering mechanisms. The polarization information contained in the backscattered wave is directly related to the geometrical structure of the scatterer, its orientation and even more important, its geophysical properties such as surface roughness, soil moisture, etc. A backscattered wave will show a different polarization state due to depolarization effects occurring when a wave travels through a certain medium.

3.1. PRINCIPLES OF POLARIMETRIC GPR SYSTEMS

Polarimetric GPR systems consists of a Vector Network Analyzer (VNA), a transmitter and a receiver Vivaldi antennas, an antenna positioner unit and a PC based control unit. The network analyzer transmits the frequency domain complex signal which has real and imaginary parts and receives the complex reflected signal at different frequencies. Fig.3.1.1 and Fig.3.1.2 show the sketch map and a photo of a polarimetric GPR system.

A set of four wideband linearly polarized antennas is used, two for transmit and two for receive, each of the two being orthogonally polarized. Vivaldi antennas are employed in this polarimetric GPR system. The Vivaldi antenna is based on a non-resonant traveling-wave structure similar to the horn antenna, but is fabricated as a printed circuit antenna. The wave guiding structure is printed slot-line. The Vivaldi

antenna has good potential for applications that require broadband end-fire radiation from elements embedded in a truncated ground plane. Return loss of the Vivaldi antenna used for the evaluation of our system is shown in Fig.3.1.3. Return loss is defined as the loss of the reflected power. Due to impedance mismatches, a part of the transmited signal is reflected and travels in the opposite direction. Return loss measures the attenuation of this undesired signal. Therefore, the bigger the value of the system's return loss is the better.

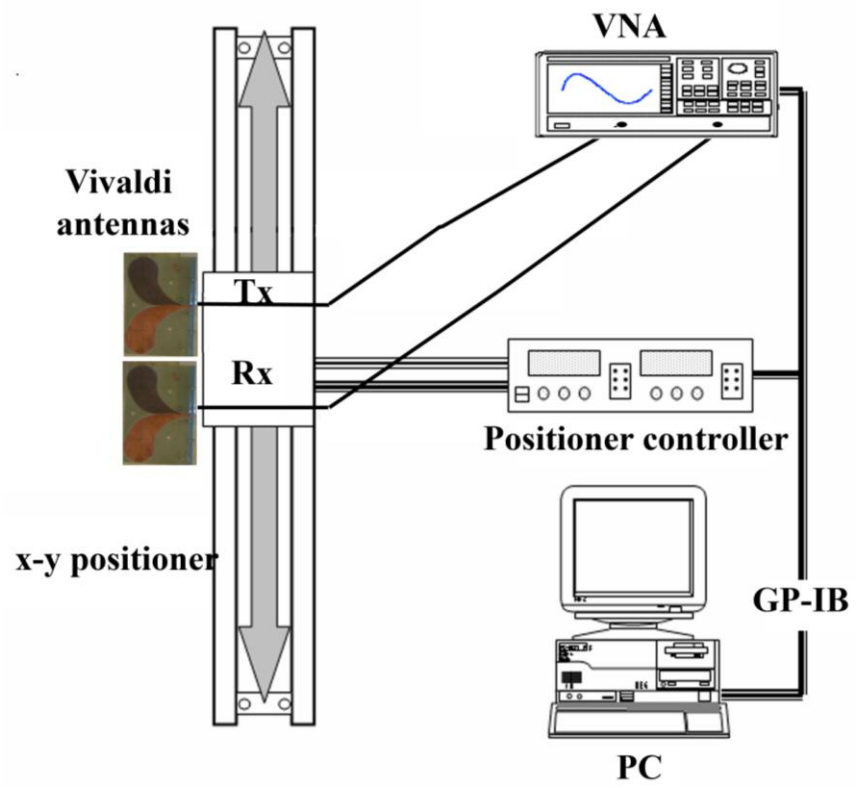

Fig.3.1.1. Sketch map of polarimetric GPR system

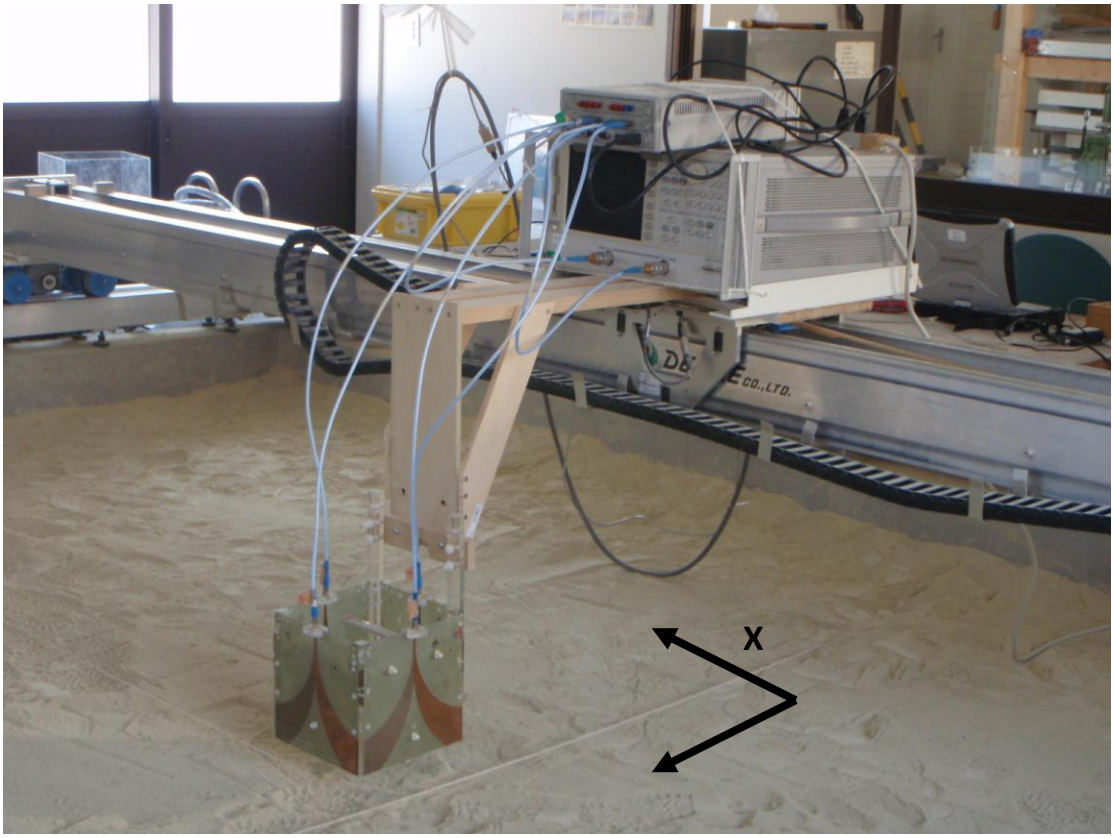

Fig.3.1.2. Polarimetric GPR system

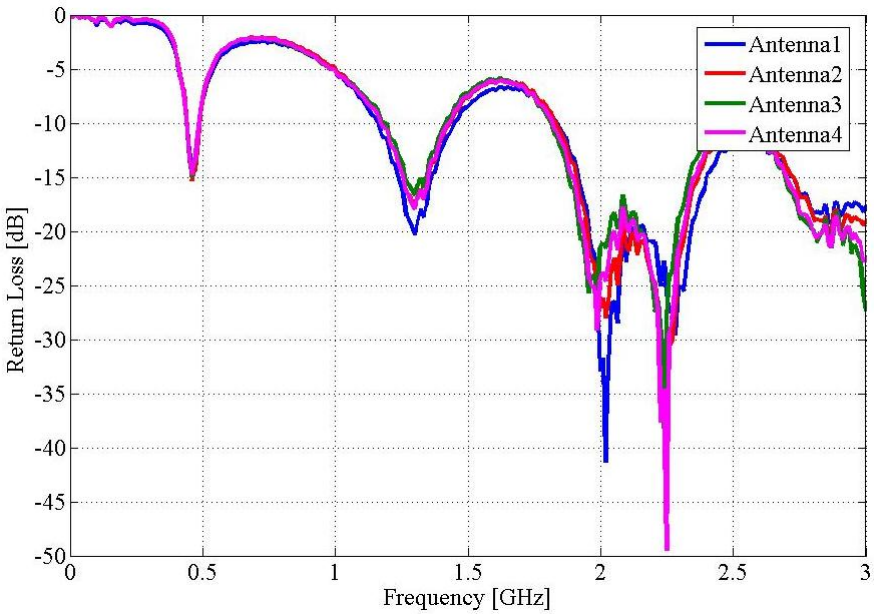

Fig.3.2.3. Return loss of Vivaldi antenna

The system sequentially transmits orthogonal polarizations, while the receiver simultaneously measures both reflected polarizations. The transmitting polarization switching rate is high enough to ensure that the successive pulses are correlated,

thereby appearing as if taken from the same location. Reflected data from all four linear combinations of transmitting and receiving polarizations are then coherently processed to yield the polarimetric image of the target.

3.2. POLARIMETRIC PERFORMANCE EVALUATION

For evaluating the polarimetric GPR system, we have performed several measurements to test the Vivaldi antenna using a linear metal wire.

3.2.1. VERIFICATION MEASUREMENT USING A METAL WIRE ORIENTED AT DIFFERENT ORIENTATION ANGLES

Verification measurements are used for monitoring simple objects in an anechoic chamber under ideal conditions. The system operates at frequencies between 30 kHz and 3 GHz. For the following test, we used as a reference target a 1m long metal wire with 6cm of diameter. The Vivaldi antennas were located at a height of 120cm above the floor. The separation between transmitter and receiver Vivaldi antennas was 20cm. Firstly, the data was taken when there was no target put in the anechoic chamber. Then, all the data were taken with the target placed in an anechoic chamber at different orientation angles, ranging from 0° to 90° with respect to the antenna system. The polarimetric GPR system measures the amplitude and phase of backscattered signals in four combinations of the linear receive and transmit polarizations, such as HH (horizontal-horizontal polarization), HV (horizontal-vertical polarization), VH and VV. These signals form the complex scattering matrix which relates the scattered to the incident electric fields.

A sketch map of the experiment is shown in Fig.3.2.1. Using this system, we examine the radar scattering behavior with the different orientation angles of the target.

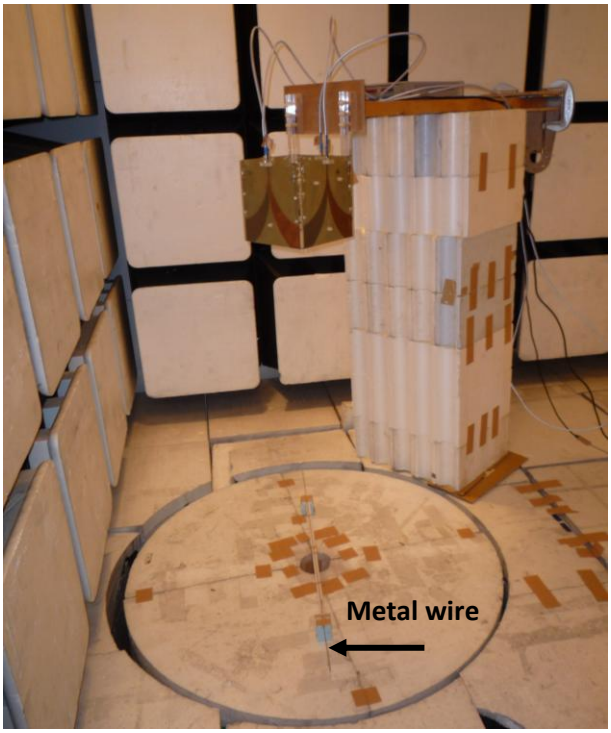

Fig.3.2.1. Experiment setup in anechoic-chamber

The transmitted signal was a predefined signal with identical phase and amplitude, the receiving signal being also a complex signal with identical phase and amplitude. Fig.3.2.2 shows the frequency spectrum in dB scale when the radar antennas were at different polarization states.

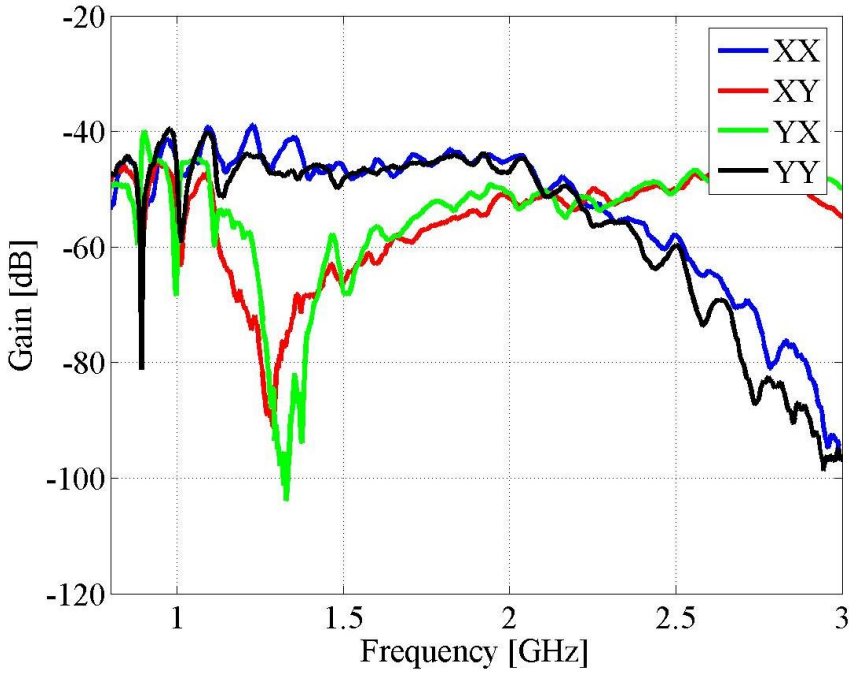

Fig.3.2.2. Power spectrum of GPR data in different polarization state

The frequency domain complex data is received by the vector network analyzer, which then sends it to the computer via a GP-IB cable using a software coded in Hewlett-Packard Visual Engineering Environment (HP-VEE). This frequency domain data was converted into a time domain signal by IFFT and showed in the computer display in real time. An example is shown in Fig.3.2.3.

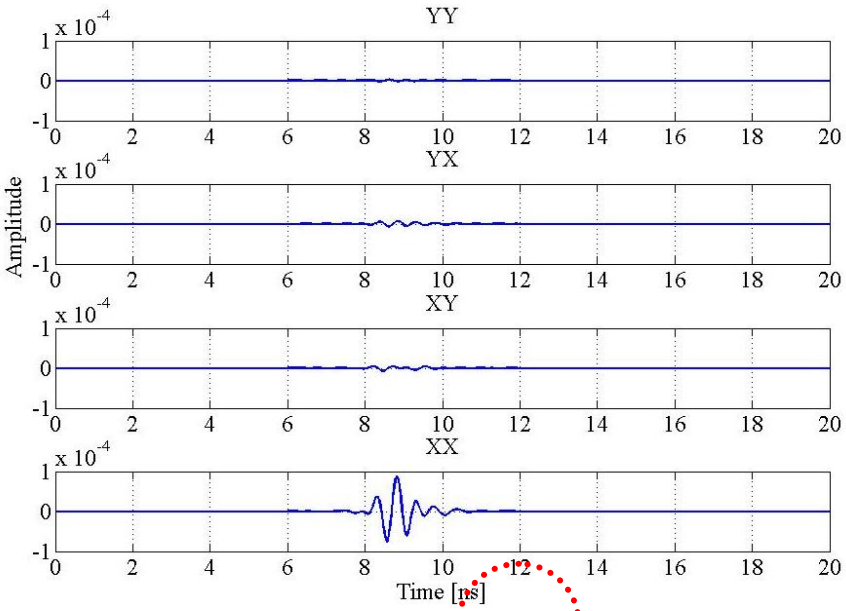

Fig.3.2.3. GPR time domain data in different polarization states

In general, the polarimetric radar response of a surface-laid or buried object depends on the orientation of the objects with respect to the transmitting and receiving antennas.

Fig.3.2.4 and Fig.3.2.5 shows the results for the metal wire given the target orientations of 0 to 90 degrees with respect to the antenna system. The scattering coefficients change with target orientation and a strong cross-polarization component is observed when the target is oriented at 45 degrees. From these results, we see that co-polarization scattering amplitude gives quite a good agreement compared to cross polarization amplitude at all orientation angles.

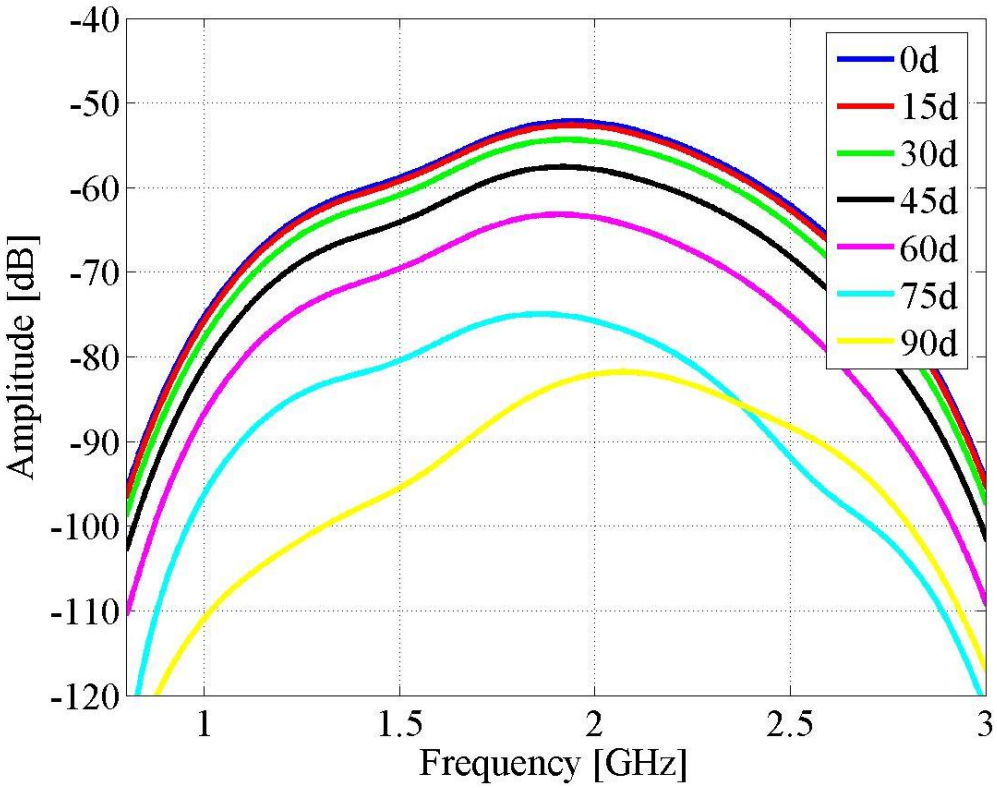

(a) XX polarization

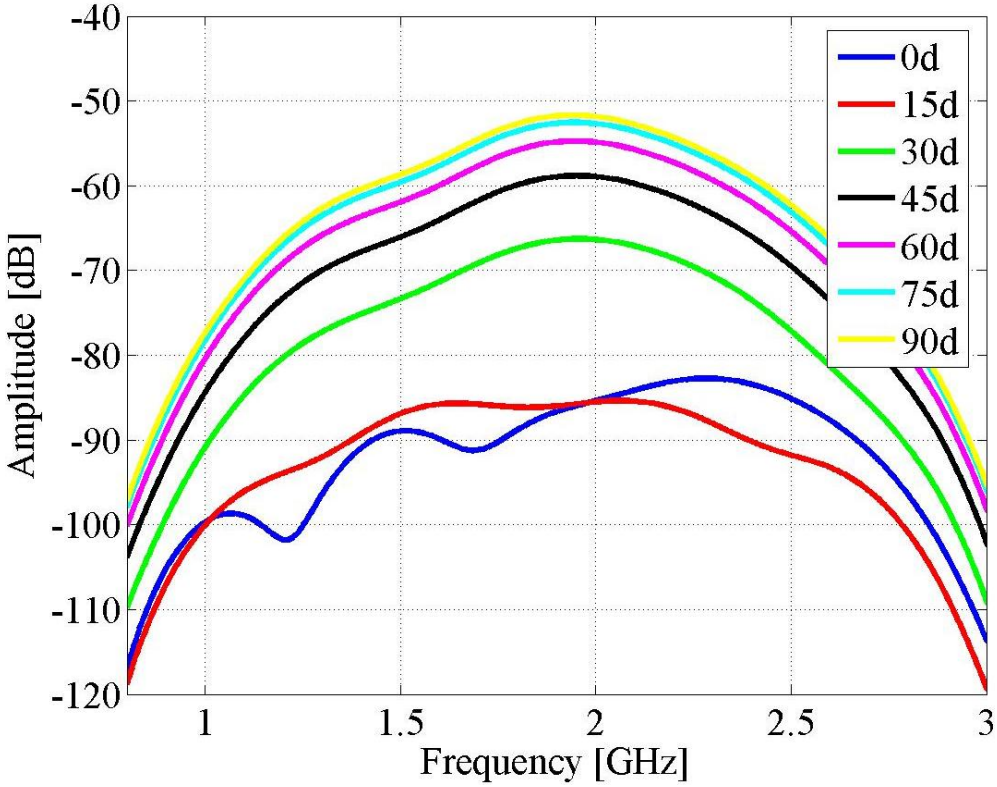

(b) YY polarization

Fig.3.3.4. Scattering coefficient of co-polarization state

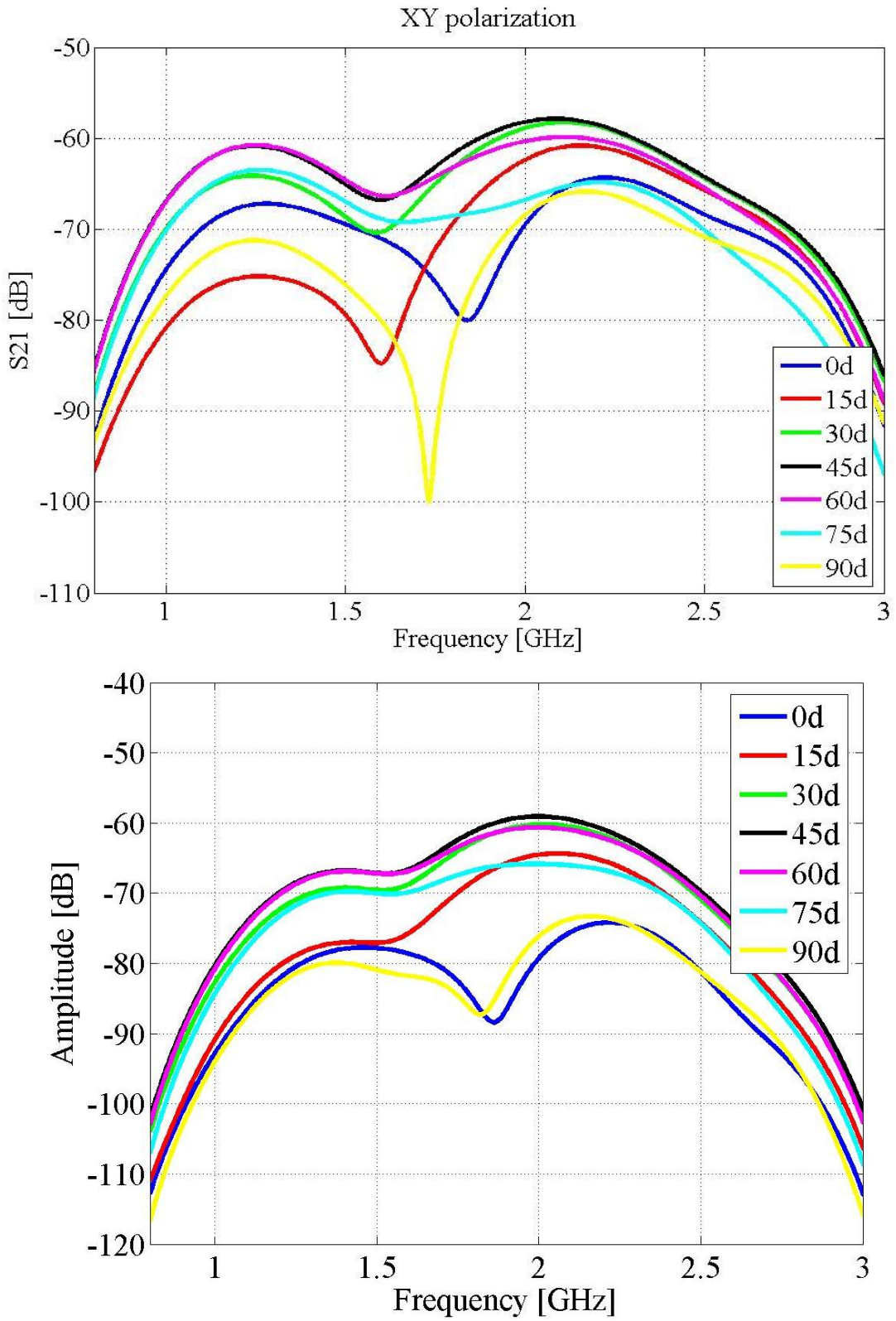

(a) XY polarization

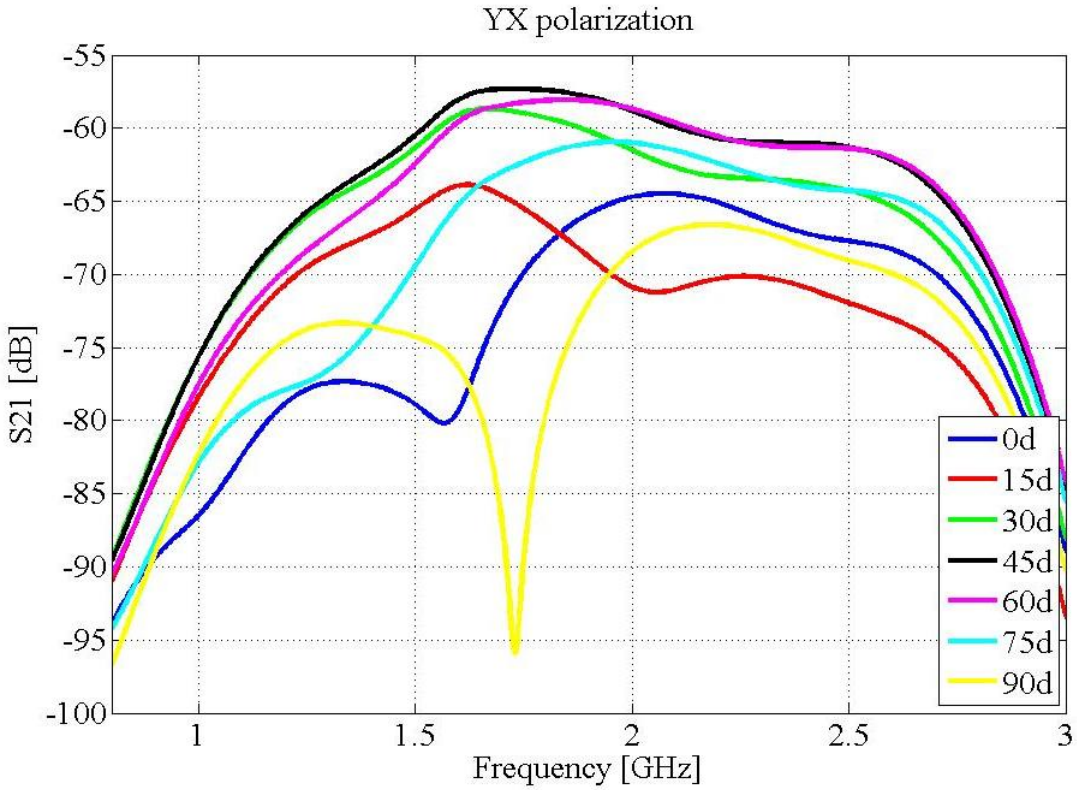

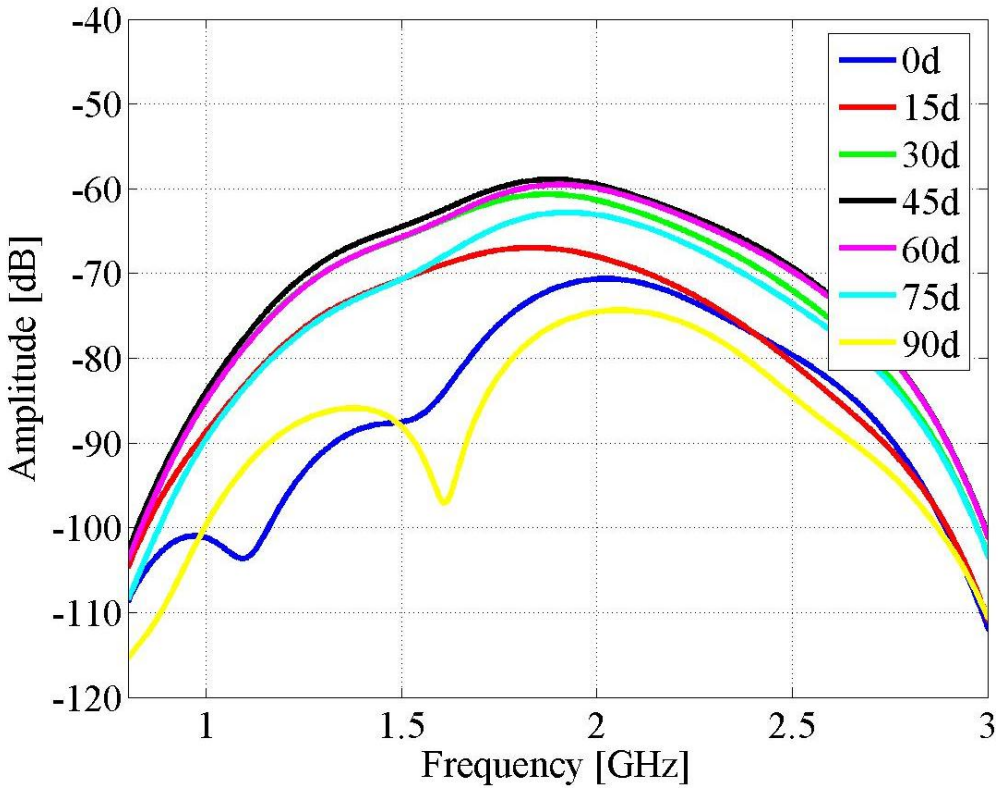

(b) YX polarization

Fig.3.3.5. Scattering coefficient of cross-polarization state

3.3. POLARIMETRIC CALIBRATION

One critical requirement of polarimetric radar systems is the need for calibration. This is because much of the information lies in the ratios of amplitudes and the differences in phase angle between the 4 transmitting and receiving polarization combinations. If the calibration is not sufficiently accurate the scattering mechanism will be misinterpreted and the advantages of using polarization will not be realized.

Knowledge of the scattering matrix is important to extract relevant information about the target. In practice, the channels of a polarimetric radar system are not always perfectly isolated and do not have identical properties; the measurements are contaminated. Therefore, calibration is necessary to get an accurate estimate from the distorted measurement. In recent years, calibration of polarimetric SAR has attracted extensive research. The major focus of such calibration has been on the removal of the effects of radar distortions by employing well characterized calibration targets.

- *Calibration algorithm*

Our Calibration algorithm used three in-scene reflectors based on the exact solution for general targets developed by S.H.Yueh and J.A.Kong [50]. This algorithm is based on modeling the transmitting and receiving ports of the polarimetric radar by two unknown polarization transfer matrices. These transfer matrices are solved in terms of measurements from three independent calibration targets with known scattering matrix. In this model we used the scattering matrices corresponding to three in-scene reciprocal reflectors as shown below. R and T indicate distortion matrices for the receiving and transmitting sub-systems.

$$X = \begin{bmatrix} X_{11} & X_{12} \\ X_{21} & X_{22} \end{bmatrix} = e^{-j\varphi_1} R S_1 T \qquad (1)$$

(Data acquired target oriented at 0 degrees)

$$Y = \begin{bmatrix} Y_{11} & Y_{12} \\ Y_{21} & Y_{22} \end{bmatrix} = e^{-j\varphi_1} RS_2T \qquad (2)$$ (Data acquired target oriented at 90 degrees)

$$Z = \begin{bmatrix} Z_{11} & Z_{12} \\ Z_{21} & Z_{22} \end{bmatrix} = e^{-j\varphi_1} RS_3T \qquad (3)$$ (Data acquired target oriented at 45 degrees)

where, S_1, S_2, S_3 are the three polarization scattering matrices of the calibration targets,

$$S_1 = \begin{bmatrix} 1 & 0 \\ 0 & 0 \end{bmatrix} \quad (4) \qquad S_2 = \begin{bmatrix} 0 & 0 \\ 0 & 1 \end{bmatrix} \quad (5) \qquad S_3 = \begin{bmatrix} 1 & 1 \\ 1 & 1 \end{bmatrix} \quad (6)$$

the matrices T and R account for the mismatch and cross-polarization coupling of the transmitting and receiving ports.

$$R = \begin{bmatrix} R_{11} & R_{12} \\ R_{21} & R_{22} \end{bmatrix} \quad (7) \qquad T = \begin{bmatrix} T_{11} & T_{12} \\ T_{21} & T_{22} \end{bmatrix} \quad (8)$$

The objective of the polarimetric calibration is to solve the normalized quantities of the X, Y and Z matrices. The normalized quantities t_{12}, t_{21}, t_{22}, r_{12}, r_{21} and r_{22} are defined by

$$t_{12} = T_{12}/T_{11} \qquad t_{21} = T_{21}/T_{11} \qquad t_{22} = T_{22}/T_{11}$$
$$r_{12} = R_{12}/R_{11} \qquad r_{21} = R_{21}/R_{11} \qquad r_{22} = R_{22}/R_{11}$$

It is useful to solve them in terms of the backscattering measurements from the three calibration targets. For the case of a H-dipole, V-dipole and inclined dipole, the normalized quantities we calculated are shown below.

$$r_{22} = \frac{c}{d}\frac{Y_{22}}{X_{11}}\frac{X_{11}Z_{21} - X_{21}Z_{11}}{Y_{22}Z_{11} - Y_{12}Z_{21}} \qquad (9) \qquad r_{12} = \frac{Y_{12}}{Y_{22}} r_{22} \qquad (10)$$

$$t_{22} = \frac{c}{d}\frac{Y_{22}}{X_{11}}\frac{X_{11}Z_{12} - X_{12}Z_{11}}{Y_{22}Z_{11} - Y_{22}Z_{12}} \qquad (11) \qquad t_{21} = \frac{Y_{21}}{Y_{22}}t_{22} \qquad (12)$$

Assuming the measured polarization matrix $\lfloor V_{ij} \rfloor$ of a target with scattering matrix S is given as

$$\begin{bmatrix} V_{11} & V_{12} \\ V_{21} & V_{22} \end{bmatrix} = e^{i\phi}\begin{bmatrix} R_{11} & R_{12} \\ R_{21} & R_{22} \end{bmatrix} \cdot \begin{bmatrix} S_{hh} & S_{hv} \\ S_{vh} & S_{vv} \end{bmatrix} \cdot \begin{bmatrix} T_{11} & T_{12} \\ T_{21} & T_{22} \end{bmatrix} \qquad (13)$$

it can be shown that the calibrated scattering matrix elements are given by

$$\begin{bmatrix} S_{hh} \\ S_{hv} \\ S_{vh} \\ S_{vv} \end{bmatrix} = \frac{e^{-j\phi}}{R_{11}T_{11}(r_{22} - r_{12}r_{21})\cdot(t_{22} - t_{12}t_{21})} \begin{bmatrix} r_{22}t_{22} & -r_{22}t_{21} & -r_{12}t_{22} & r_{12}t_{21} \\ -r_{22}t_{12} & r_{22} & r_{12}t_{12} & -r_{12} \\ -r_{21}t_{22} & r_{21}t_{21} & t_{22} & -t_{21} \\ r_{21}t_{12} & -r_{21} & t_{12} & 1 \end{bmatrix} \cdot \begin{bmatrix} V_{11} \\ V_{12} \\ V_{21} \\ V_{22} \end{bmatrix} \qquad (14)$$

where r_{12},r_{21},r_{22},t_{12},t_{21}, and t_{22} have been obtained, in terms of the measurement of the calibration targets, in Eq(9)-Eq(12).

- *Calibration procedure*

In the calibration procedure we consider three measurements. The target was a vertical, horizontal and 45 degrees oriented metal wire. First, we acquired the frequency domain data in different polarization states in an anechoic chamber. Frequency range was 30 kHz-3 GHz. Also we acquired background data, in order to subtract direct coupling and surrounding reflections (antenna support, etc). After the datasets in different polarization states are acquired, they are filtered by a broadband pass filter, with a frequency band from 800MHz to 3GHz, and transformed to time domain by IFFT.

From the time domain data we can see very clear reflections of the target occured from 5.2ns to 9.5ns. Around 12 ns we could observe other reflections probably caused by the floor of the rotation table. Time gating was employed over the time domain data selecting the range in which reflections from the target occurs; then we came back to frequency domain using FFT.

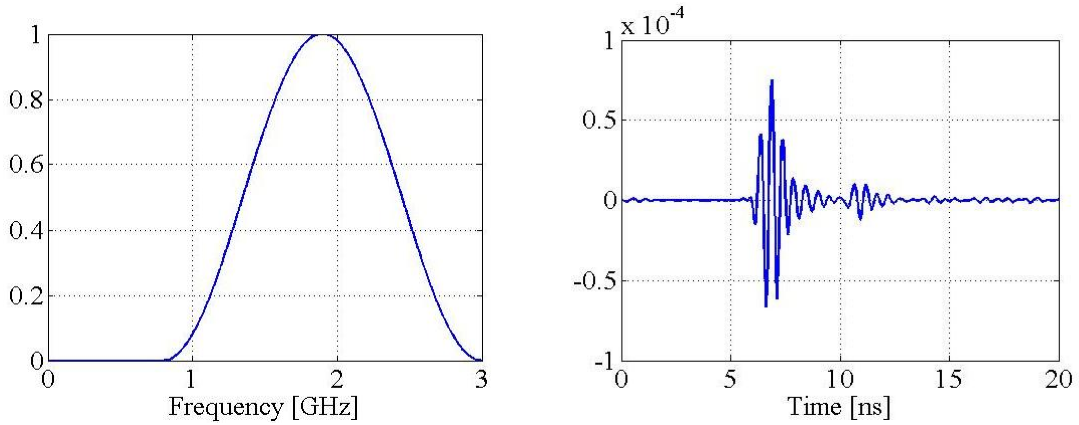

(a) Window function (b) Wave form in TimeDomain

Fig.3.3.1. Waveform of metal wire

Four polarization state datasets were processed using the same procedures. After the processed full polarization data was obtained, calibration coefficients were calculated by formulas 9-14. Fig.3.3.2 shows the scattering coefficients in different frequencies with calibration, without calibration and the theoretical values with a 30 degrees oriented target. We can find the improvements after calibration, especially in the amplitude term. Compared to the theoretical value, the difference was ~2dB in cross polarization state, and ~3dB in co-polarization state. As for the phase, we obtained a cross polarization phase difference of ~20 degrees and co-polarization phase difference of ~16 degrees. In that case, polarimetric calibration might be acceptable.

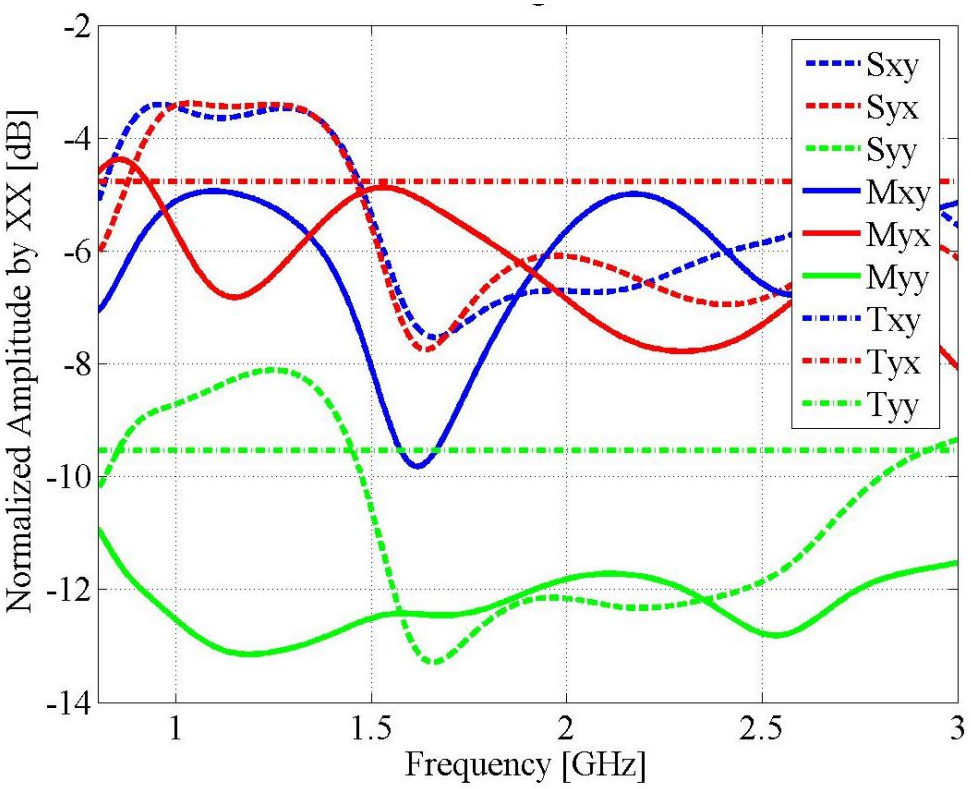

Fig.3.3.2. Calibration results of wire oriented by 30°,

"M" –indicates measured, "S" –calibrated, "T" –theoretical scattering coefficients.

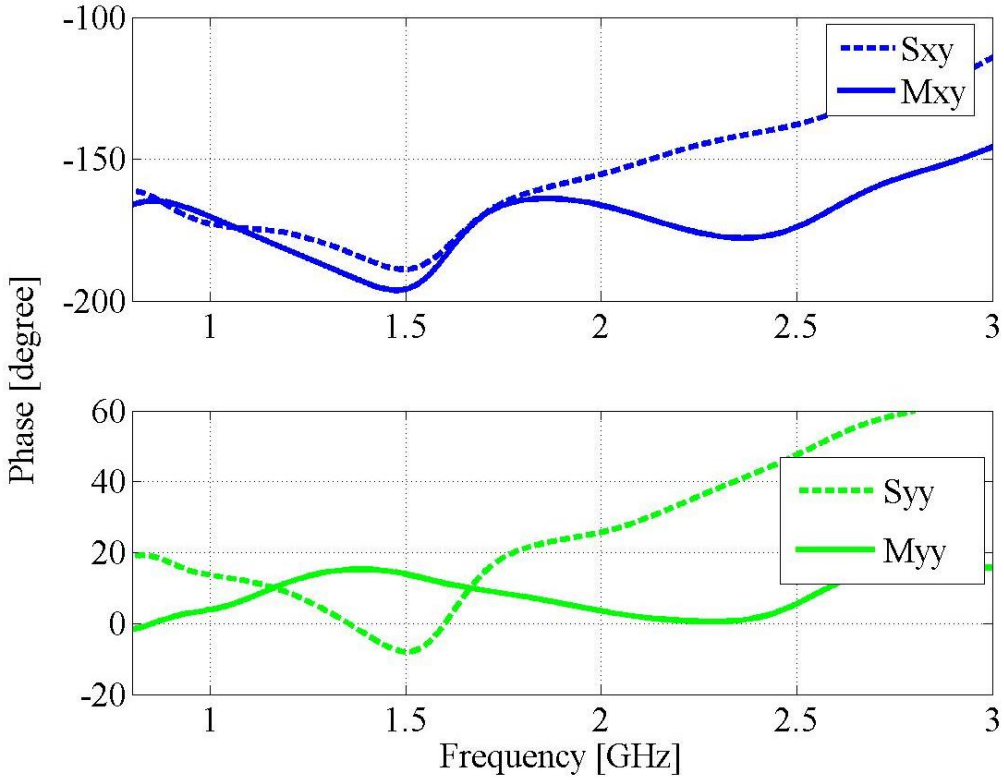

Fig.3.3.3. relative amplitude and phase characteristics of 30° oriented metal wire

Cross-polarization, b) co- polarization state.

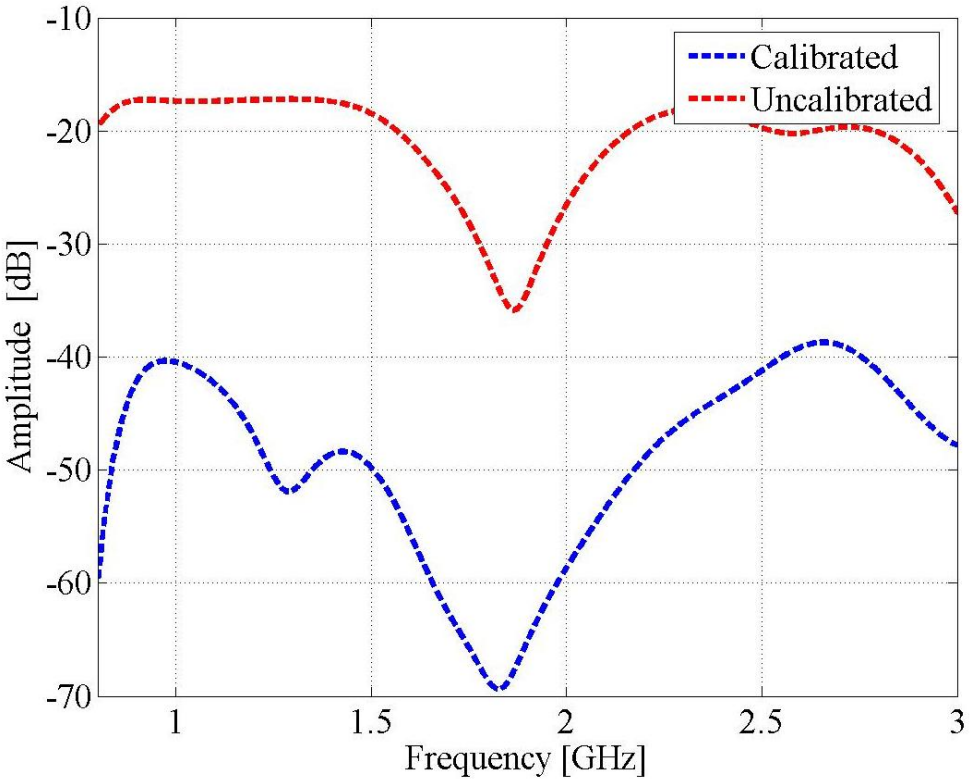

Fig.3.3.4. Cross talk

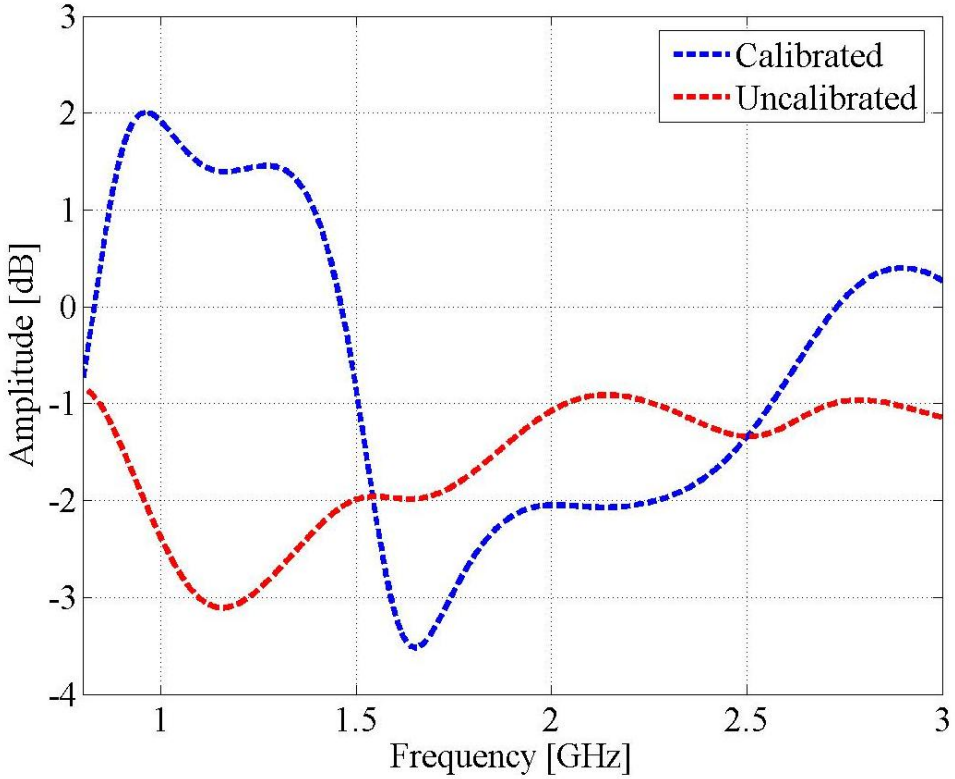

Fig.3.3.5. Gain balance

As evaluations of polarimetric effects, we compared cross-talk and gain balance at the metal wire. Based on the cross-talk and gain balance at oriented wire in both uncalibrated and calibrated data, we can recognize about 20dB improvement in cross talk and 3dB gain balance improvement as well.

3.4. SUMMARY

This chapter has outlined the fundamentals, performance and calibration of our polarimetric GPR system, which was developed by the Sato Laboratory at the Tohoku University, Japan.

The fist part of this chapter concerns the fundamentals and development of a polarimetric GPR system.

polarimetric system. It contains the results of performance test.

In the last part of this chapter, we discussed a polarimetric calibration algorithm and the obtained results from its use. We applied a calibration algorithm using three in-scene reflectors based on the exact solution for general targets developed by S.H.Yueh and J.A.Kong. The goal of the calibration procedure was to solve for unknown receiving and transmitting distortion matrices, R and T, using a set of calibration measurements. The improvement of gain balance and cross talk between H and V channels were confirmed after the calibration using the extracted distortion matrices. Results show how full polarimetric calibration improves the accuracy of scattering measurements.

CHAPTER 4

TEST EXPERIMENTS FOR BURIED OBJECT DETECTION AND DATA ANALYSIS

4.1. INTRODUCTION

An important requirement of any ground penetrating radar system is the ability to identify or determine the shape, size and material composition of buried targets. This is essential to separate the target return echoes from the radar reflections from rocks, subsurface layers, roots and other radar clutter. In order to achieve this it is necessary to relate the target return echo to the physical parameters describing the target [20],[21], [22].

The polarization of the scattered field depends not only on the polarization of the incident field but also on target characteristics such as size, shape, composition and the orientation of the target. Therefore, analysis of the polarimetric target response can provide information about these target characteristics. Moreover, in some cases it is possible to determine the orientation of the target.

4.2. POLARIMETRIC GPR MEASUREMENT SETUP

The radar system consists of a Vector Network Analyzer (VNA), a transmitter and a receiver Vivaldi antennas, an antenna positioner unit, switcher and a PC based control unit. The network analyzer operated in a stepped frequency continuous wave mode, was used to generate the transmitting signal and to detect scattered signals both in amplitude and phase. An antenna positioner was used to do an accurate measurement. In the experiment, the system was operated a frequency range in from 30 kHz to 3

GHz, with 801 scanning sampling point. We used the Vivaldi antenna array, because the Vivaldi antennas are useful for very high frequencies. Advantages of the Vivaldi antennas are suitable broadband characteristics and easy to manufacture. The Vivaldi antenna array was located at a height of 17cm above the sand surface.

4.2.1. EXPERIMENT -1

- *Data acquisition*

A linear wire is one of the fundamental targets in radar polarimetry. A metal wire was buried and placed with a different orientation with respect to survey lines. The measurements were repeated for different target orientations such as 0 or 45 degrees.
A sketch map of the experiment is shown in Fig.4.2.2. Using this system we examined the radar scattering behavior of the different orientation angles of the target.

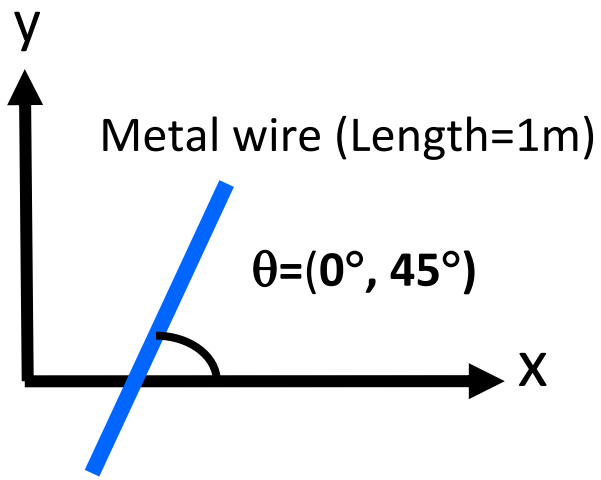

Fig.4.2.2. Sketch map of the experiment setup

Table.4.2.1 offers the measurement parameters for polarimetric GPR. We used a frequency range from 30 kHz to 3 GHz. The size of the survey area was 0.5m x 0.5m and the measurement interval was 2cm. In order to identify the target shape, polarimetric detection was examined to target a long metal wire, whose length is 3m.
Fig.4.2.3 shows the power spectrum of a wire buried at 5cm depth in different polarization state.

Table.4.2.1.Experiment Parameters

Parameters	
Start Frequency	30kHz
End Frequency	3GHz
Number of Points	801
Polarization	XX, XY, YX and YY
Measurement	S21 (Transmission)
Orientation angle	0° and 45°

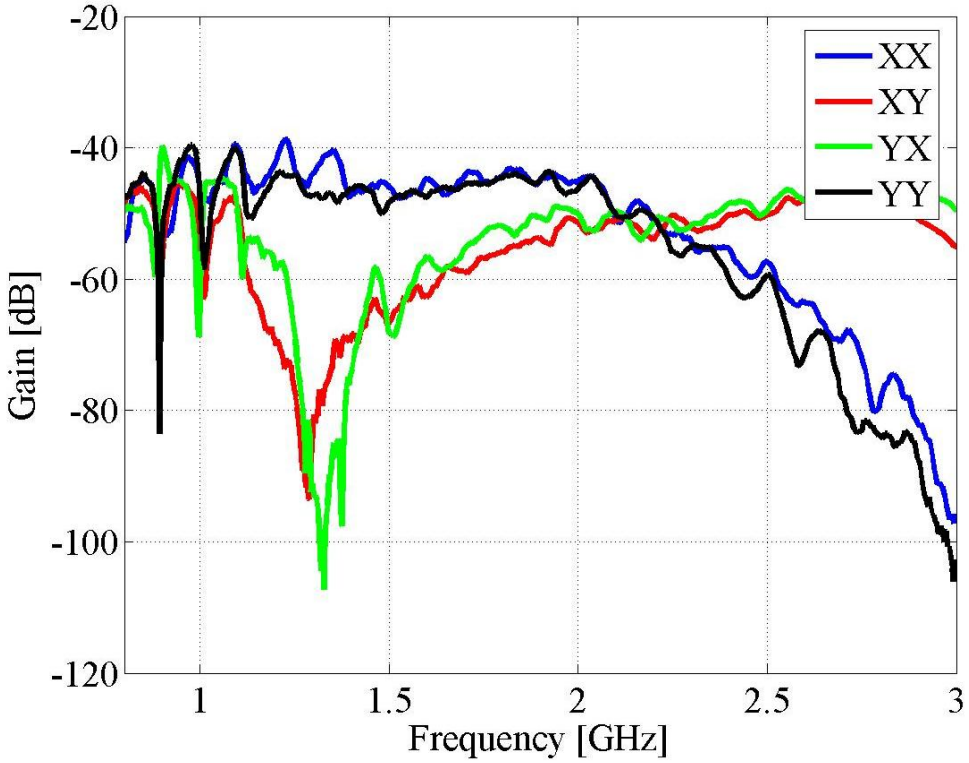

(a) Raw power spectrum

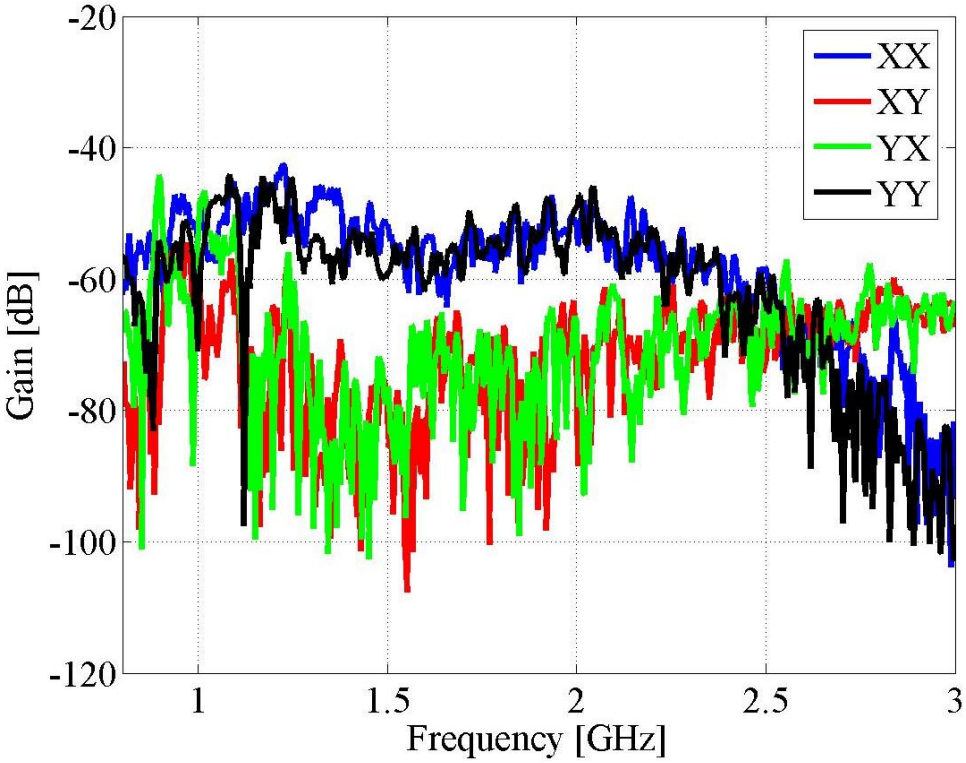

(b) Spectrum of subtracted direct coupling signal

Fig.4.2.3. Spectrum of full polarization states

- *GPR data representation*
    - *A-scan*

During the acquisition of one GPR signal, it is assumed the measurement system is not moving. A one dimensional time signal, acquired with a stationary GPR is called an A-scan. A-scan contains useful information about the target, and can thus be used directly for the distinction object-background, feature extraction and classification.

- *B-scan*

A-scan only provides a very limited amount of information. In order to have more complete view of the area under study, the GPR system shall be moved. This set of 1D A-scans can thus be assembled together in a two dimensional (2D) structure, and visualized as an image. This 2D dataset is called a B-scan. Usually it is visualized with scanning direction horizontally and the time vertically. The B-scan contains more useful information about the scatterers in the subsurface than a single A-scan, and it is also a convenient way of data representation.

- *C-scan*

We could acquire a three dimensional dataset, with the scanning coordinates in X and Y direction, and the time/depth coordinate in the Z direction. This three dimensional volume is called a C-scan. The full volume C-scan contains all possible information about the scatterers in the subsurface. It is then possible to extract out of this dataset of two dimensional slices. Using cuts along the XZ or YZ planes, will deliver more B-scans, while a slice along the XY plane shall give an overview of the reflected energy at a constant time for the various positions.

- *Signal processing*

Signal processing is a vital step for target detection with GPR as GPR signals containing not only the response from a potential target, but also unwanted coupling signals from ground surface, direct coupling between transmitting and receiving antenna, clutter signal from the homogeneous soil and buried scarps or dispersive attenuation of the radio waves during propagation. In addition, they are very sensitive

to the dielectric constant of the soil. Classifying the size, shape and material of the target is probably the most difficult aspect. The target is shallowly buried at 5 cm, and the reflected signal is very small compared to the ground reflections. In order to overcome the problems, we used the following processing steps.

First, the direct coupling was subtracted and time gating was applied in order to isolate the target response. In order to acquire the direct coupling signal, we put the antenna in the air.

Second, the scattering matrices were transformed into the frequency domain and filtered in order to eliminate high frequency noise.

In this experiment the target is buried at shallow depth and reflection of target is contaminated with ground reflection. In order to separate ground reflection and the target reflection we applied Short Time Fourier Transformation (STFT).

○ *Short Time Fourier Transformation*

STFT was used to segment the signal using a time-localized window, and performing the analysis for each segment. Since the Fourier transform was computed for every windowed segment of the signal, STFT was able to provide a true time-frequency representation. A time frequency distribution of a signal provides information about how the spectral content of the signal evolves with time, thus providing an ideal tool to dissect, analyze and interpret non-stationary signals. This is performed by mapping a one dimensional signal in the time domain, into a two dimensional time-frequency representation of the signal [30], [31], [47].

The time-frequency analysis for full polarimetric radar data is an interesting and important way to characterize the scattering behavior of targets or media. In order to enhance weak reflection of the target we applied STFT. In Fig.4.2.4, STFT was applied to polarimetric GPR data, with a target buried 5cm depth and oriented at 0°. Co-polarization state image show strong ground reflection in Fig.4.2.4. After applying STFT, the target response is still contaminated with ground reflection. For metal wire case we could observe the target reflection only in XX polarization. From this point we could subtract YY polarization, in order to represent the target response is clearer in shown Fig.4.2.5. Now we can easy determine the target response in which time and which frequency.

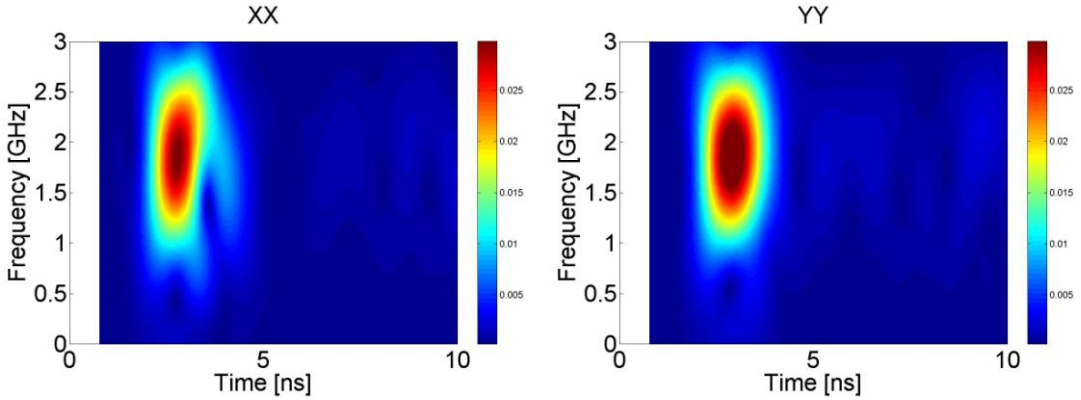

(a) Horizontal polarization (b) Vertical polarization

Fig.4.2.4. Spectrogram of STFT

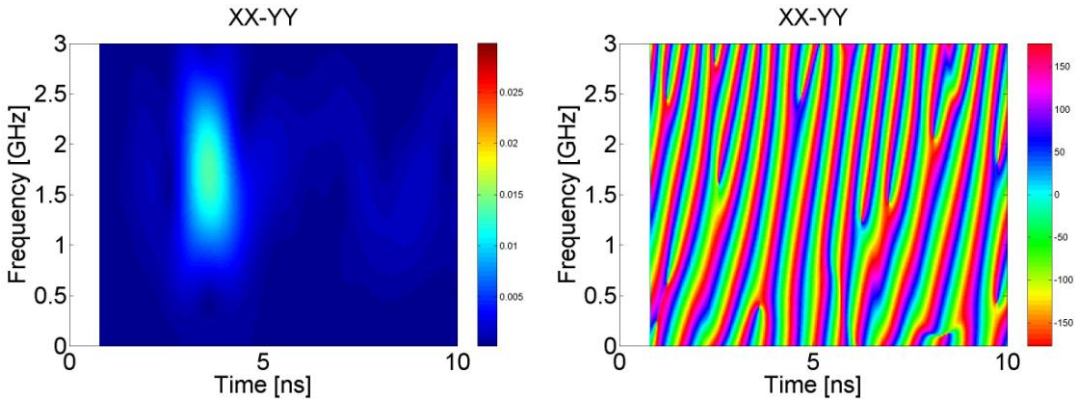

(a) Power spectrum of STFT (b) co polarized phase difference

Fig.4.2.5. Spectrogram of STFT

The polarimetric radar target scattering matrix has been studied by many authors. The matrix is defined in terms of polarization basis. The general scattering matrix is completely determined by the backscattered returns from a target for horizontally and vertically polarized target illuminations.

$$[S]=\begin{bmatrix} S_{hh} & S_{hv} \\ S_{vh} & S_{vv} \end{bmatrix} \qquad (4.1)$$

where S_{hv} is scattering matrix which is proportional to the received horizontally polarized component of the returned signal, while the target is illuminated by vertically polarized transmitted.

One of the main advantages of radar polarimetry resides in the fact that once a target response is acquired in a polarization basis, the response can be obtained in any basis

from a simple mathematical transformation and does not require any additional measurements. This transformation rotates the target response into the any basis defined by main scattering axes of the target, yielding an orientation independent response.

Scattering symmetry assumptions about the distribution of the scatterers lead to a simplification of the scattering problem and allow quantitative conclusions about their scattering behavior. For most targets, the radar cross section not only changes for different targets aspects, but also with changes of target orientation about the Line Of Sight (LOS).

.

- ***Line Of Sight Rotation***

The transformation caused by rotating the scattering object or antenna used for transmission and reception about the LOS. The LOS is defined as the line that connects the antenna phase centre with the scatterer.

- ***Scattering Matrix Rotation***

If the scatterer is rotated about the LOS by an angle θ, the scattering matrix is transformed into $[\boldsymbol{S}(\theta)]$ by the following unitary transformation.

$$[S(\theta)] = [R(\theta)] \cdot [S] \cdot [R(\theta)]^T \qquad (4.2)$$

$$[R(\theta)] = \begin{bmatrix} \cos\theta & \sin\theta \\ -\sin\theta & \cos\theta \end{bmatrix} \qquad (4.3)$$

where $[S(\theta)]$ -is the new scattering matrix after the θ -angle rotation.

Fig.4.2.6(a) shows C-scan image of full polarimetric GPR raw data at 3.3ns depth, which obtained when the target was, oriented 0 degree with respect to of the antenna. We could detect target reflection in XX polarization case. XY, YX and YY polarization we couldn't observe any reflection from target. It is proved theory of scattering matrix, where target is oriented by 0 degree.

Advantage of full polarimetric radar data is to apply a simple mathematical transformation operation and we can get a valuable information related to a target. To better understand the scattering mechanism and the components of wave target interaction, we applied some analysis on the change of polarization bases for the radar

scattering matrix. This transformation rotates the target response into the coordinate basis defined by main scattering axes of the target, yielding an orientation independent response. The scattering matrix rotation algorithm is closely related to the physics of backscattering from an elongated target. When the antenna system of the GPR rotates with respect to the target, the antenna polarization basis changes with it and different matrix elements apply. Thus, the measured target response becomes a function of the orientation of the antenna system with respect to the target.

The target response of target with a preferential scattering axis, e.g. an elongated wire depends on target orientation. Therefore, in order to be able to correctly identify target. An additional preprocessing step referred to as target scattering matrix orientation is required. In Fig.4.2.6(b), we represented the result of line of sight technique for experiment dataset, where target is oriented 0 degree. In this result we rotated scattering matrix by 45 degree by light of sight. In theory we could observe the target reflection in all polarization and the results were proved theoretical matrix. In order to prove this phenomena we choose A-A' and B-B' cross section from C-scan image as marked in Fig.4.2.6.

Fig.4.2.7(a) shows B-scan image of full polarimetric GPR raw data, which obtained by A-A' cross section. A-A' cross section target is oriented same direction. We could detect the target reflection in XX polarization case. But this case target is buried at shallow depth and reflection of target is contaminated with ground reflection. That is the reason why co-polarization case we could not observe reflection of target due to strong ground reflection and also target length is longer than survey length. We expected the reflection from the target is located at 3.2ns.

Fig.4.2.7(b) shows B-scan image acquired at 0 degree case, and then it is rotated by 45 degree using LOS. By comparing rotated image by LOS to original image, amplitude of target reflection is a little bit enhanced for cross polarization cases. When we rotated the target by 45 degree, cross polarization case contain of target information. That is why in B-scan cross polarization images we can observe enhancement of amplitude. For co-polarization case it is still affected by strong ground reflection. From this point of view we can conclude, that even if data suffers by strong reflection and noise we could obtain more target information of scattering behavior using scattering matrix rotation by LOS.

In Fig.4.2.8, we depicted B-scan image of full polarimetric GPR raw data, which obtained by B-B' cross section. From this cross section

From B-scan image it is hard to see differences how the target reflection amplitude is enhanced. That reason why we processed A-scan analysis, is to compare how reflection of a target is enhanced by line of sight (LOS). From this A-scan we clearly see how amplitude is enhanced by LOS. Specially, cross-polarization state shows more strong difference. After analyzing A-scan we applied a rotation matrix to B-scan image. Fig.4.2.9 shows A-scan traces at 0.3m from B-scan images. In this A-scan, horizontal axis indicates time [ns] and vertical axis indicates amplitude in linear scale. Fig.4.2.9(a) shows target is oriented at 0 degrees. Co-polarization represents high ground reflections. Target reflection contaminated with ground reflections. Cross-polarization did not indicate targets reflection and not affected ground reflection. When the target is rotating through the orientation angle 45 degrees cross-polarization amplitude and YY-polarization amplitude were enhanced.

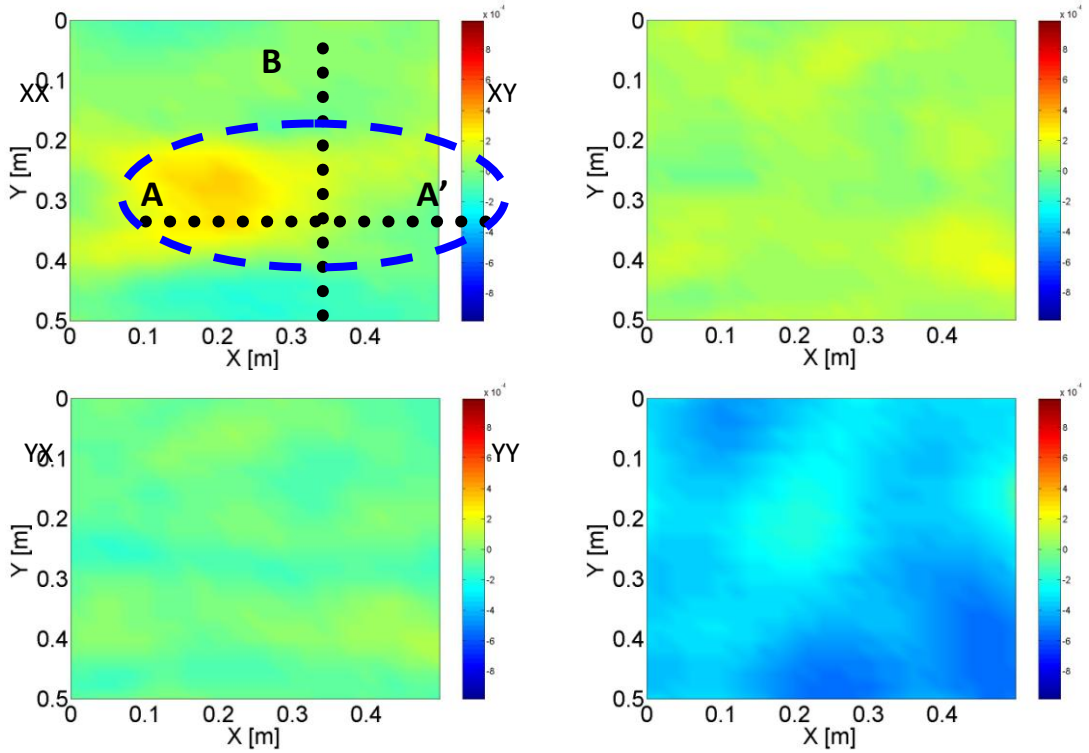

(a) target oriented at θ=0° (horizontal)

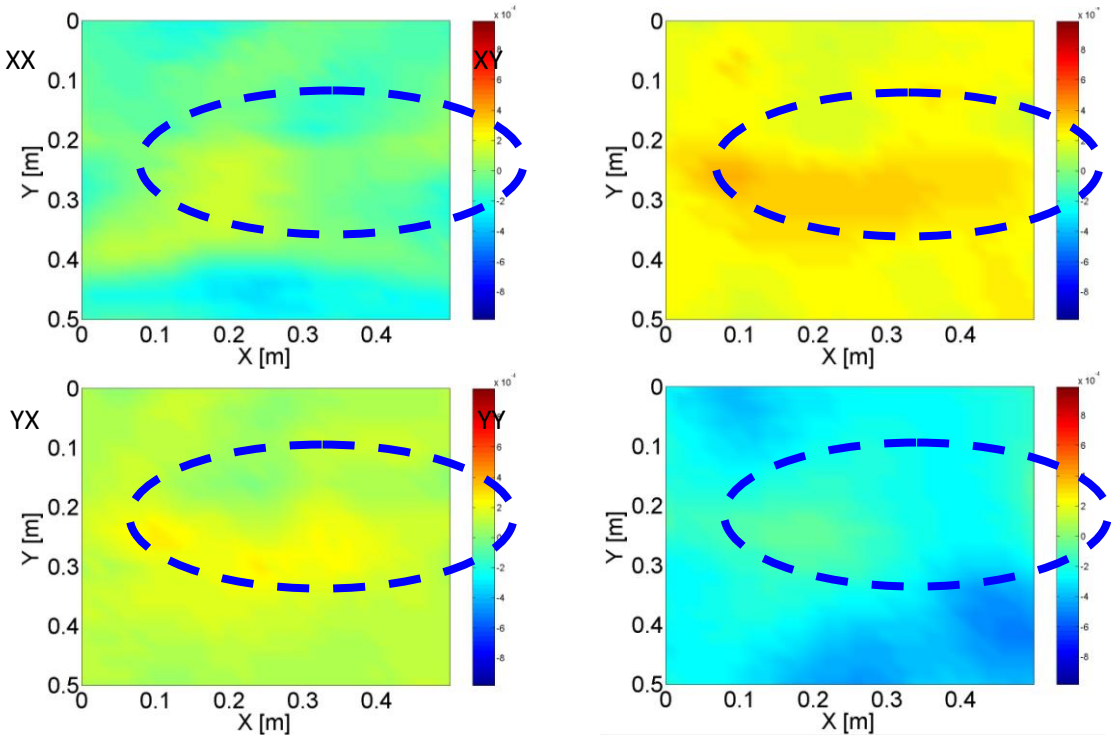

(b) target is rotating through the orientation angle θ=45°

Fig.4.2.6. Raw C-scan of metal wire buried at a depth of 5cm in sand;

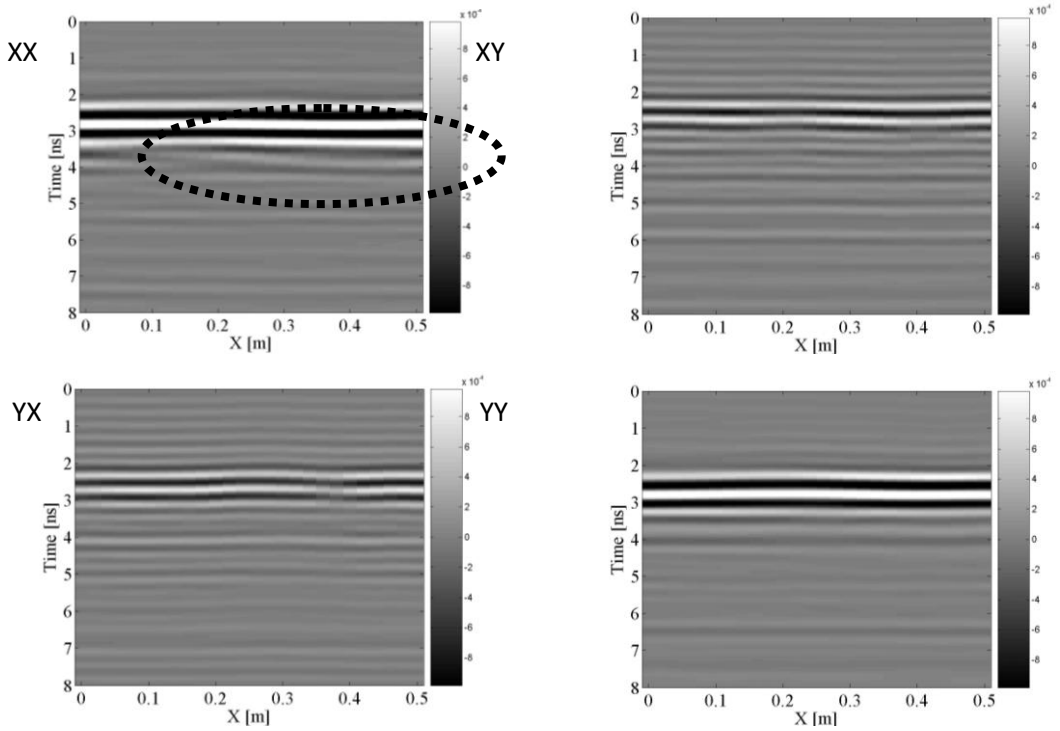

(a) target oriented at θ=0° (horizontal)

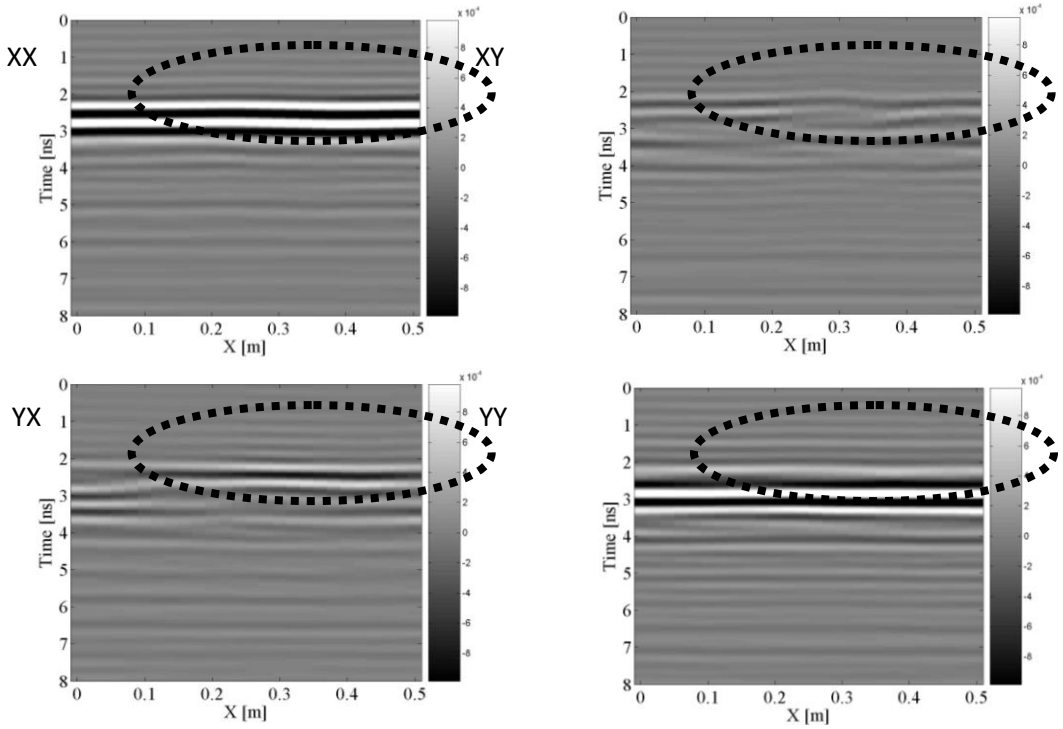

(b) target is rotating through the orientation angle θ=45°

Fig.4.2.7. Raw B-scan images extracted from A-A’ cross-section;

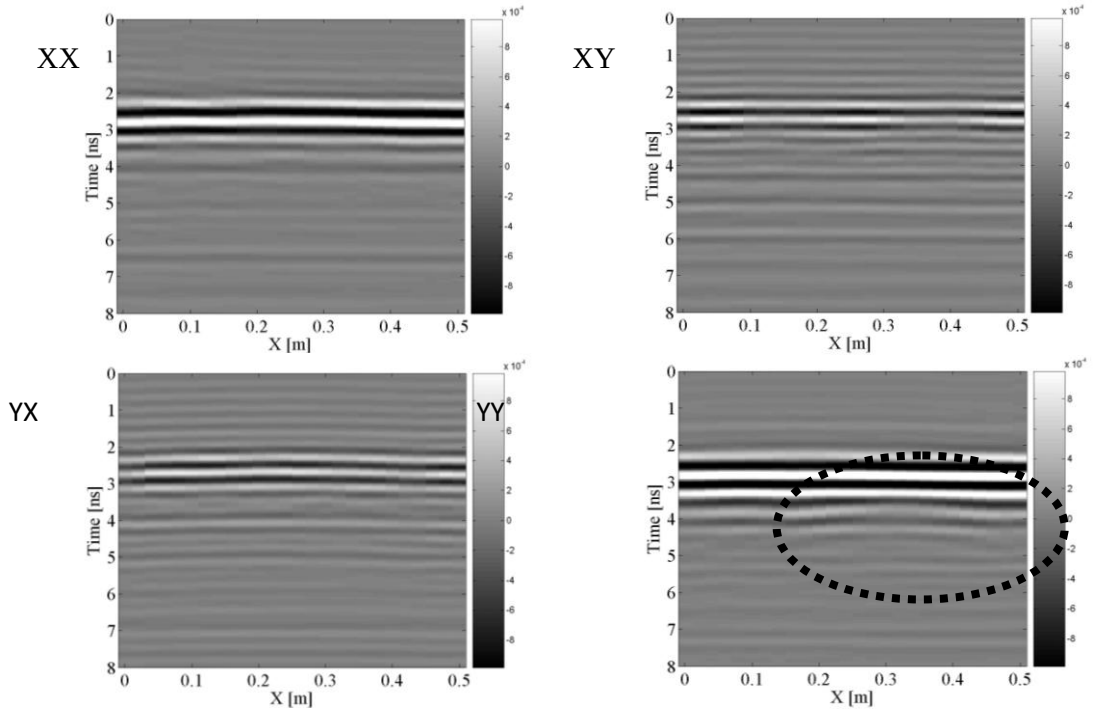

(a) target oriented at θ=0° (horizontal)

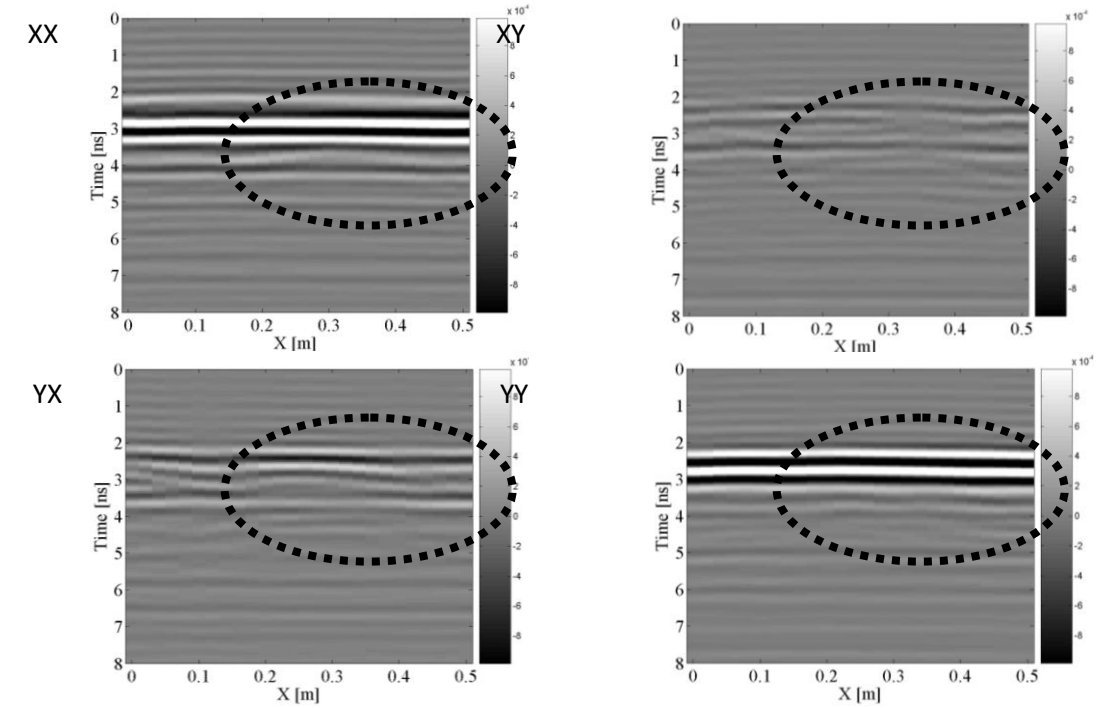

(b) target is rotating through the orientation angle θ=45°

Fig.4.2.8. Raw B-scan images extracted from B-B’ cross-section;

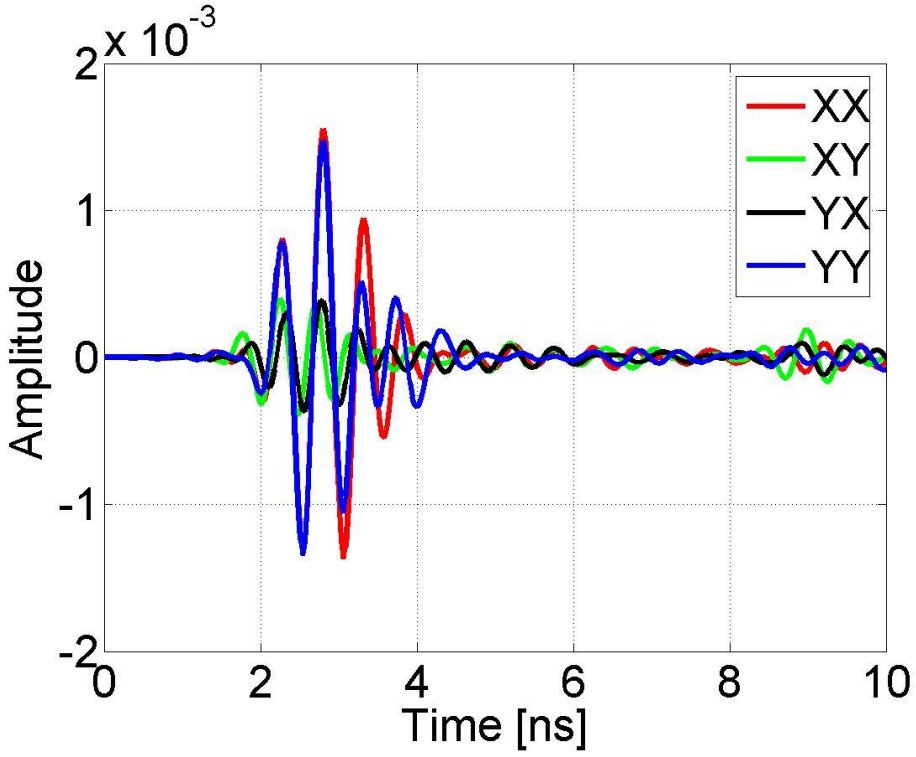

(a) target oriented at θ=0° (horizontal)

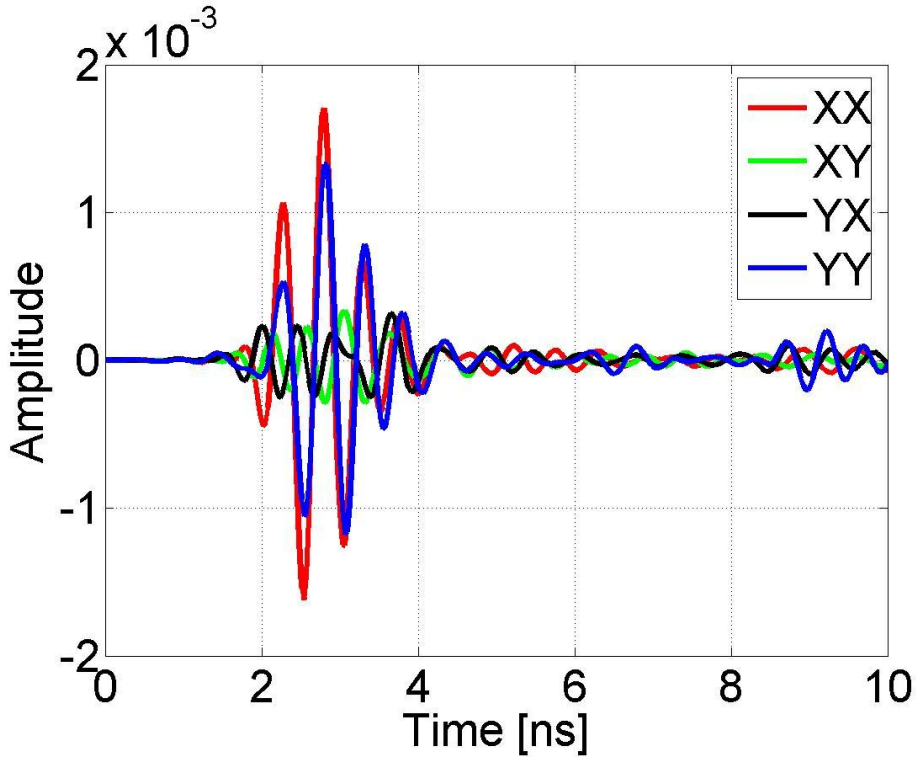

(b) target is rotating through the orientation angle θ=45°

Fig.4.2.9. Time Domain wave form of metal wire buried at a depth of 5cm in sand

- Stokes Matrix

The Stokes parameters are sufficient to characterize the magnitude and the relative phase. The Stokes vector is a convenient method for representing the polarization sate of an electromagnetic wave, and is denoted with [S], given by

$$[S]=\begin{bmatrix} S_0 \\ S_1 \\ S_2 \\ S_3 \end{bmatrix}=\begin{bmatrix} \left\langle |\mathbf{E}_X|^2+|\mathbf{E}_Y|^2 \right\rangle \\ \left\langle |\mathbf{E}_X|^2-|\mathbf{E}_Y|^2 \right\rangle \\ 2\,\mathrm{Re}\left\langle \mathbf{E}_y * \mathbf{E}_x \right\rangle \\ 2\,\mathrm{Im}\left\langle \mathbf{E}_y * \mathbf{E}_x \right\rangle \end{bmatrix} \tag{4.4}$$

The Stokes vector give in Eq.(4.4) can also be written as a function of the polarization ellipse parameters; the orientation angle θ, ellipcity angle χ and the ellipse magnitude A with

$$[S]=\begin{bmatrix} S_0 \\ S_1 \\ S_2 \\ S_3 \end{bmatrix}=\begin{bmatrix} \left\langle |\mathbf{E}_X|^2+|\mathbf{E}_Y|^2 \right\rangle \\ \left\langle |\mathbf{E}_X|^2-|\mathbf{E}_Y|^2 \right\rangle \\ 2\,\mathrm{Re}\left\langle \mathbf{E}_y \cdot \mathbf{E}_x \right\rangle \\ 2\,\mathrm{Im}\left\langle \mathbf{E}_y \cdot \mathbf{E}_x \right\rangle \end{bmatrix}=\begin{bmatrix} A^2 \\ A^2\cos(2\theta)\cdot\cos(2\chi) \\ A^2\sin(2\theta)\cdot\cos(2\chi) \\ A^2\cos(2\chi) \end{bmatrix} \tag{4.5}$$

We generated images based on the Stokes matrix formulation for facilitating the detection and recognition of targets using the polarimetric information on the buried targets. In order to improve detection and recognition probabilities, we used transformation of polarization basis. Each element of the Stokes parameters conveys useful physical and geometrical attributes about the scatterers thus augmenting the potential significant.

We recognize S_0 as the total power density of the reflected wave. S_1 is recognized as power difference between horizontal and vertical polarized components. S_2 is equal to the power difference between orientation angles θ=45° or θ=135°. S_3 is equal to the power difference between the left handed and right handed circular polarized component in the plane wave.

Fig.4.2.10(a) shows the B-scan images obtained for the horizontal buried wire given the target orientation of 0 degrees with respect to of the antenna. The scattering matrix of the target represents below.

$$[S]=\begin{bmatrix} 1 & 0 \\ 0 & 0 \end{bmatrix} \tag{4.6}$$

In this experiment we buried target at 5cm. That is why detection of object on the ground or buried very close to the ground surface is challenging problem because of the high reflectivity due to the air-ground interface. The reflection of the target is contaminated with ground reflections. In that case backscattering scattering matrix equation is given by

$$\begin{bmatrix} M_{XX} & M_{XY} \\ M_{YX} & M_{YY} \end{bmatrix} = \begin{bmatrix} S_{XX} & S_{XY} \\ S_{YX} & S_{YY} \end{bmatrix} + [G] = \begin{bmatrix} 1 & 0 \\ 0 & 0 \end{bmatrix} + \begin{bmatrix} 1 & 0 \\ 0 & 1 \end{bmatrix} \quad (4.7)$$

where $[S]$ target scattering matrix, $[G]$-is represented ground reflection matrix

In order to understand physical and geometrical attributes of scatteres we applied Stokes parameters to experimental data acquired at 0 degree oriented by LOS.

Fig.4.2.10(a) shows experiment data where the target is oriented 0 degree by applying Stokes matrix. S_0 images show total power density of the reflected wave. Our data is contaminated with ground reflection; therefore the target reflection as well as ground reflection wave was enhanced.

S_1 images represent a subtraction of horizontal and vertical polarization components, so the target reflection can be detected in horizontal polarization. Therefore from S_1 images we can see very clear of the target reflection. In S_1 image at 3.2ns occurs the target reflection, and in the S_2 image represent at 2.8ns shows strong ground reflection. S_2 images represents the linear polarized component at orientation angles θ=45° or θ=135°. In this case the target is oriented by 0°, hence S_2 image not represented the target reflection but very clear shows ground reflections. Comparing to between S_1 and S_2 we could see clear shift of reflection as marked white dotted line. Application of the Stokes matrix image processing techniques provides a method for extracting the target polarimetric reflection properties for enhancing the target detection and identification. Although the algorithm for image processing is relatively simple, it provides good results for enhancing the target detectability.

According to Eq.(4.2) the knowledge of the scattering matrix in one polarization basis allows us to derive the scattering matrix in any other orthonormal polarization cases by using the change of basis transformation. This is exactly the great advantage of polarimetric radar systems over conventional radar sensors operating in a single or dual polarization mode. The individual components of the elements of the scattering matrix in the new polarization basis are given as a complex linear combination of the

elements of the scattering matrix in the original measured basis. Fig.4.2.10(b) shows results of scattering matrix basis changing 0 degrees to 45 degrees.

Therefore from S_1 images we can see very clear of the target reflection. In S_1 image at 3.2ns occurs the target reflection, and in the S_2 image represent at 2.8ns shows strong ground reflection. S_2 images represents the linear polarized component at orientation angles $\theta=45°$ or $\theta=135°$. In this case the target is oriented by 0°, hence S_2 image not represented the target reflection but very clear shows ground reflections.

It is gives much more information about physical information of the target. This indicates that transformation of LOS is more suitable for target detection and identification.

Fig.4.2.11 shows that when the wire orientation is parallel to the transmitted polarization signal and scan direction, it is clearly detectable in the co-polarized reflectivity and depolarization images. This is due to the long interaction time that occurs during scanning, since the target is oriented along the scan axis. Fig.4.2.11(a) shows co-polarized reflectivity and depolarization images, where the target is oriented by 0 degree. Both XX and YY polarization images were very sensitive for ground reflection. Therefore co-polarized reflectivity image shows clear image of the target reflection. For depolarization image case, XY polarization is not so sensitive to ground reflection. Thus we could still observe the ground reflection. Fig.4.2.11(b) shows co-polarized reflectivity and depolarization images using scattering matrix rotation by LOS. Co-polarized reflectivity images show weak the target reflection. This indicates that the polarimetric data including strong ground reflection and system noise we still could successfully detected target buried at shallow depths.

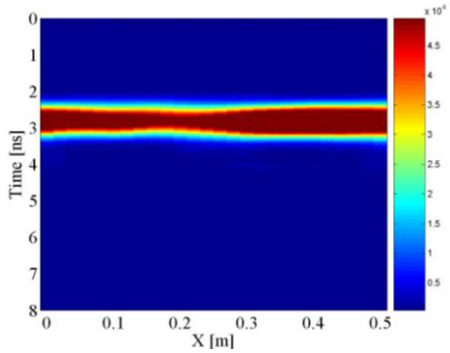

S_0 image

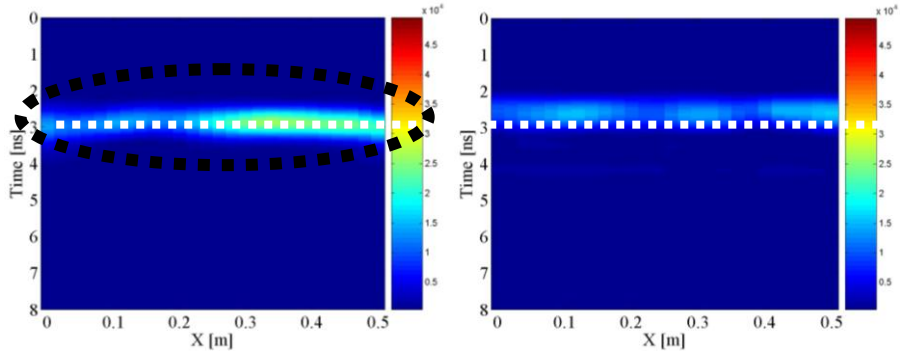

S_1 image S_2 image

(a) Stokes images target is oriented at θ=0° (horizontal)

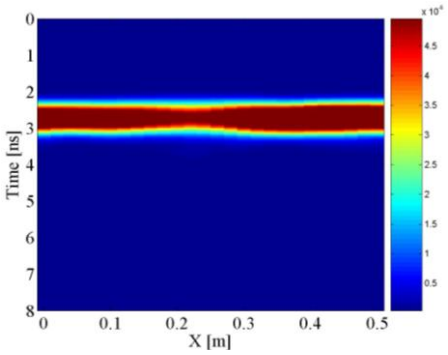

S_0 image

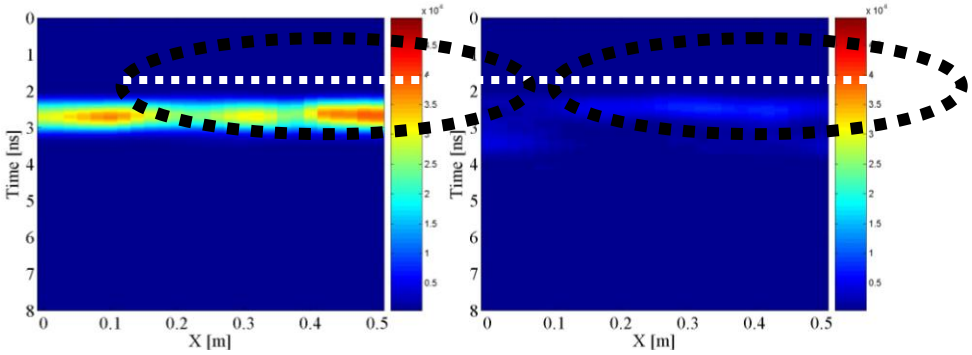

S_1 image S_2 image

(b) Stokes images; target is rotating through the orientation angle θ=45°

Fig.4.2.10. B-scan images processed by Stokes matrix;

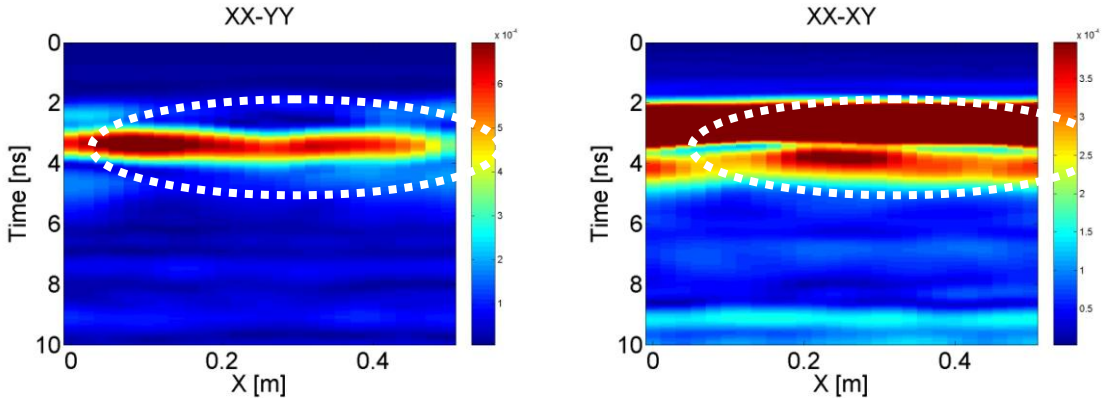

(a) Cross and co polarization images target is oriented at θ=0° (horizontal)

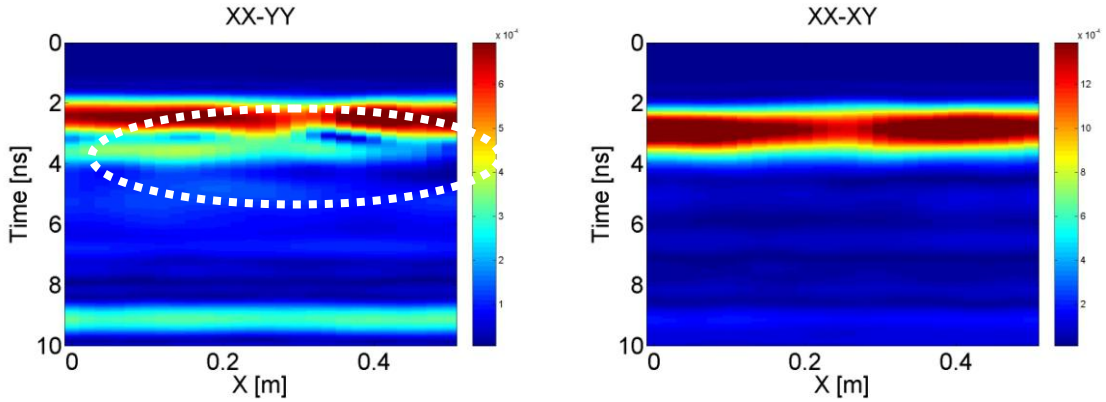

(b) Cross and co polarization images; target is rotating through the orientation angle θ=45°

Fig.4.2.11. B-scan images of polarimetric analysis

4.2.2. Experiment -2

- *Data acquisition*

The main objective of the research work is to detect and identify buried objects. 4 targets are buried in the sandpit at 10cm, 15cm respectively. The horizontal separations between 4 targets were 45-50cm. A stepped frequency continuous wave radar system based on commercial vector network analyzer was used for measurement campaign. In this measurement, frequency range was set from 30kHz to 3GHz.

Photograph of the target used in the experiment is shown in Fig.4.2.12. Table.4.2.2 descries the characteristics of targets of this experiment. We moved the GPR antenna 80cm in the y-axis 180cm in x-axis at the increment of 2cm in each axis. The number of data point in each measurement is 801.

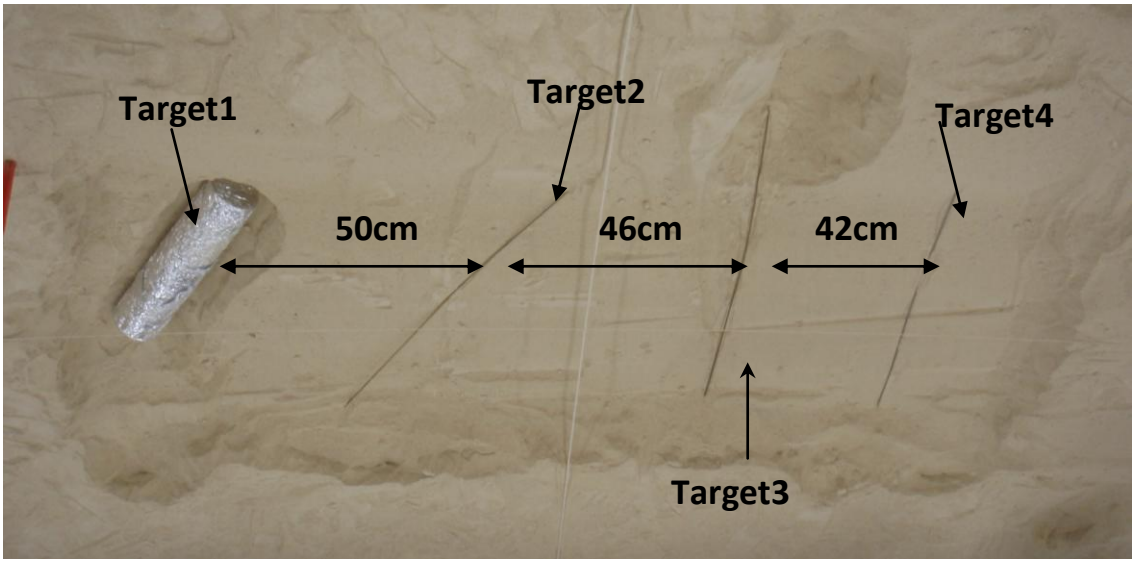

Fig.4.2.12. the targets used in the experiment

The raw time domain data obtained by full polarimetric GPR in different polarization state and with different targets are shown in Fig.4.2.13 as B-scan images. The four targets are visible in this B-scan image. The target-1 is clearly imaged in all polarization states and other targets are not so clearly imaged due to strong ground reflection.

Table 4.2.2. Characteristics of targets

Target1	Plastic pipe covered by aluminum paper	Diameter - 9cm Length - 41 cm	Oriented by 60 degree Depth 15m
Target2	Blast metal wire	Diameter – 3cm Length – 95cm	Oriented by 45 degree Depth 12m
Target 3	Blast metal wire	Diameter -3cm Length – 120cm	Oriented by 90 degree Depth 12m
Target 4	Metal wire	Diameter – 5cm Length – 120cm	Oriented by 90 degree Depth 10 cm

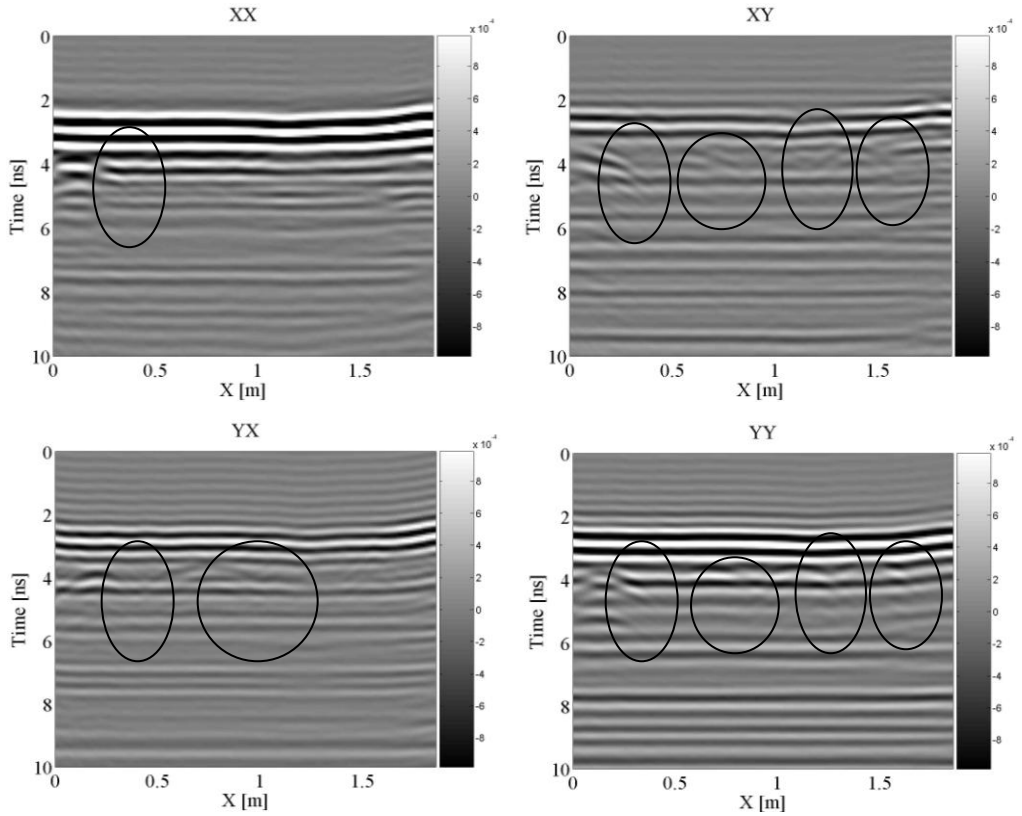

Fig.4.2.13. B-scan images of various targets in dry sand

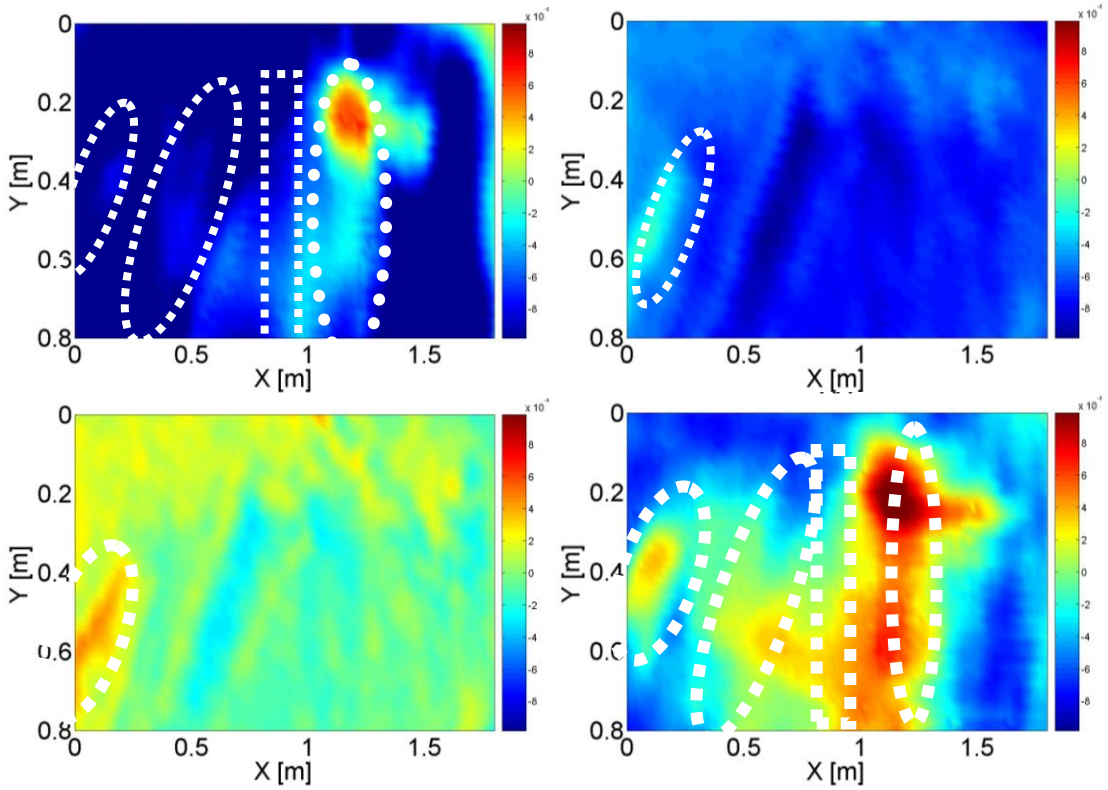

Fig.4.2.14. C-scan images of various targets in dry sand

The raw time domain data acquired by full polarimetric GPR is shown in Fig.4.1.14 as C-scan images at a time of 3.8ns, which corresponds at a depth of about 23cm. The target is detectable in this image, however also clutter can be seen and a response from the target is not so clear. Specially, the pipe and metal wire shown strong reflections compare than blast wire.

4.3. POLARIMETRIC DECOMPOSITION TECHNIQUES

Cloude defines the main idea behind Target Decomposition (TD) theorems as "expressing the average scattering matrix for a random media problem as a sum of independent elements and to associate a physical mechanism with each component". The scattering matrix is a measured quantity, often stochastic rather than deterministic in nature. The use of TD theorems to evaluate the average scattering matrix allows the various scattering mechanisms and target properties to be identified. In addition, it is possible to generate a dominant scattering mechanism for better physical interpretation. This is the main advantage of TD theorems.

4.3.1. THE H/A/α POLARIMETRIC DECOMPOSITION

The standard Cloude-Pottier eigenvalue/eigenvector decomposition is applied to the coherency matrix. The eigenvalue spectrum uniquely describes the scattering entropy, anisotropy and span (total power). In addition to the scattering mechanism and orientation angle of the scatterer that are typically extracted from the eigenvectors.

In general the polarimetric radar response of a buried object depends on the orientation of the object with respect to the transmitting and receiving antennas. In order to make the identification possible, it is crucial to measure the scattering matrix and transform the data into a target frame in which the response is orientation independent. The measurements were done for different target orientations. Transformation of the measured response into such a target frame was achieved using a matrix diagonalization technique in the frequency domain. The eigenvalues obtained with the matrix diagonalization constitute a set of orientation invariant features and have been studied as possible target discriminators. In particular we addressed the problem of classifying targets with respect to shape. The results suggest the possibility to distinguish between targets by looking at how the eigenvalues change as a function of frequency.

Second, the scattering matrices were transformed into the frequency domain and filtered in order to eliminate high frequency noise. Third, the scattering coefficient S_{yx} and S_{xy} were averaged to remove small deviation from symmetrical forms. Matrix diagonalization was applied to the real matrices obtained by taking the modulus of the scattering coefficients. Finally, the eigenvalues and eigenvectors obtained by matrix diagonalization were used to compute the estimated the power polarization anisotropy coefficient and the angle of the orientation (θ).

In this section we used full polarimetric GPR data obtained by Experiment-1. In this experiment we used single fundamental target. In order to extract clear information of target, we applied the H/A/α eigenvalue based TD for simple case.

Fig.4.3.1 shows the processing results obtained for the horizontal wire given the target orientation of 0 degree with respect to of the antenna. The plotted graphs refer to the absolute value of the scattering coefficients. In the frequency band of interest, λ_2 is

much weaker than λ_1. The polarimetric anisotropy (A) is defined as the ratio of the difference between the sum of λ_2 and λ_3 and A is close to 1. Accordingly the "metal wire" is seen as an elongated object. This indicates the presence of a strong preferential scattering axis. The orientation of this axis is clearly defined by the angle (θ). θ angle is close to 0 degrees when the wire is oriented parallel to the antenna.

Fig.4.3.2 shows the processing results obtained for the horizontal wire given the target orientation of 45 degree with respect to of the antenna. The scattering coefficients change with target orientation and strong cross-polarization components are observed when the "metal wire" is oriented at 45 degrees. The anisotropy was reached to 0. The eigenvalues λ_1 and λ_2 remain approximately the same when the target is rotated. This confirms that the eigenvalues do not depend on the orientation of the antenna system with the respect to the target and can be considered orientation invariant target features. θ angle close to 45 degrees when the target orientation of 45 degrees is considered. This proves that the preferential scattering axis of the metal wire coincides with long axis.

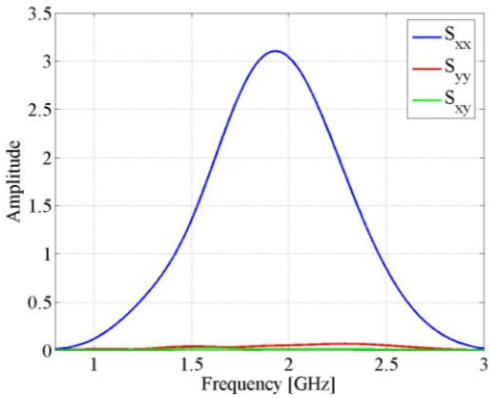

(a) absolute scattering coefficients

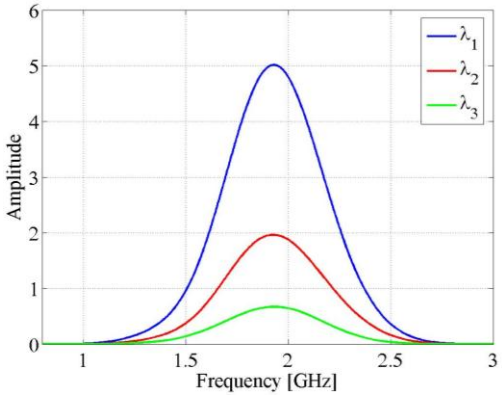

(b) the computed eigenvalues

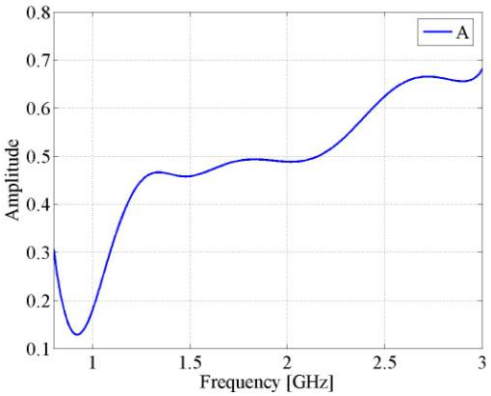

(c) estimated anisotropy

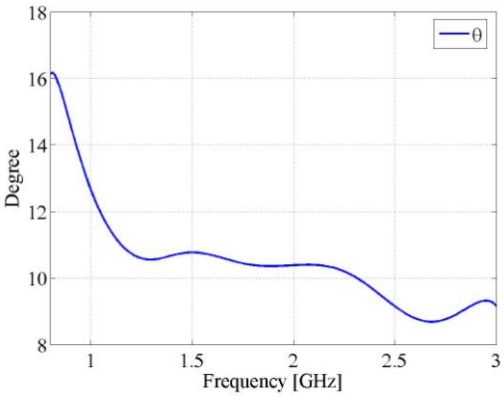

(d) estimated orientation angle

Fig.4.3.1. Polarimetric analysis of the metal wire oriented at 0 degrees

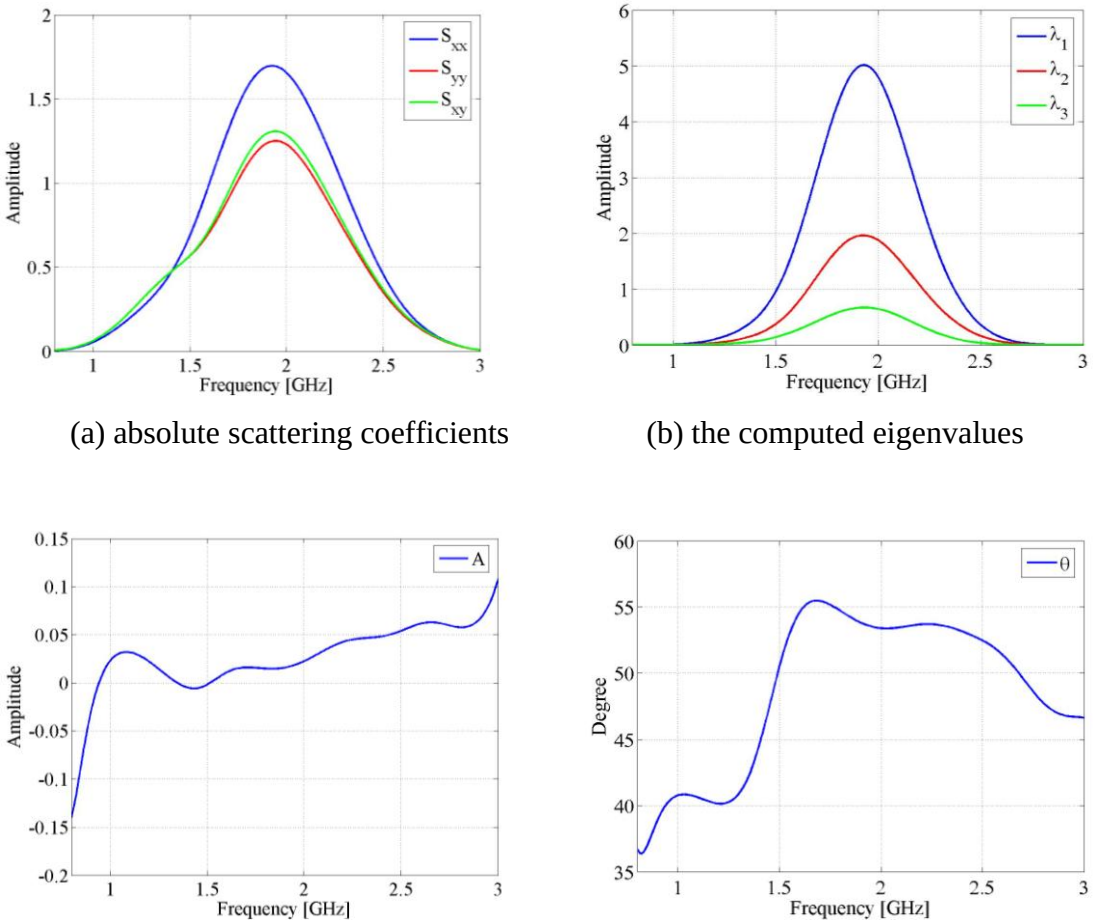

(a) absolute scattering coefficients (b) the computed eigenvalues

(c) estimated anisotropy (d) estimated orientation angle

Fig.4.3.2. Polarimetric analysis of the metal wire oriented at 45 degrees,

4.3.2. THE HUYNEN-KENNAUGH MATRIX DECOMPOSITION

The purpose of decomposition in radar polarimetry is to provide means for interpretation and optimum utilization of polarimetric scattering data. All the important target related information can be derived from the knowledge of the scattering matrix. It is known that the scattering matrix coefficient depend on radar frequency, waveform, polarization state of the transmitted wave, target structure, its conductivity.

The Mueller matrix describes a linear relation between the two Stokes vectors related to the transmitted and reflected wave. This matrix is given by

$$[M]=\begin{bmatrix} A_0+B_0 & F & C_\theta & H_\theta \\ F & -A_0+B_0 & G_\theta & D_\theta \\ C_\theta & G_\theta & A_0+B_\theta & -E_\theta \\ H_\theta & D_\theta & -E_\theta & A_0-B_\theta \end{bmatrix} \tag{4.3.1}$$

where A_0, B_0, C_θ, D_θ, E_θ, F, G_θ and H_θ are known under the name of the "Huynen parameters". The nine parameters in $[M]$ are useful for general target analysis without reference to any model, and each of them contains real physical target information.

The parameters indexed with θ mark that they depend on the target orientation relative to the horizontal direction. More specifically, the angle θ is the orientation angle of the polarization ellipse of the polarization that gives the maximum radar return from the target, for a fixed aspect angle.

If the target is rotated about the LOS to the radar so that θ becomes zero, the parameters will generally take on new values, which are donated by omission of their indexes, i.e. $B_\theta(\theta=0)=B$ etc.

$$\begin{aligned} H_\theta &= C\cdot\sin 2\theta \\ C_\theta &= C\cdot\cos 2\theta \\ G_\theta &= G\cdot\cos 2\theta - D\cdot\sin 2\theta \\ D_\theta &= G\cdot\sin 2\theta + D\cdot\cos 2\theta \\ E_\theta &= E\cdot\cos 4\theta - B\cdot\sin 4\theta \\ B_\theta &= E\cdot\sin 4\theta + B\cdot\cos 4\theta \end{aligned} \tag{4.3.2}$$

Table 4.3.1. Geometrical significance of the Huynen parameters

A_0	is related to the target symmetry: can be seen as return power from regular, even, convex parts of the scatterer; for a sphere this is only non-zero parameter
B_0	is related to target structure; can be seen as return power from the irregular, uneven,, non-convex parts
B_0-B	is related to non-symmetry
B_0+B	is related to target irregularity
C and D	are related to target shape; associated with depolarization components of symmetric targets
E and F	are related to target twist; depolarization due to non-symmetry
G and H	are related to coupling between different part of the targets
More specifically	
C	defines global shape (a line target has large C)
D	defines local shape (curvature difference; discontinuities, an edge)
E	defines local twist or surface torsion
F	defines global twist or target helicity
G	defines local coupling
H_θ	defines global coupling due to target orientation (roll angle θ)

The polarization description using the Stokes/Mueller/Huynen formalism is an example of a phenomenological approach, characterized by being essentially non-committal concerning the detailed scattering mechanism. Its aim is to draw general conclusions about every target, using the tools of linear algebra.

In that sense, the descriptive scheme is wavelength independent. However, the coefficients that appear in it are not, and some other means must be used to extract such dependence. For example, if parameter A_0 is present (non zero) for a given target at a given incident angle, that target will be symmetric for that incidence. That is all the information the Huynen method can provide in that case. A manifestation of this can be seen from Table.4.3.1 the interpretation of the Huynen parameters reflects

quite general properties of the targets. In specific applications, model-based methods can be expected to be more effective for classification.

A major problem in analyzing polarimetric radar data is in understanding the scattering mechanism of reflected targets, which are usually very complex. In order to show how it can guide the interpretation of such scattering mechanism, we applied decomposition algorithm. Once the scattering matrix S is obtained, it is used to evaluate all the elements of the Mueller matrix M. The Huynen parameters extracted from the pertinent elements of the Mueller matrix. This set of parameters is known to yield some general phenomenological information about radar target and their geometry.

In order to extract as much information as possible about the target characteristics, many polarimetric tools have been developed. They mainly deal with the recognition and classification. Among these tools, the Huynen's phenomenological theory of radar targets proposes a set of nine parameters that are related to the target physical characteristics. The target Mueller matrix is a 4×4 real matrix that is dependent of the scattering matrix polarization basis. This Mueller matrix is a power descriptor of the electromagnetic interaction between the incident wave and the target.

We processed full polarimetric data by Huynen parameter and represented the results in C-scan of the buried target in various depths in Fig.4.3.3. In Fig.4.3.3 represent full polarimetric radar data acquired in Experiment-2. In this experiment we used various target in different orientation angle. Those reasons why we are choose this experiment dataset.

C-scan images processed by Huynen parameter displayed at depth at 3.8ns. In A_0 image is related to the target symmetry. In this experiment we used metal pipe and wire. Those targets belong to irregular target. That reason we could not see clear image. But B_0 clear presents metal wire targets, where oriented by 45 and 90 degrees. C image represents the target shape. E image shows target depolarization due to non-symmetry. In all images we could not clear identify target-4. It is related to the target depth. Compare to other targets target-4, which is blast wire oriented 90 degree is buried a little bit shallow.

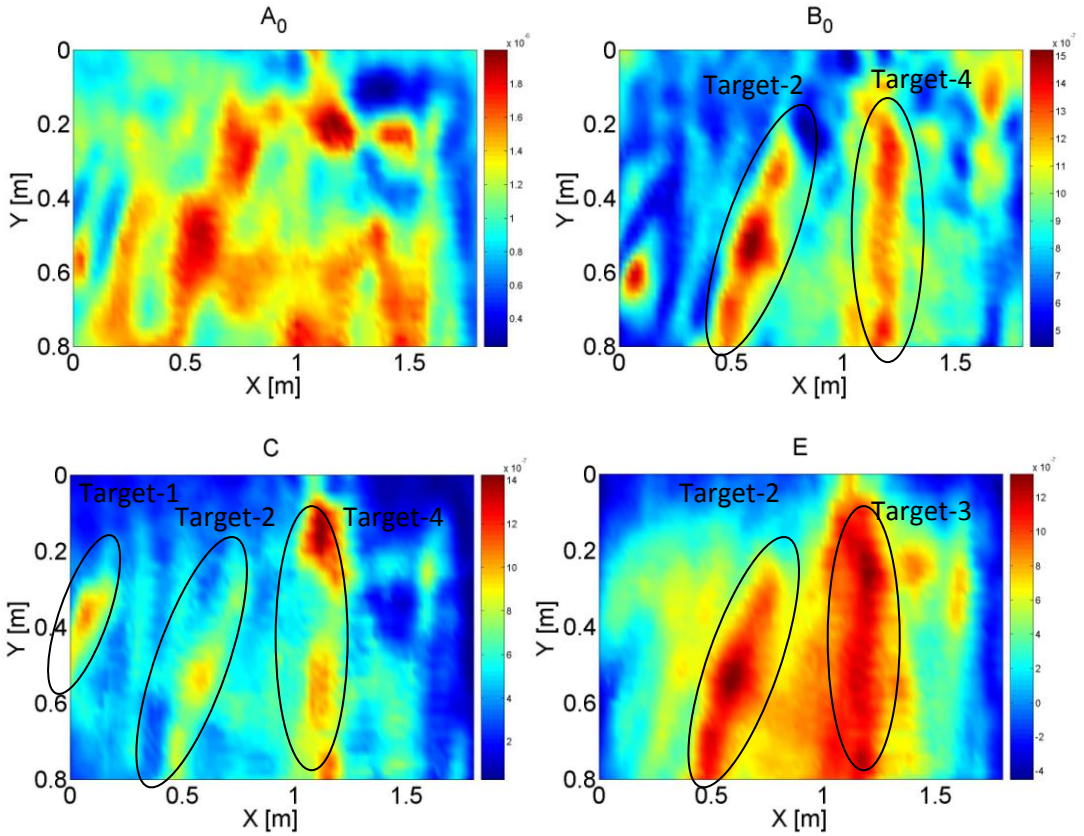

Fig.4.3.3. C-scan images processed by Huynen parameter displayed at depth at 3.8ns

4.4. SUMMARY

In chapter 4, the experiments of the result were discussed. In the first place, a polarimetric analysis of the radar backscatter response from buried target has been completed successfully. Decomposition techniques have been applied in various domains, providing a wealth of useful information about how shallow buried target is seen by a radar. Target decomposition was performed in two domains; 1) frequency domain data, and 2) time domain data.

Chapter 4 is used as a basis to determine the sensitivity to a possible detection from a certain objects. This, together with the fact that the largest reflections occur when the polarization of the electric field is parallel to the object causing reflection, shows how the sensitivity to subsurface reflections can be increased. On the other hand, these results show how to reduce the sensitivity to unwanted reflections coming from

objects on or above the surface. The concept of the target polarization basis changes has been tested using polarimetric data acquired over a buried metal wire and demonstrated the capability to accurate recover the target response signals, which would have the measured if the wire had been oriented with its preferential scattering axis aligned with antenna system. We represented the result of line of sight technique for experiment dataset, where target is oriented 0 and 45 degrees. As a result we could obtain more useful information related to the physics of scattering matrix.

In last part of Chapter 4 we addressed the result of several buried objects with different orientations. Target decomposition techniques have been applied in various domains, providing a wealth of useful information about how target where is buried at shallow depth is seen by polarimetric radar. 3D reflectivity images obtained by polarimetric GPR experiments have been employed, together with decomposition techniques, for identifying the position, orientation and characteristics of the scattering mechanism in the buried target. In order to extract clear information of target, we applied the H/A/α eigenvalue based TD and Huynen-Kennaugh TD for simple case.

.

CHAPTER 5

POLARIZATION ANAYLSIS FOR 3D GPR IMAGING

5.1. INTRODUCTION

The application of imaging radar to archaeological investigations holds great potential. The ability to detect an object within a scene is a complicated issue, the limits of which are still being explored. Target geometry, target material composition, and moisture content play very significant role.

The polarization of an electromagnetic wave is a fundamental property of propagation that provides the GPR technique with a unique opportunity for producing improved images of objects in the subsurface. Conversely, ignoring the polarization aspects of GPR can lead to false interpretations of the shape and orientation of objects in the field, and in the extreme case can cause buried objects to be totally missed in an interpretation. The effects of polarization become very critical in the case 3D imaging. The direction of measurement can strongly influence the resulting image.

5.2. METHODOLOGY

The goal of the processing was to improve the signal-to-noise ratio. Signal processing is important to recognise archaeological structures in raw data according to their geometry and despite noise contamination. Data processing included pre-processing and computation of instantaneous parameters [27]. For the analysis of this

archaeological data, it became clear that instantaneous amplitude and phase attributes provided the most detailed information for target identification. Therefore, instantaneous amplitude and phase results are presented here. The Hilbert Transform (HT) has traditionally been used in both the theory and practice of signal processing. The classic approach for estimating instantaneous parameters relies on using the Hilbert Transform. The HT method extracts the instantaneous parameters by comparing the imaginary part with the real part of an analytical signal [25], [30], [31].

Therefore, the corresponding analysis is also called complex trace analysis. Hilbert Transform relationships are relationships between the real and imaginary components of a complex sequence.

5.3. EXPERIMENT 1.
ARCHAEOLOGICAL APPLICATION

5.3.1. ARCHAEOLOGICAL BACKGROUND

The ruins of the castle of Van Khan (Wang Khan) Tooril, shown in Fig.5.3.1, are located along the Black Forest of Tuul River, 30km west of Ulaanbaatar city. The Black Forest of Tuul is mentioned several times in the Secret History of Mongols, the 13th-century account of the rise of Mongols and the life of Genghis Khan. The Mongolian archaeologists began to excavate Van Khan Tooril's castle in 2006. Archaeologists were requested to protect the excavation and to rebuild the castle as it originally appeared.

Fig.5.3.1. View of the archaeological site and the target

The size of the main castle is ~25m by 30m, and its outer walls are 300m by 300m. Before our GPR measurements archaeologists had excavated the eastern part of the main castle. In these excavations, archaeologists have found dragon, elephant statues and some pattern roofs of castle. However, the structure of the castle is mainly characterised the by brick and masonry foundations. The depth of the buried object is variable from a minimum 10cm to a maximum of ~50cm below the present ground level. Masonry structures are complicated by the array of bricks and joints. If GPR wavelength and antenna orientation are chosen correctly, then the position, internal cracking and the thicknesses of walls and bricks can be determined.

5.3.2. GPR DATA ACQUISITION AND PROCESSING

A 3D GPR survey was carried out in August 2006, and May 2007 with a $90m^2$ area. Our GPR measurement aim was to evaluate the evidence of buried structure, like walls, then delimit those structures and study the presence or absence of tiles from collapsed foundation. In preliminary work, a 3D GPR survey was conducted to estimate the archaeological target in the study area. We acquired 40 profiles 7m long at 0.2m line spacing, in a north-south survey direction. These results did not give enough information about the target. Therefore we decided to carry out further GPR measurements in the two orthogonal survey directions from north to south and west to east.

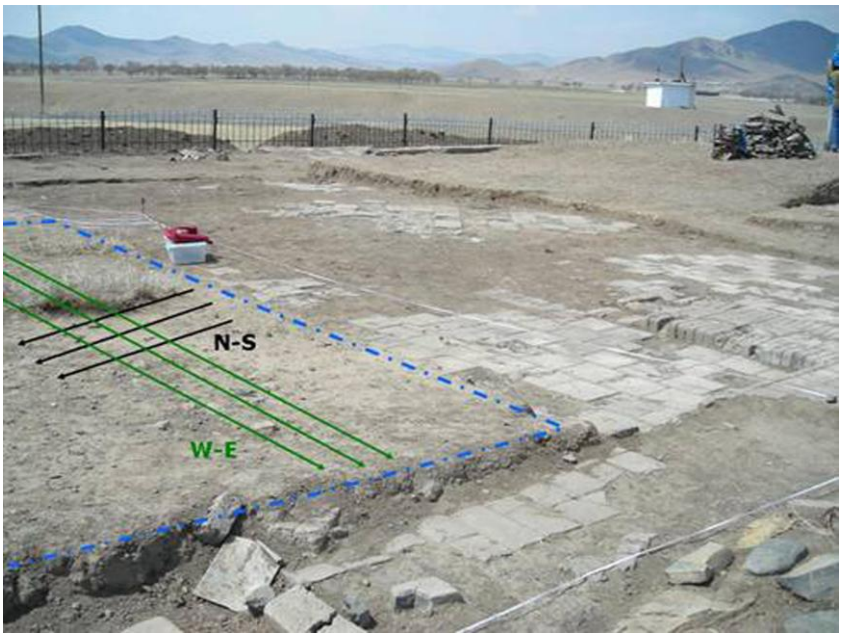

Fig.5.3.2. Sketch map of the study area

To acquire the GPR data, we used a RAMAC/GPR system. Two types of antennas were used separately, operating at 500MHz and 800MHz. The higher frequency gives good resolution at shallow depths and the lower frequency gives a larger depth of investigation. We acquired 60 profiles 9.5m long at 0.1m line spacing in the north-south survey direction, and 74 profiles 7.5m long at 0.1m line spacing in the west-east survey direction as shown in Fig.5.3.2.

The velocity of the electromagnetic waves was measured by the common mid-point (CMP) method and time-domain reflectometer measurements. From these results a velocity of 0.13 m/ns was used for time-to-space conversion.

The goal of the processing was to improve the signal-to-noise ratio. Signal processing is important to recognise archaeological structures in raw data according to their geometry and despite noise contamination. Data processing included pre-processing and computation of instantaneous parameters [27]. For the analysis of this archaeological data, it became clear that instantaneous amplitude and phase attributes provided the most detailed information for target identification. Therefore, instantaneous amplitude and phase results are presented here.

5.3.3. DATA INTERPRETATION

Before interpreting horizontal slices, we analysed the anomaly geometry in distance and direction. In order to understand reflection behaviour of the archaeological targets, we processed the data in vertical GPR profiles. To better understand the influence of spatial sampling and the position and direction of the profiles with respect to the anomalies, we compared the 2D GPR profiles in orthogonal survey directions with horizontal slices obtained from those profiles. We focused our interpretation on the strongest reflections, labelled as A-N in the figures. The final interpretation was performed on both vertical GPR profiles and horizontal slices.

5.2.3.1. B-SCAN IMAGE

Fig.5.3.3 shows Profile-4, acquired in the north-south survey direction, and Fig.5.2.4. shows Profile-10, acquired in the same survey at 60cm distance from Profile-4. The purpose of selecting these profiles was to evaluate the intensity and detecting discontinuity of the signals at the different distances. An instantaneous amplitude plot of this data is shown in Fig.5.3.3(b). The instantaneous amplitude provides a visual representation of reflection strength, and appears to be a valuable indicator of brick in the subsurface. Several reflection features can be observed in Profile-4. These features are enclosed by dashed white lines and labeled A-D. Bricks may be responsible for prominent anomalies occurring near 2 to 5m and 5.5 to 8.2m at 0.2cm depth. Additional smaller anomalies are visible near 0.5 to 1.5m at 0.2cm depth and 8.6 to 10m at 0.3cm depth. Judging by the shape and the width of the reflections, the moderate to high intensity response in instantaneous amplitude corresponds to brick and tiles. The instantaneous phase section, Fig.5.3.3(c), provided the most significant new information for our interpretation. Phase changes at the edges of the prominent anomalies (anomalies B and C) providing further strong evidence for sharp edges. Similar sharp changes marked the end of the profile.

To validate this interpretation we selected Profile-10 in north-south direction. Fig.5.3.4 shows the instantaneous amplitude and instantaneous phase attributes of the data in Profile-10. An analysis of the data acquired on different profiles along the same survey direction indicates that there is a very clear difference in instantaneous amplitude and phase between the Profile-4 and the Profile-10. The instantaneous

amplitude has greater continuity in Profile-4. Fig.5.3.4(b) shows slightly smaller multiple reflections as labelled as E, F and H. If the instantaneous amplitude data in Fig.5.3.3(b) and Fig.5.3.4(b) is overlain by the instantaneous phase data in Fig.5.3.3(c) and 5.3.4(c), a clearer image of the change in signal becomes readily apparent. From this we interpret that the change in dielectric property from bricks to soil is marked by a significant phase change that can be easily identified to enhance the interpretation. The least response in instantaneous amplitude might be related to the absence of bricks and tiles. According to these results, the moderate to high intensity response in instantaneous amplitude can be associated with presence of tiles, and lower values for these attributes can be associated with the absence of tile and bricks. Also changes of phase shift can be correlated with these to indicate presence and absence of targets.

We also acquired GPR data along west-east profiles, and one profile is shown in Fig.5.3.5. In this direction, we also observed many reflections as in the north-south profiles, but the reflections from targets did not appear as clearly compared with reflections in north-south profiles. This is explained by the fact that polarisation on the tiles and bricks was not parallel to the west-east direction. Even so, we could detect reflections from brick and tiles by using instantaneous parameters. Phase changes at the edges of the L and N anomalies provide strong evidence for sharp and discrete discontinuities there. We could also observe small phase changes at both edges of anomaly N. Between both edges of the anomaly N there is relatively good lateral continuity to the reflectors. In the instantaneous phase map we can easily distinguish phase changes due to bricks targets and filling materials.

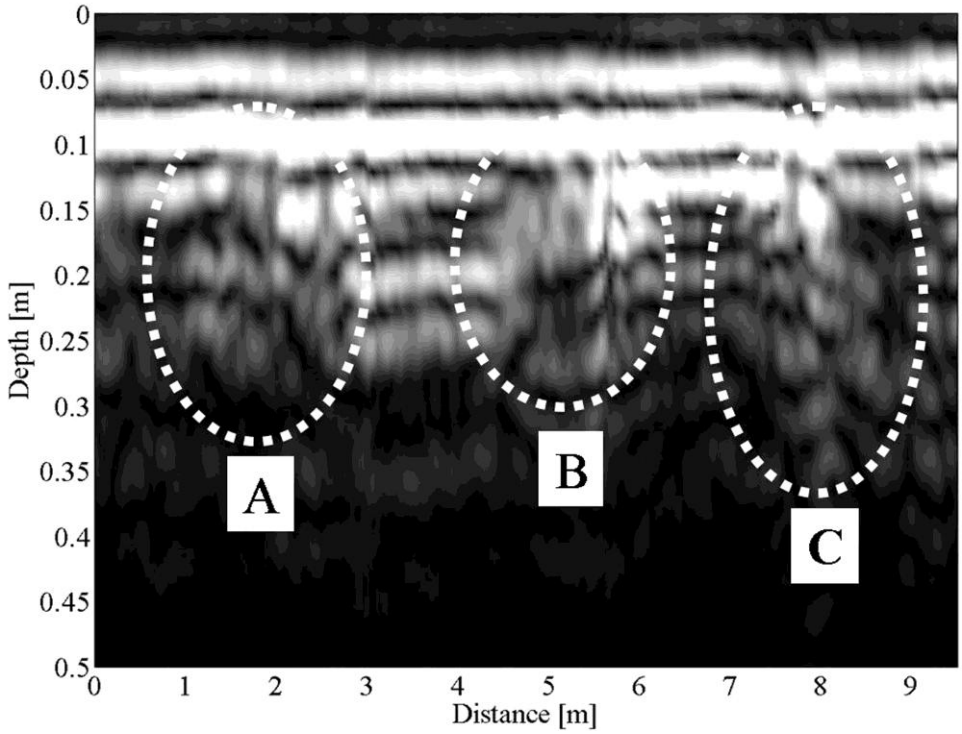

(a) Instantaneous amplitude

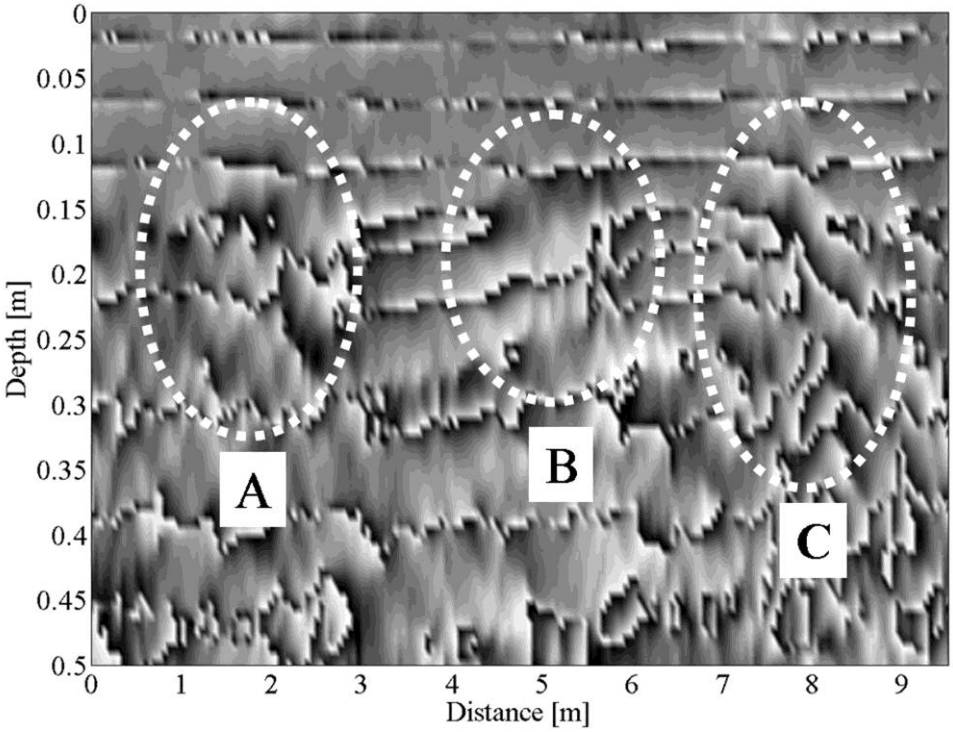

(b) Instantaneous phase

Fig.5.3.3. B-scan images;

Profile-4 acquired along NS direction dashed circles indicates reflections from tile and bricks ($v = 0.13 m/ns$)

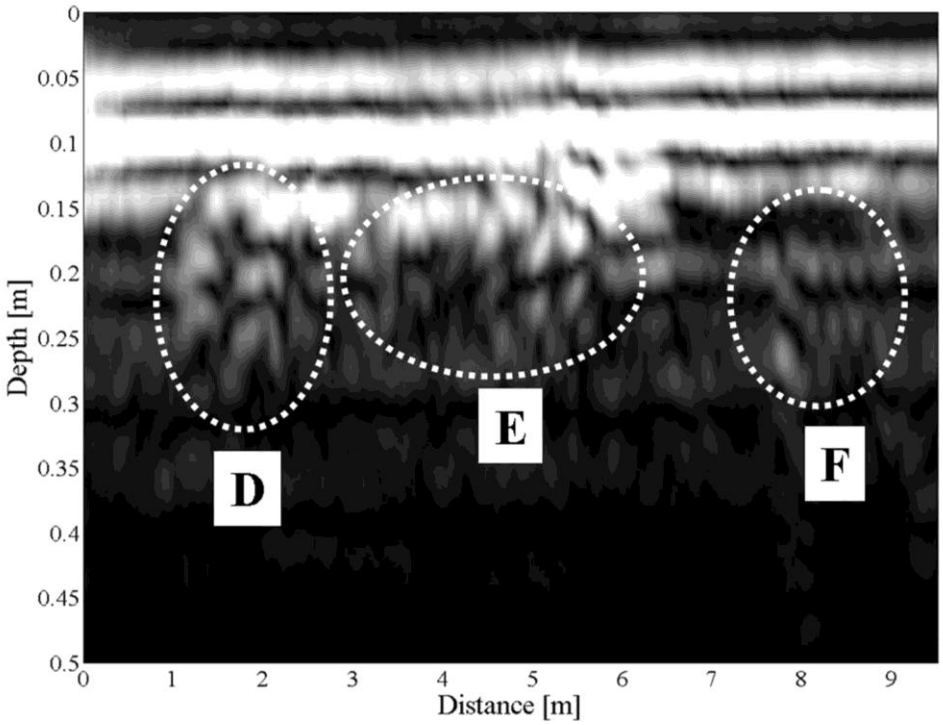

(a) Instantaneous amplitude

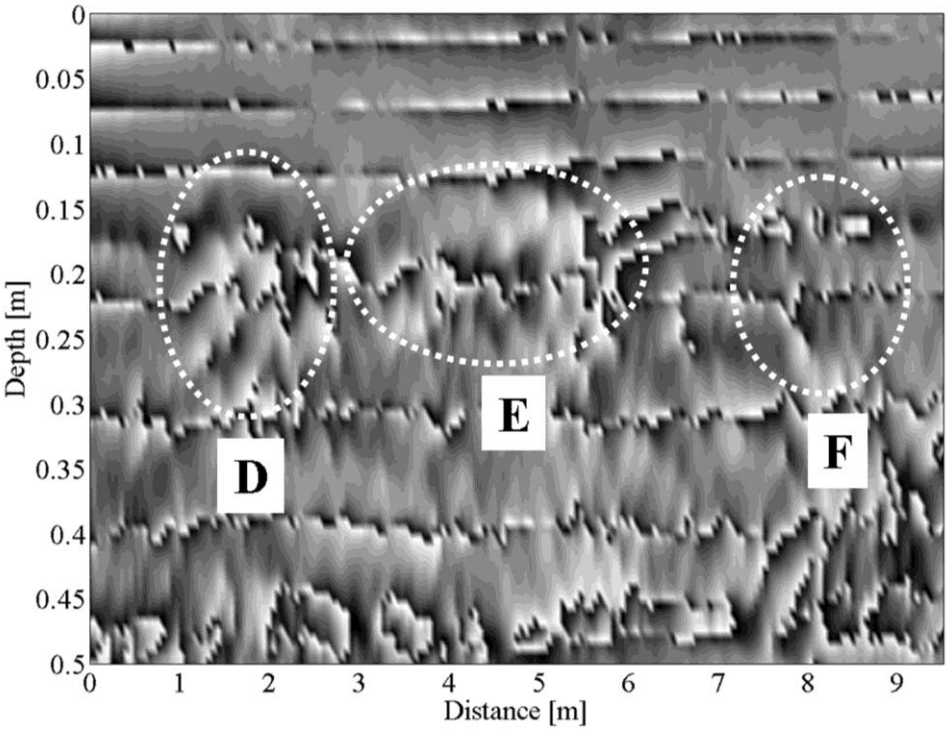

(b) Instantaneous phase

Fig.5.3.4. B-scan images;

Profile-10 acquired along NS direction dashed circles indicates reflections from tile and bricks ($v = 0.13 m/ns$)

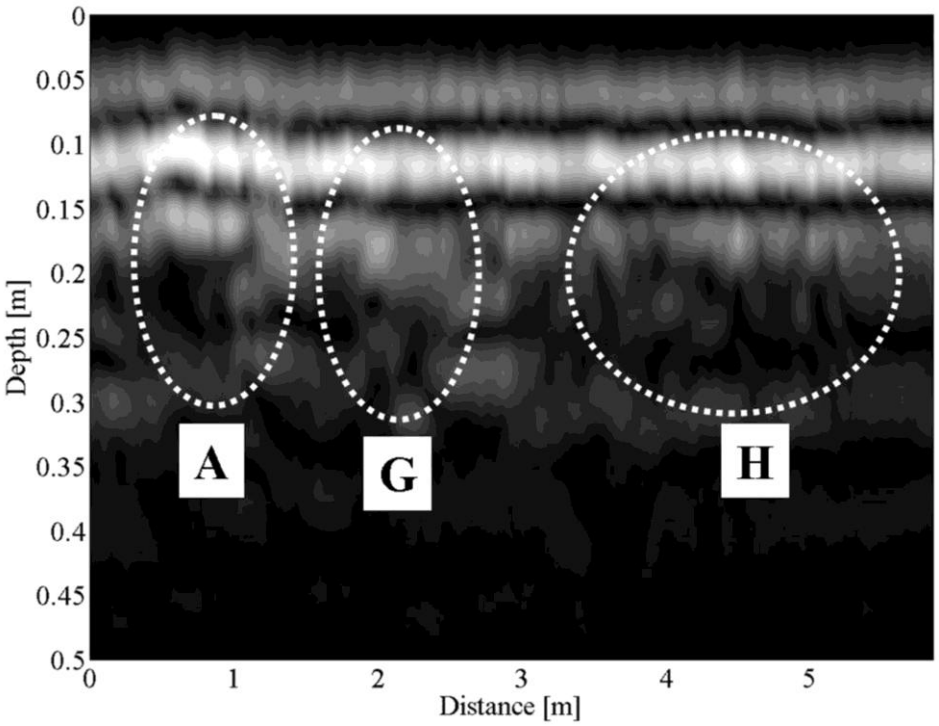

(a) Instantaneous amplitude

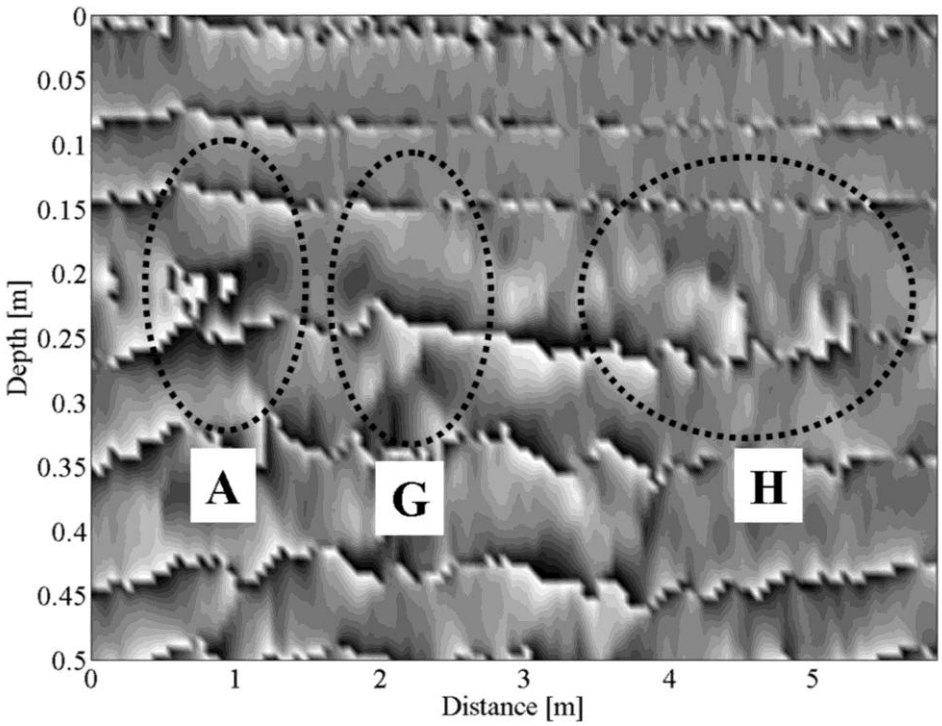

(b) Instantaneous phase

Fig.5.3.5. B-scan images;

Profile-19 acquired along WE direction

dashed circles indicates reflections from tile and bricks ($v = 0.13 m/ns$)

5.2.3.2. C-SCAN IMAGE

In order to visualise the anomaly, amplitude slice maps were created from the processed data. A GPR horizontal amplitude analysis has the ability to extract the short-wavelength reflected signal from the background noise and display it in a form that is useful for interpretation. Two-way travel times were converted to depth, using a velocity of 0.13 m/ns. Amplitude slice-maps were constructed in 2 cm horizontal slices across the surveyed area. The horizontal slice display detected many anomalies, which are not easy to interpret in terms of structures because of their indistinct shape. There might be changes in the electromagnetic impedance and therefore to the continuity in the geometries on the horizontal slices.

Fig.5.3.6 shows a GPR horizontal slice map at 15cm for data from the north-south direction surveys. The horizontal slices were used to analyze the effects on image quality of the distance between profiles and the profile direction with respect to anomaly location. Analysis of the anomalies detected detected with the horizontal slices (anomalies A-H) provided accurate results for detecting intensity, discontinuity and geometry along vertical GPR profiles. Analysis of the instantaneous amplitude and instantaneous phase maps gives significant additional information for target detection.

The amplitude map at a depth of from 0.15 to 0.21 m in Fig.5.3.7 might be used to explain a correlation between amplitude changes, distribution and geometry of the target at different depths. The horizontal slices were used to analyze the effects on image quality of the distance between profiles and the profile direction with respect to anomaly location. The advantage of using the two GPR orthogonal survey directions of the horizontal slice map is a more accurate and detailed geometry of the archaeological structure at different polarisations. A dashed white rectangular line in Fig.5.3.7 indicates room of the castle, and it matched in horizontal slice maps for the two orthogonal survey directions.

When the plane of polarisation of the transmitted wave radiation is parallel to the dominant plane of linear features, the polarised radar return will be stronger than the signal received when transmitting in an orthogonal plane. A good correlation is observed for the alignments of reflections using different polarisations, as shown in Fig.5.3.7. However, more reflections appear in the north-south survey direction than

in the west-east direction. This is due to the electric field orientation, which is in the horizontal plane for north-south survey directions, and the stronger horizontally polarised component of the backscattered energy is recorded.

By viewing appropriately combined horizontal slices maps from orthogonal survey directions, it was possible to examine detailed 3D geometries of the brick, masonry and tile structures.

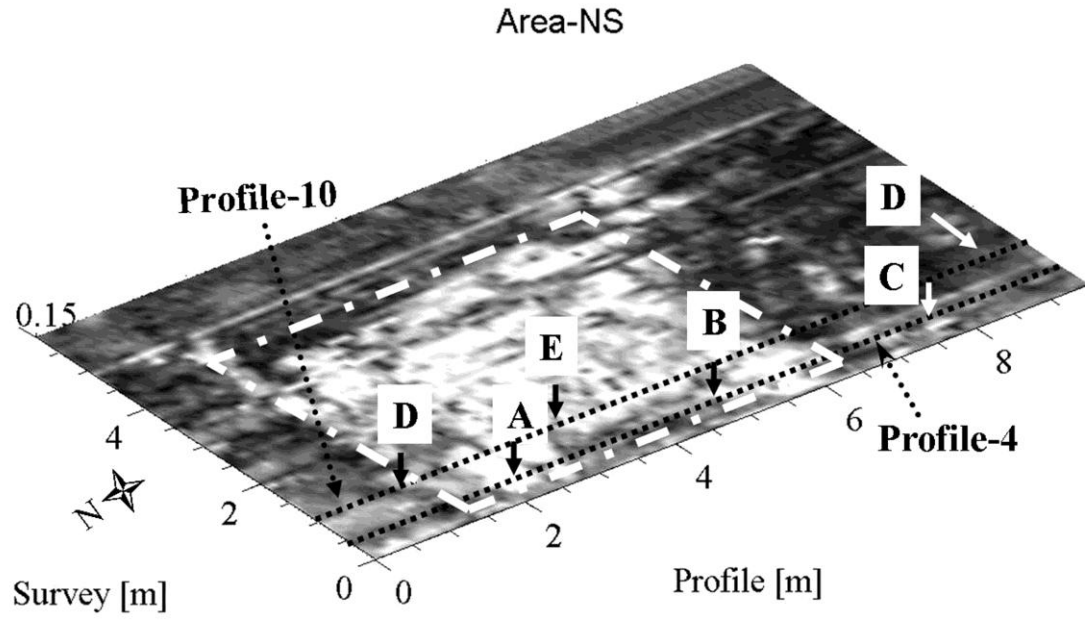

(a) Horizontal slice obtained along NS survey direction

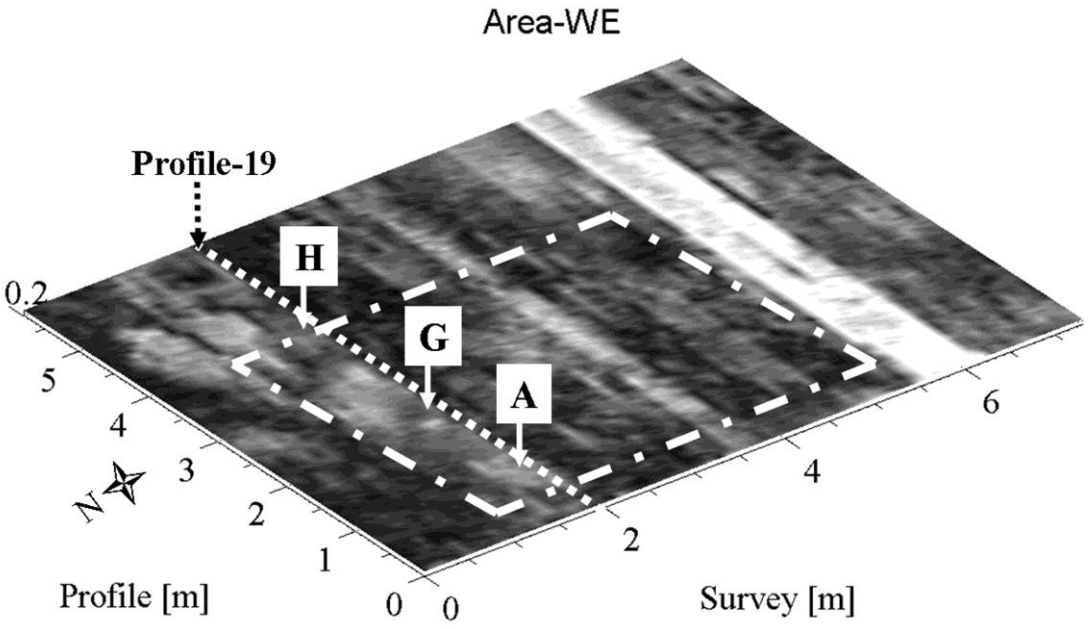

(b) Horizontal slice obtained along WE survey direction

Fig5.2.6. Instantaneous amplitude C-images at 15cm depth ($v = 0.13 m/ns$)

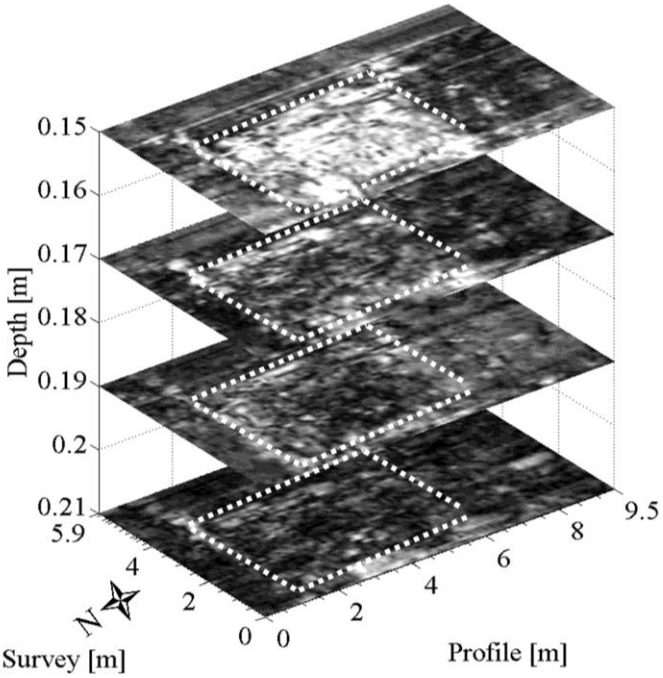

(a) Horizontal slice maps obtained along NS survey direction

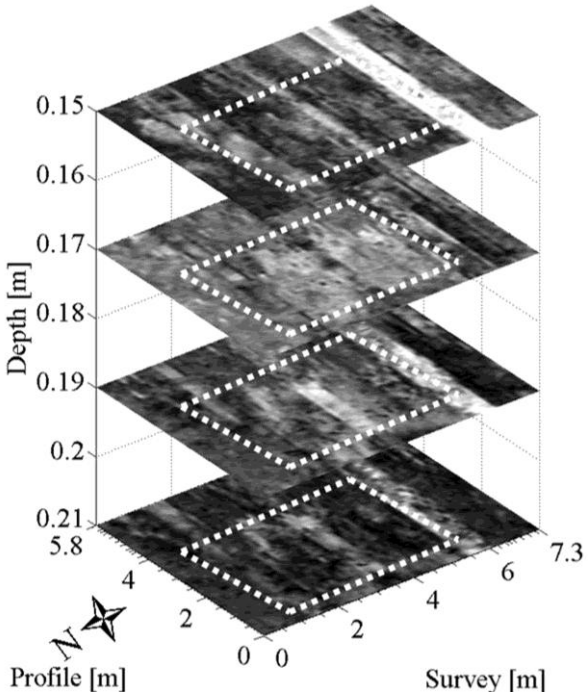

(b) Horizontal slice maps obtained along WE survey direction

Fig5.2.7. Instantaneous amplitude C-images from 15cm to 21cm depths

($v = 0.13m/ns$)

5.4. EXPERIMENT-2.

CIVIL ENGINEERING APPLICATION

In previous section we have discussed results of GPR data obtained by commercial RAMAR/GPR system. In order to apply some polarimetric processing we integrate 2 orthogonal survey directions dataset. But it was quite difficult to integrate 2 datasets obtained by commercial RAMAR/GPR system due to adjust the coordinate.

In this experiment we used a high resolution new 3D-GPR, which is a combination between commercial GPR and rotary laser position system (RLPS) developed by Miami University. The laser positioning enables acquisition of centimeter accurate x, y, and z coordinates from multiple small detectors attached to moving GPR antenna. Positions streaming with 20 updates/second from each detector are fused in real-time with the GPR data. Rotary laser positioning has the flexibility to be integrated with multiple moving GPR antenna and other geophysical sensors enabling simple and efficient high resolution 3D data acquisition at different GPR frequencies and polarizations. Fig.5.4.1 shows principles and schematic diagram of the new 3D GPR system.

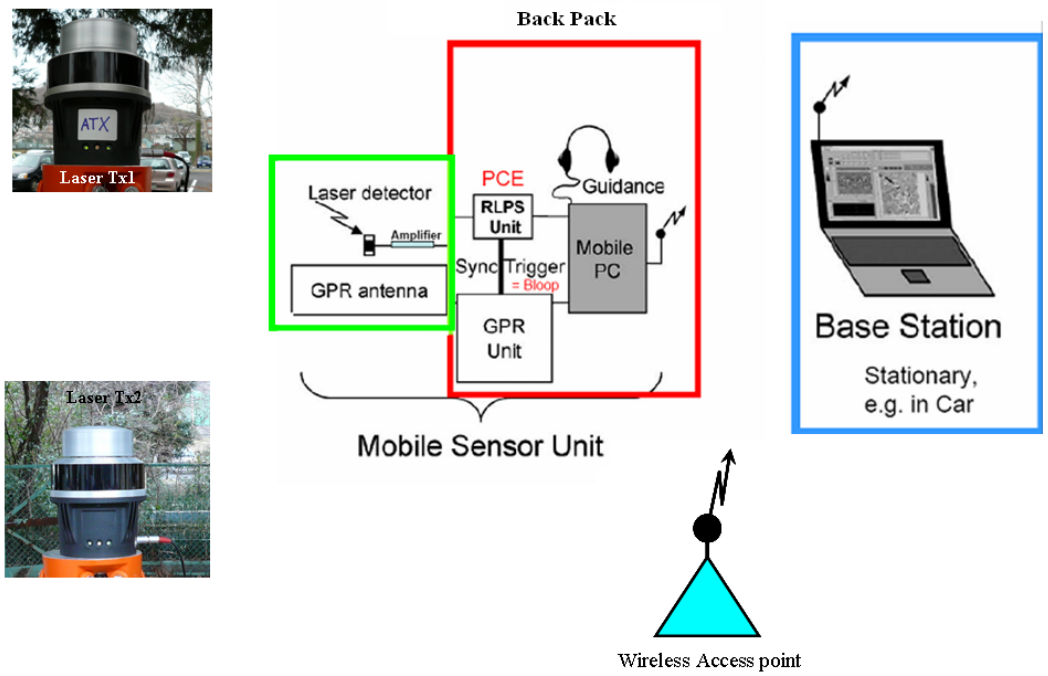

Fig.5.4.1 Schematic diagram of the new 3D GPR system

The stationary base station computer wirelessly links to the mobile sensor unit controlling both GPR and RLPS. There are no long cables connecting the mobile sensor unit to the base station. This allows the person moving the antennas to concentrate on the terrain without being distracted by cable management or checking a computer screen. The GPR and PLPS electronics are connected to the mobile computer via parallel (GPR) and serial (RLPS) port. The trigger link between GPR and RLPS is for data synchronization purposes.

5.4.1. GPR DATA ACQUISITION

Graduate School of Environmental studies of Tohoku University is planning to have a new building behind the main building. It was great chance to measure and to make comparison 2 different orthogonal directions using a high resolution new 3D-GPR.

Laser positioning system enables acquisition of millimeter accurate coordinates from a small detector attached to the moving GPR antenna as shown in Fig.5.4.2. The position data streaming with 20 update/second were fused in real time with the GPR antenna is automatically guided by LED array elements.

The survey area of 10.5 m × 10m area was covered with 101 parallel GPR lines spaced by 10cm recording a GPR trace ever 5cm in order to obtain 3D GPR surveys. Both orthogonal direction GPR measurements used the same shielded 250MHz RAMAC/GPR antenna and the experiment area shown in Figure 5.4.3.

Two antenna configurations were considered in this study: perpendicular broadside (YY) and parallel broadside (XX). Objective of this experiment was to detect buried object by dual polarization radar measurement.

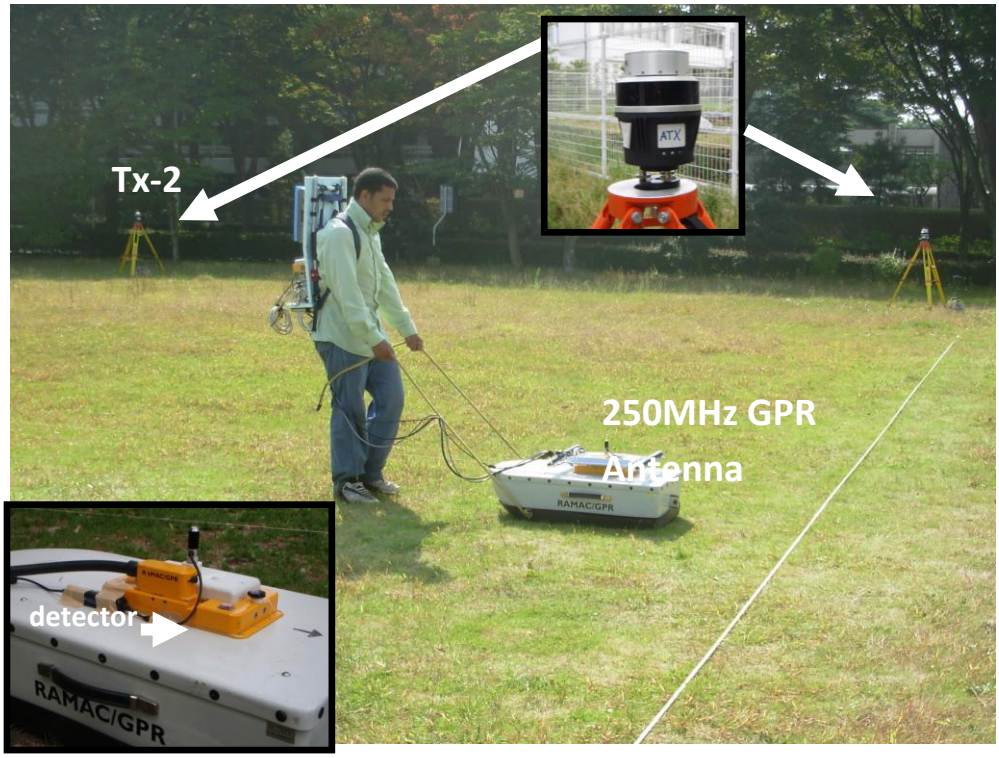

Fig.5.3.2. Data acquisition by 3D GPR with PLPS;
Two rotating laser transmitters (Tx1, Tx2) emit pulse sequences received by the laser detector mounted on the GPR antenna

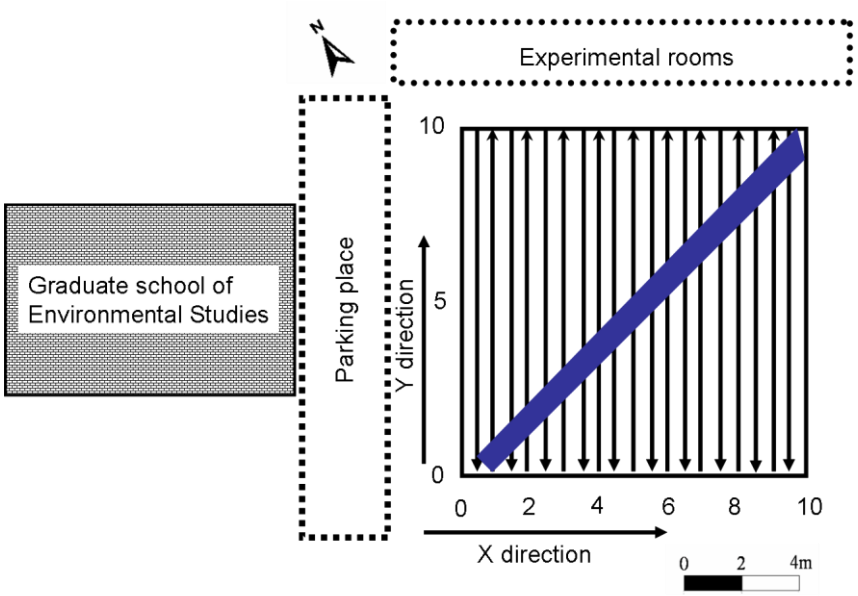

Fig.5.3.3. Sketch map of 3D GPR experiment; blue line indicates location of buried pipe

5.4.2. SIGNAL PROCESSING RESULT

Compare to previous archaeological dataset we could obtain more precise GPR data sets using new GPR with IGPS system. In that case we could obtain dual polarization measurements in horizontal and vertical polarization.

The data processing consists of the following steps: The “Fuse” module continuously reads the raw GPR and RLPS files while they were generated during the survey. Data fusion assigns x, y and z laser coordinates to each radar trace by interpolation between the two nearest available RLPS points, based on the laser-detector clock time when the trace was acquired. The “Dewow” step removes the low frequency components of the data associated with the system dependent noise.

The results of two different orthogonal direction measurement 3D imaging have been presented in Fig.5.4.4. Horizontal slices at depths of around 35cm contain the signature of the pipe and dotted white line indicates location of the target. The amplitudes of the images resulting from 2 different orthogonal direction horizontal imaging of the oblique pipe were large amplitude. This is probably caused by data which has its maximum response when both antennas are oriented almost at a 45° angle to the pipe.

When the plane of polarisation of the transmitted wave radiation is parallel to the dominant plane of linear features, the polarised radar return will be stronger than the signal received when transmitting in an orthogonal plane. A good correlation is observed for the alignments of reflections using different polarisations, as shown in Fig.5.4.4.

The Hilbert transformation is applied in 3D GPR dataset. In Fig.5.4.5 represented the result of the phase images obtained by Hilbert transformation. Phase changes provide strong evidence for sharp and discrete discontinuities there. Instantaneous phase map illustrated distinguishable phase changes due to pipe and ground soil. From this phase image we could identify the pipe orientation.

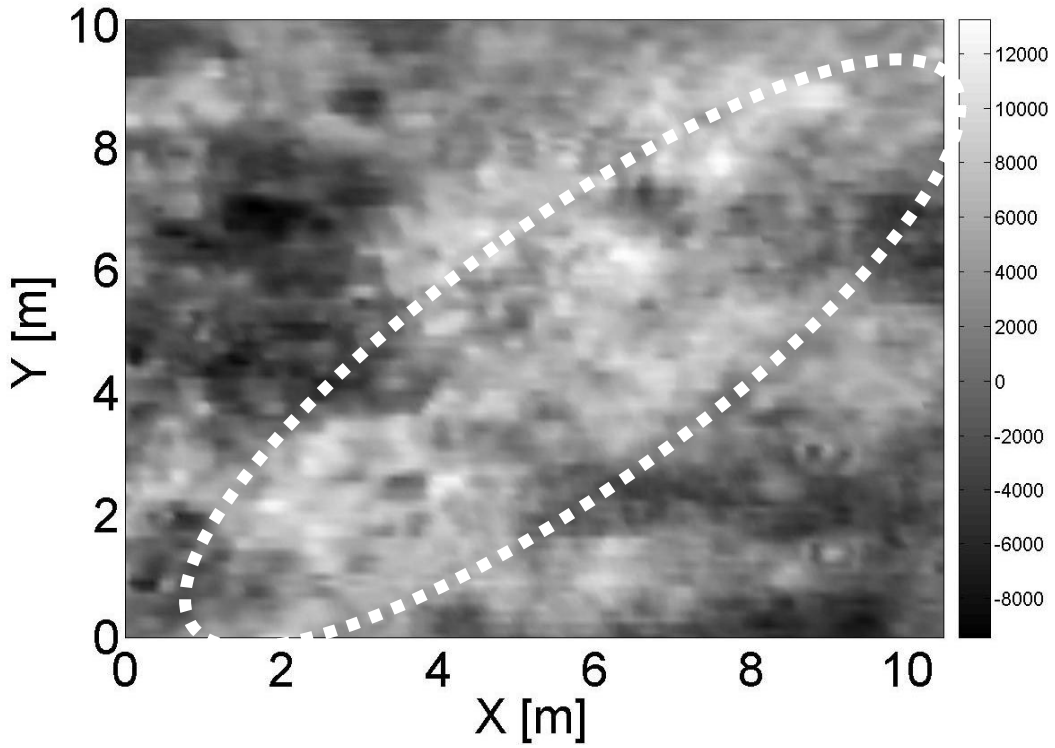

(a) XX polarization

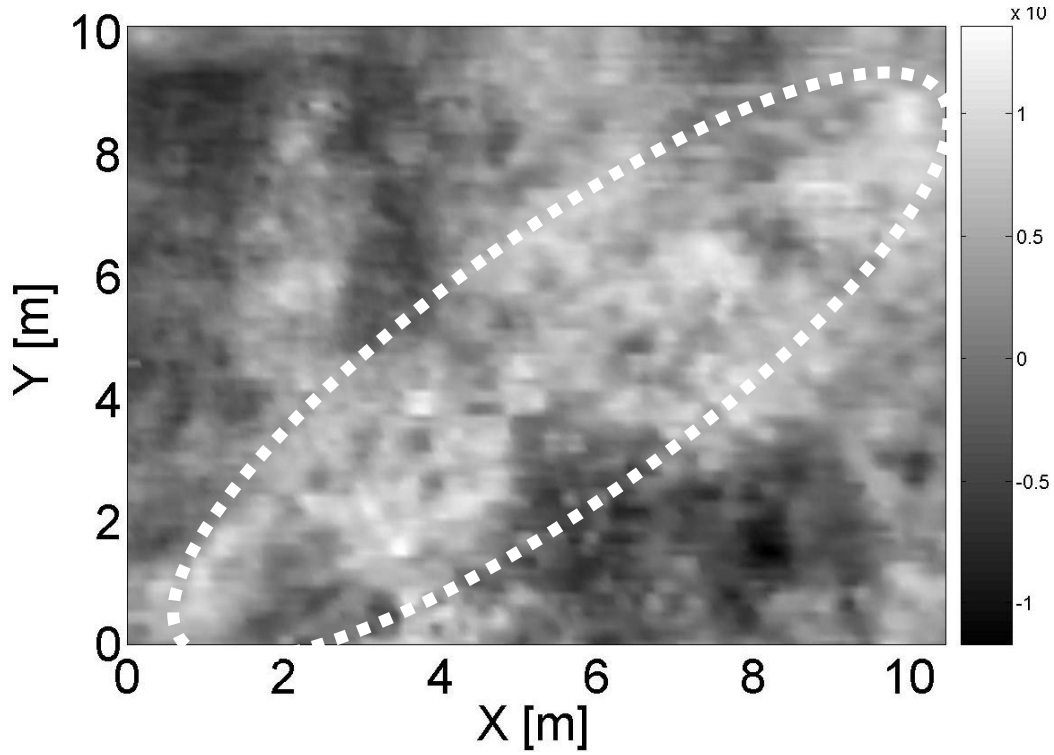

(b) YY polarization

Fig.5.4.4. C-scan images of 3D GPR in 2 different orthogonal directions at 35 cm depth; dotted white lines indicates location of pipe

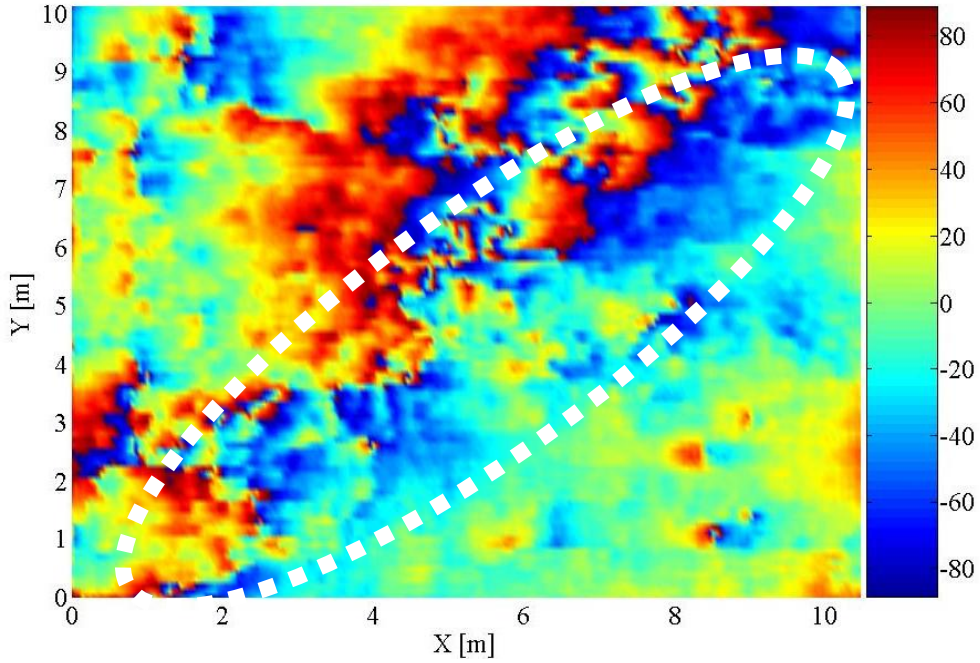

(a) XX polarization

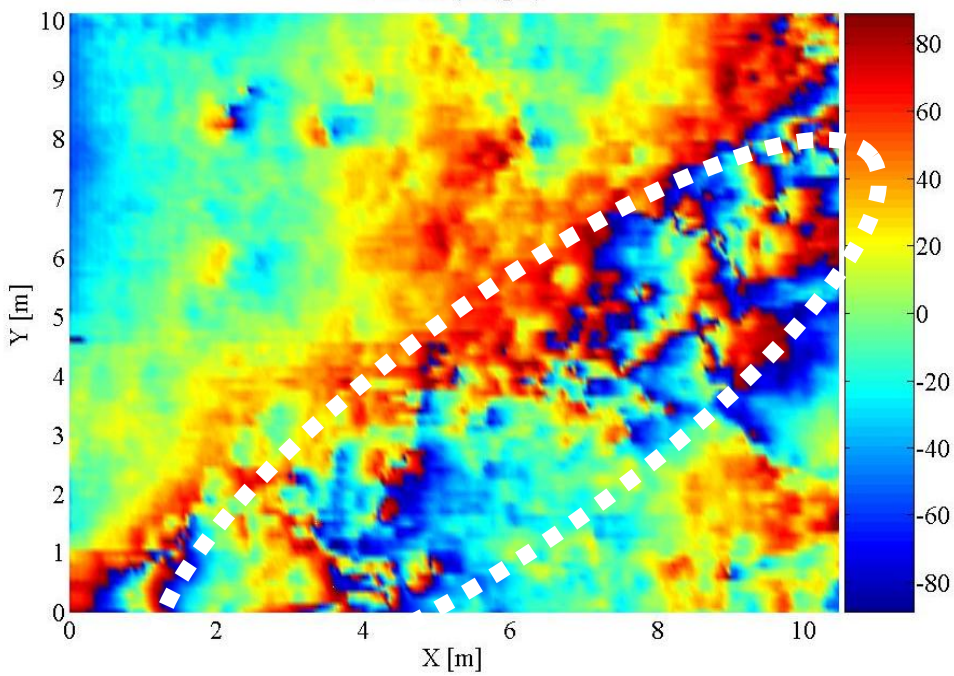

(b) YY polarization

Fig.5.4.5. Phase images obtained by Hilbert transformation;
Dotted white line indicates location of target

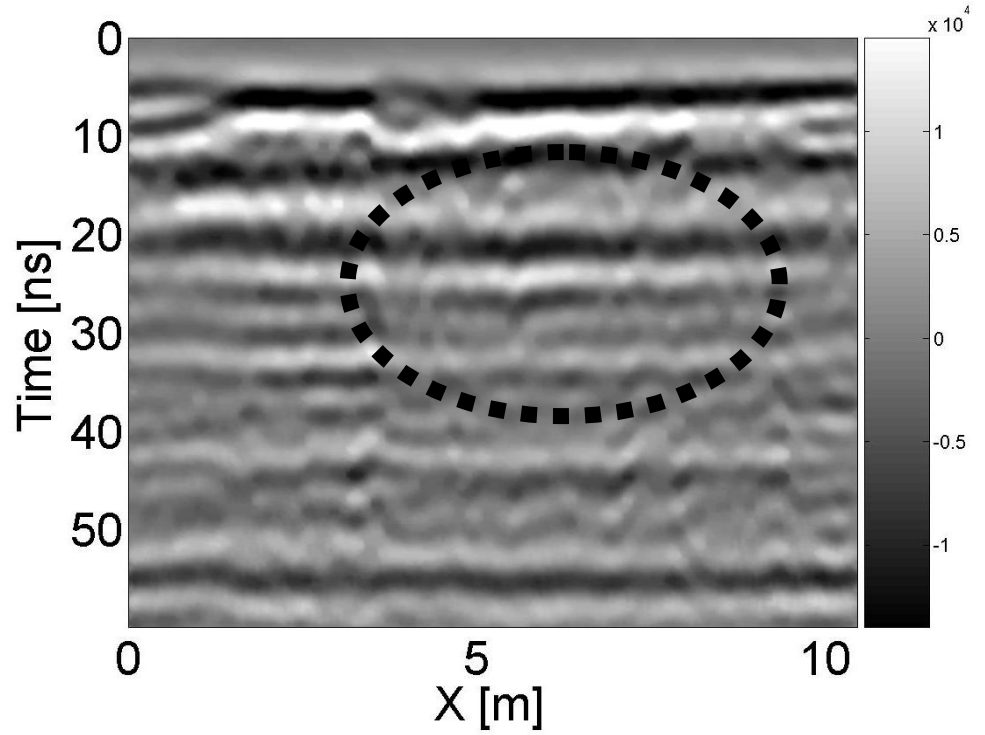

(a) XX polarization

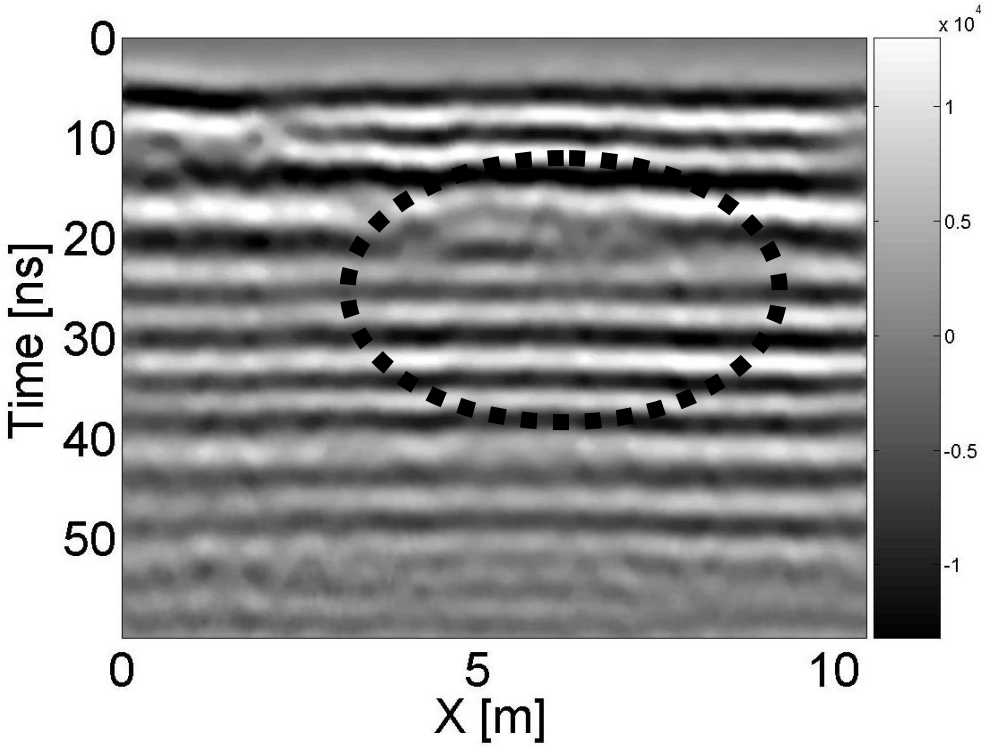

(b) YY polarization

Fig.5.4.6. B-Scan images extracted from 3D GPR imaging;

Dotted black line indicates hyperbola, where is representing location of the target

Reflexw was used to for processing and visualizing the 2D GPR parallel profiles to extract the subsurface horizontal time (C-scan) slices. In order to keep the horizontal slice as close as the slice created from the 3D GPR care was taken to exactly process the 2D GPR data with the same processing steps as described in the 3D GPR processing. Fig.5.4.6 is B-scan images extracted from C-scan image. In this figure B-scan represent Profile-6, acquired in the XX and YY survey directions. The purpose of selecting these profiles was to evaluate the intensity and detecting discontinuity of the signals at the different polarization. The target response is shown clear by hyperbolic reflection. Judging by the shape and the width of the reflections, the moderate to high intensity response in instantaneous amplitude corresponds to pipe. Comparing C-scan and B-scan we can get more information about location of the target, orientation and other properties.

5.4.2.1. DATA INTERPRETATION

- **C-SCAN IMAGE**

If we acquired GPR dataset in two different orthogonal direction and precise coordinate system, we could apply some polarimetric processing to experiment datasets. For dual polarization case Stokes matrix algorithm is more suitable.

Application of the Stokes matrix image processing techniques provides a method for extracting the target polarimetric reflected properties for enhancing target detection and identification. Although the algorithm for image processing is relatively simple, it provides good results for enhancing target delectability.

In response to quasi-monochromatic illumination of a known polarization, the total power of the backscatter will have two components; unpolarized and polarized. The polarized component can be presented with two orthogonal polarizations, which traditionally are expressed in terms linearly polarized basis vectors. For a given incident polarization, the Stokes parameters of the backscattered field, expressed in linear polarization basis, are given by Eq.4.3.1.

Several useful measures follow the Stokes formalism for coherent dual polarized radar data. In particular one may calculate the degree of polarization. The orientation of the effective polarization ellipse is given by

$$\theta = \frac{1}{2}\tan^{-1}\left(\frac{S_2}{S_1}\right)$$

We have successfully applied the Stokes matrix image processing technique to full polarimetric GPR data. For 3D GPR/RAMAC with iGPS system measurement case we could not obtain cross polarization state. That is why Stokes matrix image processing technique is more suitable to target identification and recognition of target shape and orientation.

Fig.5.4.7 shows images processed by Stokes matrix images S_1, and S_2. For S_1 case it equal to power of horizontal or vertical polarized component. Even this target is still detectable. It is related to target orientation. S_2 –is equal to the linear polarized component at orientation angles θ=45° or θ=135°. It is coincide result of C-scan raw image and phase image processed by Hilbert transformation. Comparing the raw and phase C-scan images with Stokes matrix processing technique gives quite useful information related for target identification. Applying Stokes matrix technique we could decrease clutter information.

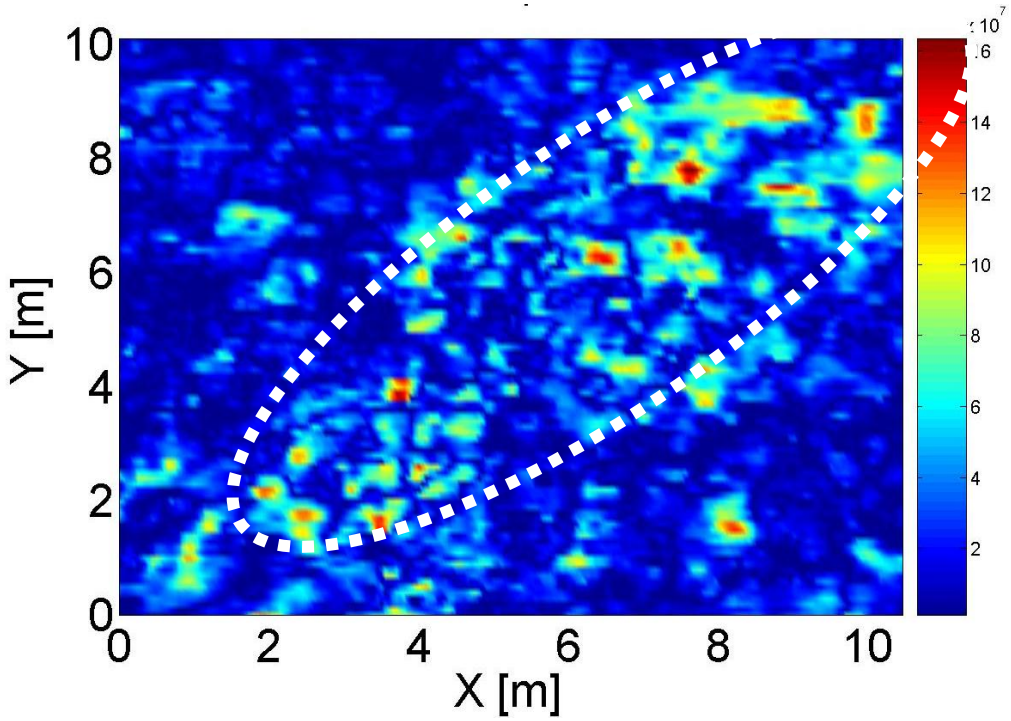

(a) S_1 image processed by Stokes matrix

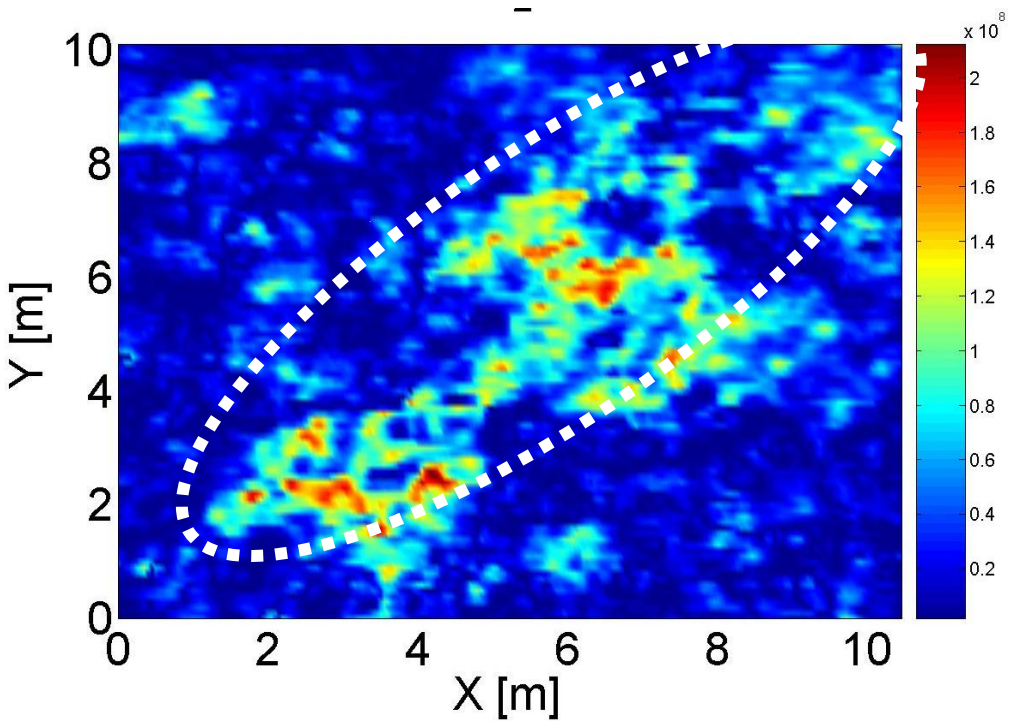

(a) S_2 image processed by Stokes matrix

Fig.5.4.7. Polarimetric images processed by Stokes matrix;
Dotted white line indicates location of the target

5.5. SUMMARY

Polarization analysis of 3D GPR datasets for two different orthogonal directions has been presented. Polarization analysis applied two different applications.

Fist section this chapter discussed polarization analysis for archaeological application. We applied the 3D GPR imaging method to detect and locate anomalous zones that could be associated with buried structures. Instantaneous phase map gave information about the location of targets, edge appearing as discontinuities of the signal. In order to enhance our ability to interpretation the archaeological targets and to recognise major reflections, we compared the GPR datasets acquired in two orthogonal survey directions. A good correlation is observed for the alignments of reflections acquired in the two directions.

3D GPR imaging has successfully mapped the 13th-century "Van Khan Tooril's" castle.

Second section covered by civil engineering application experiment. In order to apply some polarimetric processing we need to integrate 2 orthogonal survey directions dataset to adjust precise coordinate. In this section we described principles of a high resolution new 3D-GPR system. Also we present experiment results of GPR dataset acquired by new GPR system and result of polarimetric analysis processed by Stokes matrix algorithm.

CHAPTER 6

CONCLUSION

The main objective of this research work was to examine the application possibility of polarimetric GPR for detection and identification of subsurface objects at shallow depths. A number of new developments of in the theory of electromagnetic scattering from buried targets and in GPR data processing were necessary to perform at shallow depths target identification. This dissertation presents description of polarimetric GPR system, calibration of system, some polarimetric signal processing algorithm and application of signal processing algorithm in experimental data. This work involves proposal of polarimetric decomposition algorithms to improve the target detection and identification at shallow depths. A review of the results is presented in the following.

- In this research work, polarimetric GPR system, which was developed by the Sato Laboratory at the Tohoku University, Japan is proposed and evaluated for the detection and discrimination of the target at shallow depth. Polarimetric GPR system is stepped frequency continuous wave radar systems operates in frequency domain. The Polarimetric radar system consists of a Vector Network Analyzer (VNA), a transmitter and a receiver Vivaldi antenna array, an antenna positioner unit, switcher and a PC based control unit. The network analyzer operated in a stepped frequency continuous wave mode, was used to generate the transmitting signal and to detect scattered signals both in amplitude and phase.
- A linear wire is one of the fundamental targets in radar polarimetry. A metal wire was buried and placed with a different orientation with respect to survey lines. In order to identify the target shape, polarimetric detection was examined to target a long metal wire, whose length is 3m. Using for known target we can understand and interpreted behavior of electromagnetic wave and scattering mechanism. Mainly we focused how we will acquire precise measurement using polarimetric GPR.

- In Chapter 3 presents principles of polarimetric GPR and performance measurements of polarimetric system. It contains the results of performance test. In the last part of this chapter, we discussed a polarimetric calibration algorithm and the obtained results from its use. We applied a calibration algorithm using three in-scene reflectors based on the exact solution for general targets developed by S.H.Yueh and J.A.Kong. Compared to the theoretical value, the difference was ~2dB in cross polarization state, and ~3dB in co-polarization state. As for the phase, we obtained a cross polarization phase difference of ~20 degrees and co-polarization phase difference of ~16 degrees. As evaluations of polarimetric effects, we compared cross-talk and gain balance at the metal wire. Based on the cross-talk and gain balance at oriented wire in both uncalibrated and calibrated data, we can recognize about 20dB improvement in cross talk and 3dB gain balance improvement as well. Results show how full polarimetric calibration improves the accuracy of scattering measurements.
- The key point of polarimetric GPR data is that measurements are carried out at multiple frequencies and polarizations. The obtained multidimensional information allows the identification of different scatterers via discrimination of different scattering mechanisms. In experiment we buried target at 5cm. That is why detection of object on the ground or buried very close to the ground surface is challenging problem because of the high reflectivity due to the air-ground interface. The reflection of the target is contaminated with ground reflections.
- Chapter 4 is used as a basis to determine the sensitivity to a possible detection from a certain objects. This, together with the fact that the largest reflections occur when the polarization of the electric field is parallel to the object causing reflection, shows how the sensitivity to subsurface reflections can be increased. On the other hand, these results show how to reduce the sensitivity to unwanted reflections coming from objects on or above the surface. The concept of the target polarization basis changes has been tested using polarimetric data acquired over a buried metal wire and demonstrated the capability to accurate recover the target response signals, which would have the measured if the wire had been oriented with its preferential scattering axis aligned with antenna system. We represented the result of line of sight technique for experiment dataset, where target is oriented 0 and 45 degrees. As a result we could obtain more useful information related to the physics of scattering matrix. In last part of Chapter 4 we addressed the result of several buried objects with different

orientations. Target decomposition techniques have been applied in various domains, providing a wealth of useful information about how target where is buried at shallow depth is seen by polarimetric radar. 3D reflectivity images obtained by polarimetric GPR experiments have been employed, together with decomposition techniques, for identifying the position, orientation and characteristics of the scattering mechanism in the buried target. In order to extract clear information of target, we applied the H/A/α eigenvalue based TD and Huynen-Kennaugh TD for simple case.

- Polarization analysis of 3D GPR datasets for two different orthogonal directions has been presented in Chapter 5. Polarization analysis applied two different applications. First section this chapter discussed polarization analysis for archaeological application. We applied the 3D GPR imaging method to detect and locate anomalous zones that could be associated with buried structures. Instantaneous phase map gave information about the location of targets, edge appearing as discontinuities of the signal. In order to enhance our ability to interpretation the archaeological targets and to recognize major reflections, we compared the GPR datasets acquired in two orthogonal survey directions. A good correlation is observed for the alignments of reflections acquired in the two directions. 3D GPR imaging has successfully mapped the 13th-century "Van Khan Tooril's" castle. Second section covered by civil engineering application experiment. In order to apply some polarimetric processing we need to integrate 2 orthogonal survey directions dataset to adjust precise coordinate. In this section we described principles of a high resolution new 3D-GPR system. Also we present experiment results of GPR dataset acquired by new GPR system and result of polarimetric analysis processed by Stokes matrix algorithm.

APPENDIX 1

A.1. Hilbert transformation

The Hilbert Transform (HT) has traditionally been used in both theory and practice of signal processing. The classic approach for estimating instantaneous parameters relies on using the Hilbert Transform. The HT method extracts the instantaneous parameters by comparing the imaginary part with the real part of an analytical signal [27], [30], [31]. Therefore, the corresponding analysis is also called complex trace analysis. HT is relationships between the real and imaginary components of a complex sequence. The complex trace $f(t)$, is defined as:

$$f(t) = f_r(t) + jf_i(t) \tag{A.1}$$

where $f_r(t)$ and $f_i(t)$ are real and imaginary sequences. The real trace $f_r(t)$ is the already available GPR trace. The imaginary trace $f_i(t)$ is the HT of the real GPR trace. The HT is basically a special filter that shifts the phase of all positive frequencies of an input signal by -90° and all negative frequencies by +90°. Therefore, the Fourier Transforms $F_r(e^{j\omega})$ and $F_i(e^{j\omega})$ are directly related by

$$F_i(e^{j\omega}) = H(e^{j\omega})F_r(e^{j\omega}) \tag{A.2}$$

Where

$$H(e^{j\omega}) = \begin{cases} 2F_r(e^{j\omega}) & 0 \le \omega < \pi \\ 0 & -\pi \le \omega < 0 \end{cases} \tag{A.3}$$

and

$$F(e^{j\omega}) = \begin{cases} 2jF_i(e^{j\omega}) & 0 \le \omega < \pi \\ 0 & -\pi \le \omega < 0 \end{cases} \tag{A.4}$$

where $F(e^{j\omega})$ -is the Fourier transform of the complex trace. Therefore, a kind of "causality" is applied to the Fourier Transform of the complex trace sequence:

$$F(e^{j\omega}) = 0 \quad -\pi \le \omega < 0 \tag{A.5}$$

The magnitude sequence $A(t)$ is given by

$$A(t) = \sqrt{f_r^{\,2}(t) + f_i^{\,2}(t)} \tag{A.6}$$

and is called the instantaneous amplitude. It is the envelope of the complex trace sequence $f(t)$. It may have its maximum at phase points other than peaks or troughs of the real trace especially where an event is a composite of several reflections. The magnitude of the complex trace is a measure of the total energy involved in the GPR reflection response. The instantaneous phase is given by

$$\theta(t) = \tan^{-1}\left[\frac{f_i(t)}{f_r(t)}\right] \tag{A.7}$$

and emphasizes the continuity of the events. It often makes weak coherent events clearer.

By deriving the instantaneous parameters from the GPR data, we extract more accurate information about targets, such as their distribution. Instantaneous parameters such as the instantaneous amplitude, phase and frequency are directly related to geometry and physical property variations of the medium through which the radar signal propagates. HT will decompose a radar signal, represented as a time series, into its magnitude, instantaneous phase, or instantaneous frequency component. HT expresses the relationship between the magnitude and phase of a signal, or in other words, differentiates between its real and imaginary parts [30], [31].

BIBLIOGRAPHY

[1] Ainsworth, T. L., "Eigenvector Analysis of Polarimetric SAR Data", Pro. Geoscience and Remote Sensing Symposium, IGARSS 02. vol.1, pp.626-628, 2002.

[2] Bickel, S. H., "Some invariant properties of the polarization scattering matrix", Pro. IEEE, vol.53, pp.1070-1072,1965.

[3] Boerner, W.M., Mott, H. et al., "Polarimetry in Radar Remote Sensing; Basic and Applied Concepts", Chapter 5 in Hendersen, F.M. and Lewis, A.L. (eds.), Principles & Applications of Imaging Radar, Vol. 2 of Manual of Remote Sensing, New York, 1988.

[4] Boerner, W.M., and Cloude, S. R., "Radar Polarimetry and Interferometry: Past, Present and Future Trends", Chapter 5 in Hendersen, F.M. and Lewis, A.L. (eds.), Principles & Applications of Imaging Radar, Vol. 2 of Manual of Remote Sensing, New York, 1988.

[5] Bourgeois, J. M., and Smith, G. S., "A fully three-dimensional simulation of a ground penetrating radar: FDTD theory compared with experiment", IEEE Trans. Geoscience and Remote Sensing. Vol.34, pp.36-44, 1996.

[6] Cohen, L., "Time-frequency analysis", Prentice Hall PTR, Englewood Cliffs, New Jersey, 1995.

[7] Conyers, L. B., "Moisture and Soil Differences as Related to the Spatial Accuracy of GPR Amplitude Maps at Two Archaeological Test Sites", 11th International Conference on Ground Penetrating Radar, ARC.1, 435-438, 2004.

[8] Conyers, L. B. and Goodman, D., "Ground Penetrating Radar: An Introduction for Archaeologists", Altimira Press, Walnut Creek, 1997.

[9] Conyers, L. B. and Osburn, T., "GPR Mapping to Test Anthropological Hypothesis: A Study from Comb Wash, Utah, American Southwest", 11th International Conference on Ground Penetrating Radar, Extended Abstracts, 2006.

[10] Cloude, S. R,.. and Pottier. E., "A review of target decomposition theorems in radar polarimetry", IEEE Trans.Geocience and Remote Sensing, vol.34, pp.498-518,1996.

[11] Cloude, S. R.., Papathanassiou, K P., "Polarimetric SAR Interferometry", IEEE. Transactions on Geoscience and Remote Sensing, Vol 36. No. 5, pp 1551-1560.

[12] Eriksson, L. B., "Satellite-borne L-band Interferometric Coherence for Forestry Applications in the Boreal Zone", Ph.D. thesis, Friedrich-Schiller University Jena, Germany, 2004.

[13] Feng, X. and Sato, M., "Pre-stack migration applied to GPR for landmine detection", Inverse Prob., vol. 20, pp. 99-115, 2004.

[14] Feng, X, and Jin, Y. Q., "Numerical Simulation of Targets Deorientation and Its Application to Unsupervised Classification in Polarrimetric SAR images", Pro., In Electromagnetics Research Symposium, pp. 364-368, 2005.

[15] Gader, P. D., Mystkowski, M., and Zhao, Y., "Landmine detection with ground penetrating radar using Hidden Markov Models", IEEE Trans. Geo-science and Remote Sensing, vol. 39, pp.1231-1244, 2001.

[16] Gazdag, J., “Wave equation migration with the pulse shift method”, Geophysics, vol. 43, pp.1342-1351, 1978.

[17] Grandjean, G., Gourry, J., and Bitri., “Evaluation of GPR techniques for civil-engineering applications: study on a test site”, Journal of Applied Geophysics, vol. 45, no. 3, pp. 141-156, 2000.

[18] Graves, C.D., “Radar polarization power scattering matrix”, Pro.Ins.Radio Engrs, vol.44, pp.248-252, 1956

[19] Hamasaki, T., “Polarimetric Three-Dimentional Imaging”, PhD thesis, Tohoku University, 2005.

[20] Helloco, Y. L., Priou, L., Uguen, B., and Chassay, G., “A study of the desying process of a radar target applied to A critical analysis of the meaning and the sensibility of some measured Huynen parameters”, Microwave and Optical Technology, vol.14, pp.191-196, 1997.

[21] Helloco, Y. L., Priou, L., Uguen, B., and Chassay, G., “A study of the desying process of a radar target applied to A critical analysis of the meaning and the sensibility of some measured Huynen parameters”, Microwave and Optical Technology, vol.14, pp.191-196, 1997.

[22] Huynen,J.R., “A new extended target decomposition scheme”, Pro. Geoscience and Remote Sensing Symposium, IGARSS 94, vol.2, pp.1124-1125, 1994.

[23] Huynen,J.R., “Measurement of the target scattering matrix”, Pro. IEEE Trans, pp.262-271, 1981.

[24] Iizuka, K., Freundorfer, A., Wu, K., Mori, H., Ogura, H., and Hguyen, V., “Step Frequency Radar”, Journal of Applied Physics, vol. 56, no. 9, pp.2575-2583, 1984.

[25] Lanbo, L., "GPR signal analysis: Instantaneous parameter estimation using the wavelet transform", Proc. of the 7th International Conference on Ground Penetrating Radar, Extended Abstracts, 219–223, 1998.

[26] Lee, J. S., and Pottier, E., "Polarimetric Radar Imaging", 2009.

[27] Lu, Q., "Monitoring of Subsurface Environment by Ground Penetrating Radar", Ph.D. thesis, Tohoku University, 2002.

[28] Osella, A., de la Vega, M., and Lascano, E., "3D electrical imaging of an archaeological site using electrical and electromagnetic methods", Geophysics, **70**, G101–G107, 2005

[29] Olhoeft, G. R., "Application of Ground Penetrating Radar", In Proc. GPR'96, pp. 1-3, 1996.

[30] Qian, S., and Chen, D., "Joint Time-Frequency Analysis, Methods and applications" Prentice Hall PTR, New Jersey, 1996.

[31] Qian, S., "Introduction to Time Frequency and Wavelet Transformations", Prentice Hall PTR, New Jersey, 2002.

[32] Papathanassiou, K. P., "Polarimetric SAR Interferometry", PhD thesis, Technical University Graz, Germany, 1999.

[33] Peter, L., Daniels, J. J., and Young, J. D., "Ground Penetrating radar as a subsurface enviromental sensing tool", Proc, IEEE, vol.82, pp.1802-1822, 1994.

[34] Raney, R. K., "Dual Polarized SAR and Stokes Parameters", IEEE Geoscience and Remote Sensing, vol. 3, No. 3, pp. 317-319, 2006.

[35] Sciotti, M., Colone, F., Pastina, D., and Bucciarelli, T., "GPR for archaeological investigations; real performance assessment for different surface and subsurface conditions", in Proc. of IGARSS 03, pp. 2266-2268, 2003.

[36] Schnaider C. T., "Extension of the Huynen theory to bistatic coherent mechanism", Pro. Of the IEEE, pp.249-254, 1988.

[37] Stolt, R., "Migration by Fourier Transform", Geophysics, vol. 43, pp. 23-48, 1978.

[38] Streich, R., and van der Kruk, J., " Three-dimensional multicomponent georadar imaging of sedimentary structure", Near Surface Geophysics, **4**, 39-48, 2006.

[39] Shrestha, S. M., "High Resolution Signal Proceesing Technique for Ground Penetrating Radar Combining MUSIC and FFT Algorithms", PhD thesis, Tokyo University, 2004.

[40] Takahashi, K., "Detection and localization of subsurface objects by Ground Penetrating Radar", PhD thesis, Tohoku University, 2006.

[41] Tillard, S., "Radar experiments in isotropic and anisotropic geological formations (granite and schists)", Geophysical Prospectings, **42**, 615–636 doi:10.1111/j.1365-2478.1994.tb00232.x., 1993.

[42] Touzi, R., "Target Scattering Decomposition in Terms of Roll-Invariant Target Parameters", IEEE Trans. Geo-science and Remote Sensing, vol. 45, pp.73-84, 2007.

[43] Tseedulam, Kh., and Sato, M., "Evaluation of Van Khan Tooril's castle, an archaeological site in Mongolia, by Ground Penetrating Radar", Exploration Geophysics, vol.40, pp. 69-76, 2009.

[44] van Kempen, L., "Ground Penetrating Radar for Anti-Personnel Landmine Detection", PhD thesis, Vrije University Brussels, Belgium, 2006.

[45] van der Kruk, J., and Wapenaar, C., "Three-dimensional imaging of multicomponent ground penetrating radar data", Geophysics, **68**, 1241-1254, 2003.

[46] Yamaguchi. Y., "Radar Polarimetry from Basics to Applications: Radar Remote Sensing using Polarimetric Information" , Japan, 2007.

[47] Zhou, S. Z., "Application of a Ground-Based Polarimetric SAR system for Environmental Study", PhD thesis, Tohoku University, Japan, 2003.

[48] Deschamps,G. A., "Part II: Geometrical representation of the polarization of a plane electromagnetic wave", Proc. IRE, vol. 39, pp. 540-544, 1951.

[49] Copeland, J. R., "Radar target classification by polarization properties", Proc. IRE, vol. 48, pp. 1290-1296, 1960.

[50] Yueh, S. H., and Kong, J. A., "Calibration of Polarimetric Radars using In-scene Reflectors", Journal of Electromagnetic Waves and Applications", vol. 4, no.1, pp. 27-48, 1990.

PUBLICATION BY THE AUTHOR

Conference papers:

- Khuut Tseedulam and Motoyuki Sato,

Evaluation of “Van Khan Tooril’s ruin” –an archaeological site in Mongolia by GPR, Archaeological Conference, June, 2007, Akita, Japan

- Khuut Tseedulam and Motoyuki Sato,

GPR investigation for archeological site "Van khan Tooril's ruin"in Mongolia, Proceeding of the 116th SEGJ Conference, The Society of Exploration Geophysics Japan, May, 2007, Tokyo, Japan.

- Khuut Tseedulam and Motoyuki Sato,

Experimental approaches to understanding scattering behavior byPolarimetric GPR, Proceeding of the 118th SEGJ Conference, The Society of Exploration Geophysics Japan, May, 2008, Tokyo, Japan.

Journal:

- Khuut Tseedulam and Motoyuki Sato,

Evaluation of Van Khan Tooril's castle; an archaeological site in Mongolia by GPR, Exploration Geophysics journal, 40(1), pp-69-76